COUPLED WAKE AND BLOCKAGE MODELLING FOR A WIND FARM

A Thesis submitted to
the Graduate School of Engineering and Sciences of
İzmir Institute of Technology
in Partial Fulfilment of the Requirements for the Degree of

MASTER OF SCIENCE

in Energy Engineering

by
Janset Betül ÇAM

October 2022
İZMİR

ACKNOWLEDGMENTS

First, I would like to express my deepest gratitude to my supervisor Asst. Prof. Dr. Ferhat BİNGÖL for his inspiring guidance, mentorship, support, kindness, tolerance, patience and trust. I would not have been able to complete this study without his enthusiasm for teaching and unlimited knowledge sharing. I am grateful to him for allowing me to take part in this study and for providing a comfortable studying process.

I would like to thank Taylan KABAŞ, Wind Energy Power Plant Manager at Egenda Ege Enerji Üretim A.Ş. and Egenda Ege Enerji Üretim A.Ş. for their support, contribution, and collaborations.

Lastly, I would like to express my most tremendous most significant appreciation to my mother Selvinaz ÇAM, my father Suat ÇAM, my brother Ömer Bertan ÇAM and my sister Fatma Betül ÇAM for their endless love, great effort, support, belief, and encouragement throughout my life.

ABSTRACT

COUPLED WAKE AND BLOCKAGE MODELLING FOR A WIND FARM

One of the significant reasons for the power loss in wind farms is the wake effect. Therefore, the wake effect is crucial for designing a wind farm. However, only wake modeling is not sufficient to explain power losses. Wake is the turbulent, complex, and relatively weak flow behind the wind turbine. The wake effect is not required for the front row turbines in wind farms, and the wake model cannot be applied. It is assumed that the wind farm directly encounters the free stream wind speed. However, the blockage effect, also known as the induction zone effect, is observed at the front of the wind turbines. Due to this effect, the wind farm encounters a lower wind speed than the free-stream wind speed. This situation reduces the accuracy of the Annual Energy Production (AEP) calculation in wind farms.

The motivation of this study is to obtain an improved coupled wake and blockage model that converges to the accurate SCADA data of a wind farm more than the wake-only or blockage-only models. This study applies seven wake and six blockage models to the wind farm. The similarities and differences between the coupled models and the wind farm SCADA data and their reasons are discussed.

ÖZET

BİR RÜZGAR ENERJİSİ SANTRALİ İÇİN BİRLEŞTİRİLMİŞ RÜZGAR İZİ VE BLOKAJ MODELLEMESİ

Rüzgar çiftliklerinde meydana gelen güç kaybının önemli nedenlerinden biri de iz etkisidir. Bu nedenle, bir rüzgar çiftliği tasarlamak için iz etkisi çok önemlidir. Ancak sadece iz modellemesi güç kayıplarını açıklamak için yeterli değildir. İz, rüzgar türbininin arkasındaki türbülanslı, karmaşık ve nispeten zayıf akıştır. Rüzgar çiftliklerinde ön sıradaki türbinler için iz etkisi gerekli değildir ve iz modeli uygulanamaz. Rüzgar çiftliğinin doğrudan serbest akım rüzgar hızıyla karşılaştığı varsayılmaktadır. Ancak indüksiyon bölgesi etkisi olarak da bilinen blokaj etkisi rüzgar türbinlerinin ön kısmında gözlenmektedir. Bu etki nedeniyle, rüzgar çiftliği, serbest akış rüzgar hızından daha düşük bir rüzgar hızıyla karşılaşır. Bu durum, rüzgar santrallerinde Yıllık Enerji Üretimi hesaplamasının doğruluğunu azaltmaktadır.

Bu çalışmanın motivasyonu, bir rüzgar çiftliğinin doğru SCADA verilerine yalnızca iz veya yalnızca blokaj modellerinden daha fazla yakınsayan gelişmiş bir birleşik iz ve blokaj modeli elde etmektir. Bu çalışma, rüzgar çiftliğine yedi farklı iz modeli ve altı farklı blokaj modeli uygulamaktadır. Birleştirilmiş modeller ile rüzgar santrali SCADA verileri arasındaki benzerlikler ve farklılıklar ve bunların nedenleri tartışılmıştır.

TABLE OF CONTENTS

LIST OF FIGURES

Figure **Page**

Figure **Page**

Figure **Page**

Figure **Page**

Figure **Page**

LIST OF TABLES

LIST OF SYMBOLS

A	Swept Area
C_P	Power Coefficient
C_T	Thrust Coefficient
D	Wind Turbine Rotor Diameter
e_x	x-direction Yawed
e_y	y-direction Yawed
k^*	Wake Growth Rate
k_w	Wake Decay Coefficient
P	Power
r_r	Rotor Radius
T	Thrust Force
u	Axial Component of the Flow Velocity
U_0	Free Stream Velocity
u_1	Inflow Wind Speed
u_2	Downstream Velocity
U_∞	Undisturbited Wind Speed
U_W	Wake Velocity
V	Wind Speed
x	Streamwise Coordinate
y	Spanwise Coordinate
z	Vertical Coordinate
z_h	Hub Height Level

θ_{yaw}	Yaw Angle
ρ	Air Density
x	Distance Behind the Turbine
ε	Function of Thrust Coefficient

LIST OF ABBREVIATIONS

AEP	Annual Energy Production
CFD	Computational Fluid Dynamics
DTU	Technical University of Denmark
DWM	Dynamic Wake Meandering
GCL	Wake Model of G. C. Larsen
IEA	International Energy Agency
NOJ	Wake Model of Niels Otto Jensen
RHB	Rankine Half Body
SCADA	Supervisory Control and Data Acquisition
WD	Wind Direction
WS	Wind Speed
WTG	Wind Turbine

CHAPTER 1

INTRODUCTION

Nowadays, the world's energy demand is increasing day by day. Countries that plan to increase their electricity production capacity to meet the increasing energy demand by moving away from energy sources that are exhaustible and unfavorable in many respects; aim to advance clean, green, renewable, and sustainable energy sources. With targets such as climate awareness, sustainable development goals, carbon footprint reduction, and Net Zero by 2050, the renewable energy capacity of 290 GW as of 2021 is projected to increase rapidly worldwide by 2030 and 2050 [1]. For the Net Zero by 2050 target, a leap in solar and wind energy is expected by 2030 [2]. On the other hand, the 3Ds of energy, decarbonization, digitization, and decentralization, play a crucial role in clean energy. While most renewable energy sources are close to each other for decarbonization and digitization principles, wind power is also essential for decentralization. The reason for this importance is especially the off-grid industrial zone targets. It is beneficial to have a wind farm around to meet the electricity demand of industrial areas. Having a mesoscale wind farm once the appropriate site is obtained is an impressive step towards decentralization in that area. Considering the existing wind power plants, the capacity of a single turbine is 2-3 MW on average in onshore applications. Considering that the wind farm consists of many wind turbines, even a tiny improvement can produce satisfactory results.

Efficiency in wind energy can be examined from two different perspectives. The first of these is the aerodynamic efficiency of the wind turbine. Wind turbines that convert the wind's kinetic energy into mechanical energy and then into electrical energy are subject to Betz's law. Therefore, the theoretical limit of this energy conversion is about 59 percent. Today, many industrial turbines have come close to the theoretical limit. Therefore, achieving aerodynamic improvement by focusing on turbine efficiency is exceptionally challenging. Various methods can be used for aerodynamic improvement. Some are unaffordable and unfeasible to adapt to the industry. When looking at wind energy efficiency from another perspective, it is realized how substantial it is to examine the effect of the wind farm, which is formed by many wind turbines, on electricity

production. The site's geological and meteorological features and the turbines' positions have an outstanding role in the electricity generation of the wind farm. Geological and meteorological studies at the preliminary project stage are valuable for techno-economic feasibility. Thanks to the studies, consistent capacity factor and AEP estimations can be made, or production improvement scenarios can be prepared for the already operating power plant.

Apart from that, due to the variety of industrial turbines dominating the wind energy market, it is farm or site-based optimizations suitable for an industrial level enhancement or an already operational power plant. In other words, aside from the importance of turbine efficiency, the fact that two different wind farms using the same turbine will have different AEP values with the correct analysis of the sites shows the importance of site assessment. Since the wind power is directly proportional to the cube of the wind speed, the turbine that catches the optimum wind shows a high level of performance.

Although the performance of wind energy is satisfactory, one of the most critical challenges affecting the industry in wind energy can be considered as fluctuating electricity generation. Wind energy, the best solution to the problem of foreign dependency on electricity demand, causes fluctuating-intermittent electricity production. This is no longer a problem favoring various supports (such as hydrogen storage). The second major challenge is that wind energy projects need long-term measurements in the preliminary phase. Meteorological analyses must proceed at required often, at different altitudes, and over a long time. If the wind turbines are not positioned correctly in the field, the electricity generation will be far below the rated power value of the turbines. Therefore, capacity factor and AEP decrease. Making site assessment consistent is a substantial step in preventing these problems. Besides the significance of terrain structure and roughness in the preliminary phase of field assessment, wake modeling is the most crucial part of wind energy meteorology [3]. In wind energy, wake is the irregular characteristic flow that the turbine leaves behind after capturing the wind [3]. According to the first and second laws of thermodynamics, the kinetic energy in the wind flow is not entirely captured by the wind turbine, leaving behind an irregular, weak kinetic energy. That is, while the wind flow in front of the wind turbine is strong and relatively more regular, the remaining flow is irregular, relatively more turbulent, and reduced after the wind turbine captures some wind. Many wake models emerge to be able to understand

and clearly observe the wind turbine wake, then position the turbines in an optimum way or make improvements-corrections in the wind farms currently in force. Since many parameters are considered while creating wake models, different wake models are designed for different field conditions and wind farms of various sizes. Wake is divided into two parts: near wake and far wake. The near wake represents the flow just behind the wind turbine, which equates to an average of 1 turbine rotor diameter (D) to 3 turbine rotor diameter (D) downstream [4]. Far wake is downstream in the extensive environment.

Studies on wake for many years explain the flow characteristic in wind farms. However, the wake is defined by downstream flow, and the upstream flow is mainly ignored. Blockage effects are examined with upstream flow [5]. For instance, the turbines in the first row of the wind farm are not under the wake effect. However, this does not mean that the turbines in the first row are not under any influence. This is explained by the blockage effect [6]. Therefore, the blockage effect gives results that cannot be calculated with wakes. Examining these two effects together for site assessment is expected to converge more to actual production values (SCADA Data). In addition, the thrust coefficient is the input for the blockage model and the wake model's output. Thus, the two models can be combined easily [6].

The motivation of this study is to model the wake and blockage, which affect the wind farm's performance, and to optimize the wind farm with a coupled model consisting of these two effects. Only wake is usually considered in performance improvements of wind farms. However, it is impossible to predict upstream flow with wake modeling. The subject argued in this thesis is that wake modeling alone is insufficient to analyze the wind farm from all sides and make predictions of electricity production consistent. The results of wind farms for which only wake modeling is created are relatively inconsistent due to the blockage in the front of the turbine and the wide-spreading lateral areas. Therefore, it is advocated to combine wake and blockage models. Early-stage studies of this coupled model idea are reviewed to validate further enhanced unified wake and blockage modeling. The research problems questioned for this purpose are as follows:

1. How to filter SCADA data obtained from a wind farm?

2. How to choose the suitable wake model for the wind field, and what parameters are considered during the selection?

3. Which blockage models are suitable for the wind farm?

4. What is the relationship between wake and blockage?

5. Where are the areas exposed to wake and blockage effects in the wind farm?

6. What parameters are considered to examine the wake and blockage effects?

7. How to combine wake and blockage models? How to determine the compatibility of models with each other?

8. How close are the results of the developed coupled wake and blockage model to SCADA data? What is the difference between only the wake model works and coupled model works?

CHAPTER 2

LITERATURE SURVEY

In this chapter, there is a literature review on the researched topics. This section aims to understand the sub-titles of the research topic, to be familiar with the definitions covered by the subject, and to have information about the methodology, process, and result discussions of the studies carried out from the past to the present.

In the first part, the principles of wind energy are examined. The basic concepts of wind energy are familiarized. Wind turbine aerodynamics are briefly discussed. The flow characteristic around the wind turbine is explained. The basics of wind energy meteorology, related to the flow characteristic, are presented. Definitions associated with the study are detailed. The following parts examine the rotor average models, and the superposition models used with the wake and blockage models are explained.

Last but not least, the wake effect in wind energy is defined, and types of wake are explained. The area affected by the wake and its parameters is described. The development of wake from past to present is observed. State-of-the-art technology is researched. Wake models are explained, and their areas of influence and features are supported by references. The blockage is defined, and its types are described. The area where it is effective is examined, and the blockage parameters are explained. The blockage is reviewed from the past to the present. State-of-the-art technology is explored.

2.1. The Essentials of Wind Energy

The wind is occurred by the pressure difference of the air. Wind turbines capture wind flow and convert existing flow energy into another form of energy: mechanical energy. Wind turbines generate power with this mechanical energy. When this fundamental process is examined, the sections before the energy production phase can be examined under two main headings: meteorology and aerodynamics. Topics such as wind profile, atmospheric forces, and the effect of the wind turbine on flow characteristics are mainly studied within the framework of meteorology, and issues such as momentum

theorem, Betz law, and rotor model are studied within the framework of aerodynamics. Wind energy meteorology and aerodynamics are interactive subjects. This section explains the definitions required for wind energy and wind turbine before the meteorology and aerodynamic explanations.

One of the most fundamental parameters in wind energy is wind speed. Especially considering the power equation of wind energy; the power is directly proportional to the cube of the wind speed. A slight increase in wind speed affects power. In addition to the speed of the wind, it is essential to capture free stream wind that has not encountered any obstacles. The flow becomes more irregular when it hits the inherently solid body. In addition to this irregularity, a weak flow will remain downstream due to the flow captured by the wind turbine. Hence, the flow that encounters a wind turbine continues after the turbine as both turbulent and weak flow. This is explained by the wake effect [7].

Another fundamental parameter in wind energy is wind direction. Due to their aerodynamic structure, horizontal axis wind turbines must catch the wind perpendicular to the hub. The wind flow becomes normal to the wind turbines thanks to the yaw mechanism. Apart from that yaw mechanism is a substantial control method for wind farm optimization [8].

Hub height is simply the height of the rotor hub from the ground. Hub height is required for meteorological approximations. Also, the met mast should have a measuring device close to the hub height. The blades of wind turbines sweep the rotor swept area.

Wind power is calculated as follows.

$$P = \frac{1}{2}\rho A V^3 \qquad 2.1$$

Where ρ is the air density, A is the swept area, V is the wind speed. The wind power equation represents the absolute power of the wind. However, the power obtained by the turbine is less than the wind power. Betz's law explains this. The theoretical limit for converting wind to mechanical energy is the Betz limit of 16/27 [9]. Since this is the theoretical limit, it is the maximum power coefficient Betz limit.

The power coefficient represents the performance of the wind turbine and is defined as follows.

$$C_P = \frac{Rotor\ Power}{Wind\ Power} \tag{2.2}$$

Thrust force is calculated as follows.

$$T = \frac{1}{2}\rho A V^2 \tag{2.3}$$

When the thurst is dimensionless, the thrust coefficient is obtained.

$$C_T = \frac{Thrust\ Power}{Dynamic\ Power} \tag{2.4}$$

2.2. Rotor Average Models

Rotor performance is examined to observe wake interactions. Rotor averaged models are applied to the wind farms to observe turbine-based wake and near wake. Thus, it is defined the kinematics of the wake and predicted the power production of the wind turbine. There are two different rotor average models which are the actuator disk model and the actuator line model.

2.2.1. Actuator Disk Model

The actuator disk principle can analyze wind turbine rotor behavior in the flow domain [10]. The actuator disk is a vital theorem for wind turbine aerodynamics. The Actuator Disk model is the simplest method developed with CFD methodology in wake

models[11]. Models the effect of the wind turbine rotor on the wind flow as a force disk [11]. Because it is a fast and basic model, it is frequently used in model validation comparisons. It is not as detailed as the Actuator Line Model [11].

In Figure 1, the velocity at the disk u is the arithmetic mean of the free-stream V_o and the slipstream velocity u_1 [10].

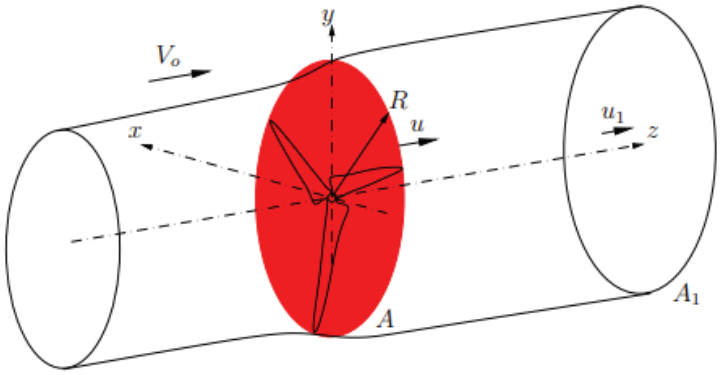

Figure 1. Flowfield around an actuator disk [10].

2.2.2. Actuator Line Model

The Actuator Line Model is the radial distribution of body forces along lines representing wind turbine blades [12]. The Actuator Line Model is more advanced compared to the Actuator Disc Model. The vortex structures are elaborate. Figure 2 is a comparison of the actuator disc and actuator line models.

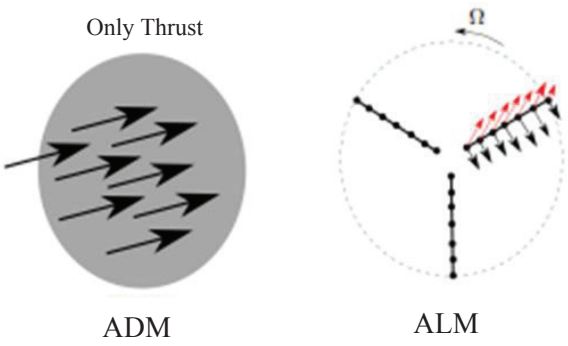

Figure 2. Actuator Disk and Actuator Line Model [13].

2.3. Wake Summation

Superposition models are inputs for the wake model. There are four commonly used superposition models [14]; however, only the linear sum is used in this study.

$$\left(1-\frac{u_{n+1}}{U_{\infty}}\right)=\sum_{j=1}^{n}\left(1-\frac{u_j+1}{u_j}\right) \qquad 2.5$$

2.4. Wake Effect

Airflow tends to be irregular. When the airflow encounters the wind turbine, the wind turbine captures some of the airflows. Thus, the wind turbine generates power with part of the airflow. The remaining airflow becomes irregular and loses some energy [15]. When this weaker airflow encounters another wind turbine, the wind turbine captures less airflow. As a result, it produces less power than the previous turbine. This is explained as the wake effect of wind energy. The development of wake that occurs downstream of one wind turbine on another wind turbine is illustrated in Figure 3.

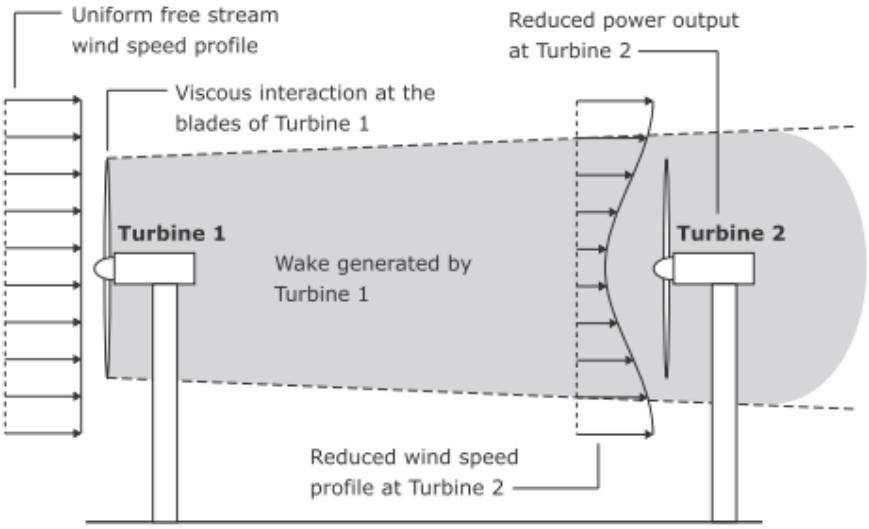

Figure 3. The phenomenon of aerodynamic coupling between two wind turbines aligned with the free stream wind [16].

For the wake effect to be observed, there must be more than one wind turbine, a cluster, or a wind farm. In a wind farm, the wake can reduce the power production of wind turbines by 40-45% [17]. The wake is divided into two in terms of the area where it is effective. These are near-wake and far-wake. Near-wake is the downstream air flow just behind the turbine. Far-wake starts from a distance of approximately 4D wind turbine rotor diameter. In Figure 4, while the blockage area is located as the induction region, near-wake and far-wake are schematized.

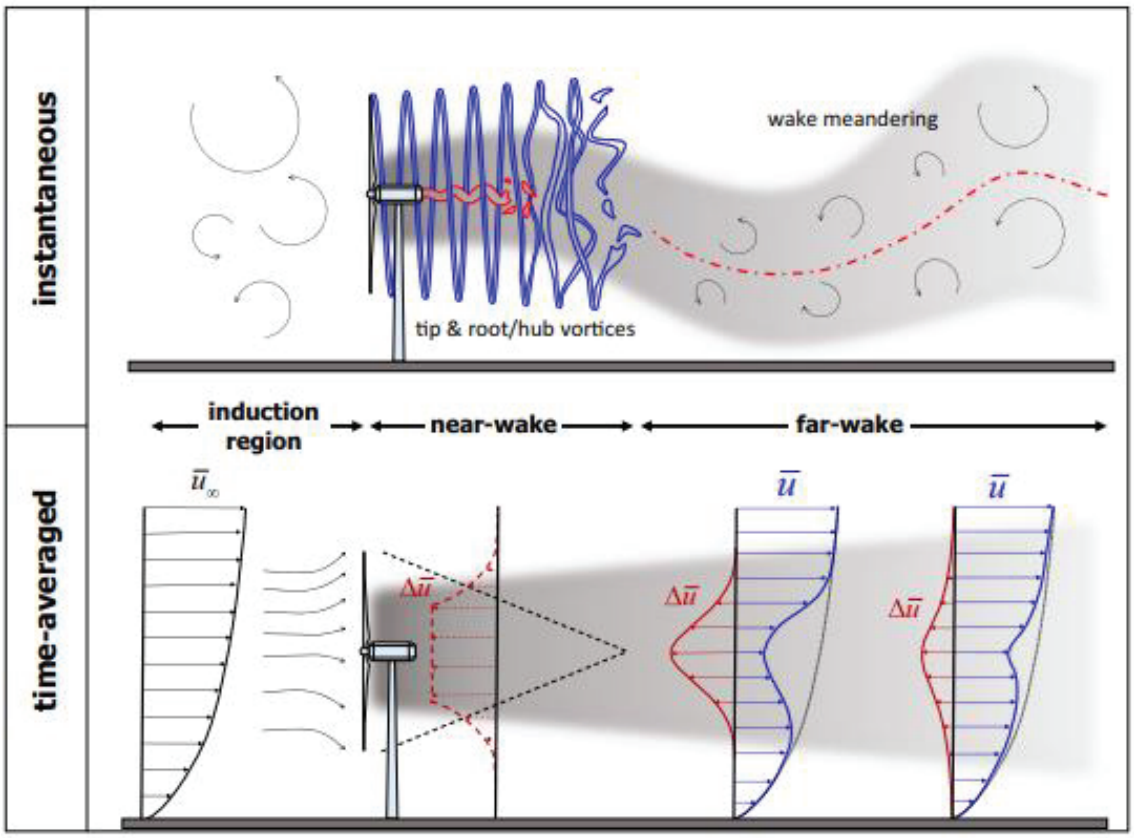

Figure 4. Schematic figure showing the flow regions resulting from the interaction of a wind turbine and incoming turbulent boundary layer. Depicted are the most characteristic instantaneous (top) and time-averaged (bottom) flow features [7].

2.4.1. The Jensen Wake Model

Niels Otto Jensen developed the Jensen Wake Model in 1983 [18]. It is one of the most common wake models. It was formulated simply under the influence of its development in the early 1980s. An elementary calculation method compared to other models makes it a fast model. The fact that it gives immediate results and is comprehensible is the most significant reason for its widespread use [19].

$$1 - \frac{u_2}{u_1} = \frac{1 - \sqrt{1 - C_t}}{(1 + k_w\, x/r_r)^2} \qquad 2.6$$

Where u_2 is the downstream wind speed of a turbine at a distance x, u_1 is inflow wind speed, Ct is the thrust coefficient, r_r is the rotor radius, and k_w is the wake decay coefficient. The schematic view of the Jensen wake model is as in Figure 5

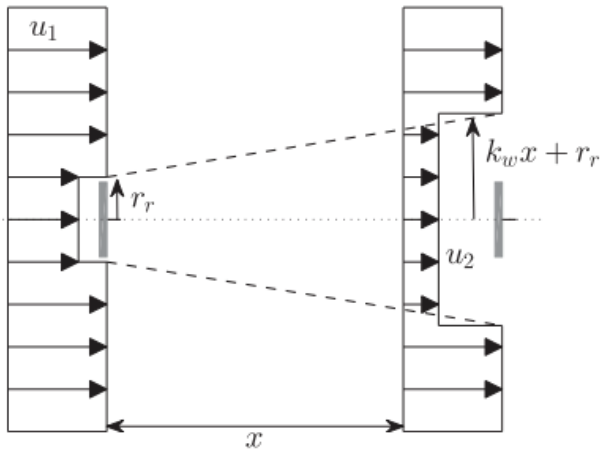

Figure 5. The Jensen wake model concept [19].

The two models obtained by further development on the Jensen Model are the Jensen Local Wake Model and the Turbo Jensen Wake Model.

The Jensen Local Wake Model is similar to the Jensen Model in general. However, local data are used for inflow wind speed and turbulence intensity. Since Jensen

and Gaussian wake models have the same expansion rate process, Jensen Local is sampled from the linear connection in the Gaussian wake model [20].

The Turbo Jensen Wake Model is turbulence-optimized. The expansion rate of the wake is related to the amount of turbulence [7]. This relationship is studied by Nygaard and modified for the Jensen model in the PyWake Tool [21].

2.4.2. The Gaussian Wake Model

Bastankhah and Porte-Agel [22] create a new wake model. This model is created using the laws of conservation of mass and conservation of momentum. Apart from that, a Gaussian distribution for velocity deficit is assumed.

$$\frac{\Delta U}{U_\infty} = \frac{U_\infty - U_W}{U_\infty} = \left(1 - \sqrt{1 - \frac{C_t}{8(k^*(x/d_0) + \varepsilon)^2}}\right) \times exp\left(-\frac{1}{2(k^*(x/d_0) + \varepsilon)^2}\left\{\left(\frac{z - z_h}{d_0}\right)^2 + \left(\frac{y}{d_0}\right)^2\right\}\right) \quad 2.7$$

$$\varepsilon = 0.2\sqrt{\frac{1 + \sqrt{1 - C_t}}{2\sqrt{1 - C_t}}} \quad 2.8$$

Where U_∞ is the undisturbed velocity, U_w the wake velocity, C_T the thrust coefficient, d_0 the wind turbine diameter, and x the distance behind the turbine. x, y, and z are streamwise, spanwise, and vertical coordinates, respectively, and z_h is the hub height level. k^* denotes the wake growth rate s a function of the thrust coefficient and local turbulence intensity [22]. ε is a function of the thrust coefficient. Bastankhah and Porte-Agel [22] create a new wake model. This model is created using the laws of conservation of mass and conservation of momentum. Apart from that, a Gaussian distribution for

velocity deficit is assumed. As seen in Figure 6, the downstream region of the gaussian wake model takes the shape of a hat.

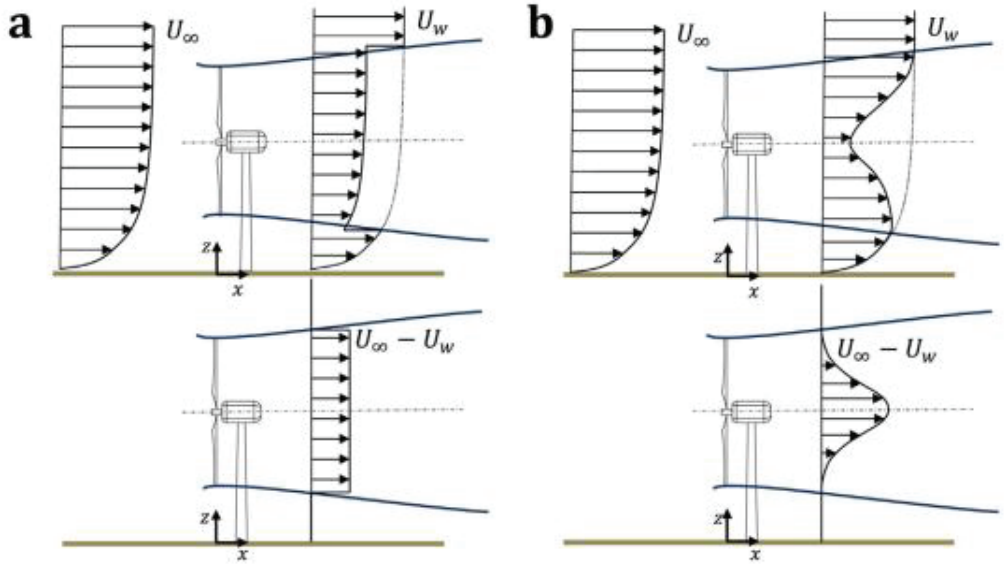

Figure 6. Schematic of the vertical profiles of the mean velocity (top) and velocity deficit (bottom) downwind of a wind turbine obtained by assuming: (a) a top-hat and (b) a Gaussian distribution for the velocity deficit in the wake [22].

2.4.3. The Larsen Wake Model

Larsen Wake Model is an elementary wake calculation developed by Larsen [23]. The first version, released in 1988, is suitable for single wake conditions. In the expanded version, boundary conditions are enhanced. Two different boundary conditions are included in The Further Larsen version. The first is for the rotor plane, and the second is for the fixed frame [24].

As in the Jensen Local Model, local data are used for inflow wind speed and turbulence intensity in the Larsen Local Model.

2.4.4. The Dynamic Wake Meandering

The dynamic wake meandering (DWM) model was developed to model wind wake and unsteady fluctuating flow. According to the DWM model, the wind wake is the passive tracer triggered by the large-scale turbulence structure [25]. According to the model, the wake dynamics are as in Figure 7. The red symbol represents the motion, and the black line represents the wake without fluctuation. The figure shows the system is dynamic in two ways [25]. The combination of these two situations gives more realistic results for instant calculations. When the DWM model is applied to a wind farm, the deviation between the expected and simulated results is about 10% [25]. This level of departure can be considered normal.

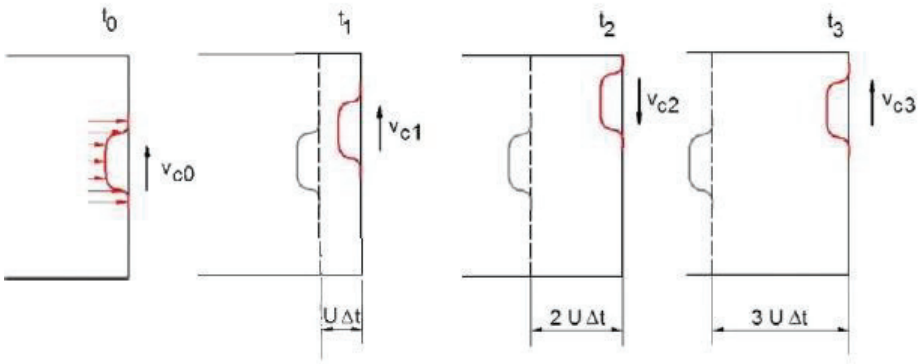

Figure 7. The Dynamic Wake Meandering [25].

2.5. Blockage Effect

The interactions of turbines with each other in wind farms have been explained only by a wake for many years. When the wake was not sufficient to explain the power losses in the wind farm and after the experiences with high error rates, it was concluded that the missing connection was the blockage effect [26]. The blockage effect decreases as the distance between turbines increases. In the study of Bleeg [27], the wind speed deceleration is 3.4% at the distance of 2 D, and the wind speed deceleration is 1.9% at the distance of 7-10 D.

Although the blockage effect is not as massive as the wake effect, it causes a significant power loss, especially for large wind farms [26]. Blockage is the reduction or change of direction of wind flow by encountering an obstacle. This obstruction can occur not only as a solid body (wind turbine) blockage but also due to wake. In this case, it can be examined under two main headings as solid-body blockage and wake blockage in terms of blockage types. Also, the blockage can be divided into local and global blocks in terms of scope and predictability. Local blockage represents the blockage effect on a wind turbine basis [28]. Global blockage can be seen as a meteorological effect. The wind covers the entire field and is associated with the atmosphere. It's uncertain compared to local blockage. Its remarkable feature is that it affects the first turbine in the wind farm [29]. Although it is thought that there is no obstacle in front of the first turbine, the spherical blockage affects the first turbine and then all the turbines in the wind farm. The global blockage is difficult to measure and is an essential parameter for wind farm power production forecasts.

2.5.1. Self Similarity Blockage Model

The self-similarity blockage model is calibrated by RANS simulation. The radial velocity, a parameter for the blockage model comparison, is not available in the self-similarity blockage model. Therefore, the self-similarity model cannot calculate the wind flow's direction change (bias). The first Self-Similarity Model developed did not include the ground effect, but nowadays ground effect can also be calculated using various techniques. Despite its low cost, it does not have the features considered in comparing the blockage model [30].

2.5.2. Vortex Cylinder Blockage Model

In the Vortex Cylinder Model, the wake is assumed to be of constant density and a semi-infinite cylinder. The Vortex Cylinder Model is suitable for all blockage parameters [30]. When Figure 8 is examined, U_0 is the free stream velocity norm. For aligned flow, the free-stream velocity is along x, $U_0 = U_0 e_x$. For yawed inflow, it is

$$U_0 = U_0 \cos\theta_{yaw}\, e_x + U_0 \sin\theta_{yaw}\, e_y \qquad 2.9$$

with θ_{yaw} is the yaw angle.

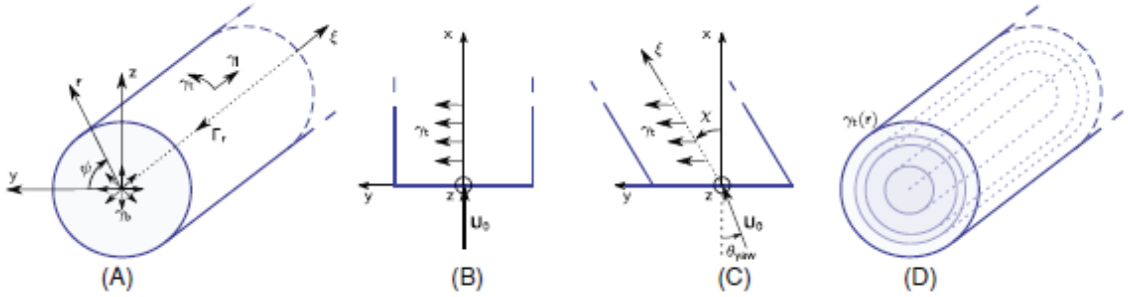

Figure 8. The vortex cylinder model. (A) 3D representation of the model, (B) Top view for aligned flow. (c) Top view for yawed flow [31].

2.5.3. Vortex Dipole Blockage Model

The Vortex Dipole Model examines distant induction. In this respect, it differs from the Vortex Cylinder Model [20], [28].

2.5.4. Rankine Half Body Blockage Model

The Rankine Half Body is a simple model based on potential flow theory. Since it is a newly discussed model, its development continues. Although it is an uncertain approach, it is similar to the vortex cylinder model. The Rankine Half Body model is shown in Figure 9.

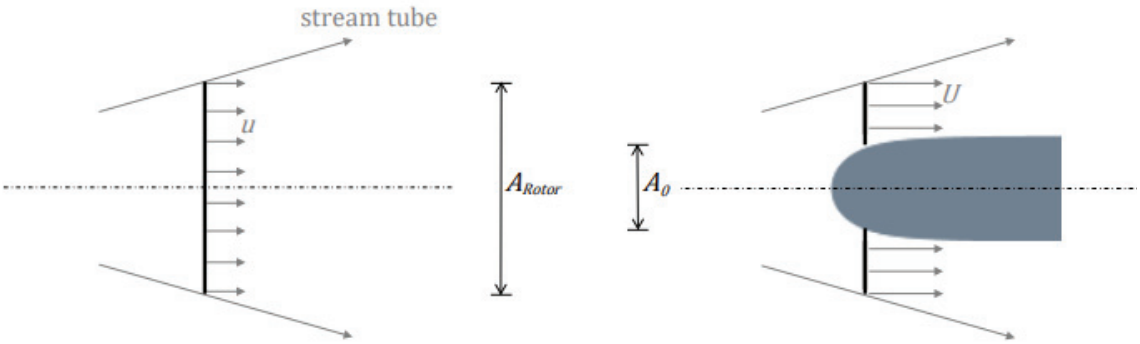

Figure 9. Sizing the RHB flow to approximate the flow ahead of and around an actuator disc (left) by matching the mass flow around an RHB (right) through a stream tube of the equivalent area [32].

2.5.5. Hybrid Induction Blockage Model

This model is based on the idea of combining far-zone and near-zone induction. The reason for this is to simplify the calculation. The self-similarity is used for rotor close, and the vortex dipole is used for rotor distance. Therefore, the two blockage models are hybridized [21], [31].

CHAPTER 3

SITE DESCRIPTION

Since comparing the wake and/or blockage models among themselves will not lead to a satisfactory result, the examined models are validated with the power production data of a wind farm. With this, the models can be interpreted and compared with each other and the SCADA data of an operating wind farm. In this study, the examined models are compared with SCADA data and validated to correlate them with the theoretical basis and obtain consistent results.

In this chapter, various specifications of the wind farm where the models are validated are explained. Site description, the definition of WTG used in the wind farm, and the wind characteristics of the field are the most basic features that need to be explained.

The wind farm investigated in this study is located in the western part of İzmir, on the coast of the Aegean Sea. It is an onshore wind farm consisting of five turbines. Due to the small number of turbines, it consists of only one row. In this case, it is sufficient to examine the wind directions in which the turbines are lined up, rather than all wind directions, to explore the wake effect.

This wind farm is located on a complex terrain at an average height of 450 m above sea level. The single row with all the wind turbines has a length of 930 m. The distance between the wind turbines is 230 m.

The wind farm has five 3 MW wind turbines. These turbines have a rotor diameter of 82 m and a hub height of 78 m.

In other words, the distance of 230 meters between the turbines corresponds to approximately 2.8 D.

Figure 10 shows the image of the Urla Wind Farm. The complex terrain and the height difference of the turbines are visible.

Figure 10. Urla Wind Farm [33].

The field's elevation is examined to observe the height difference in the area better. Figure 11 shows the heights of the turbines in the wind farm above sea level. It is observed that the height of WTG0 is less than other turbines.

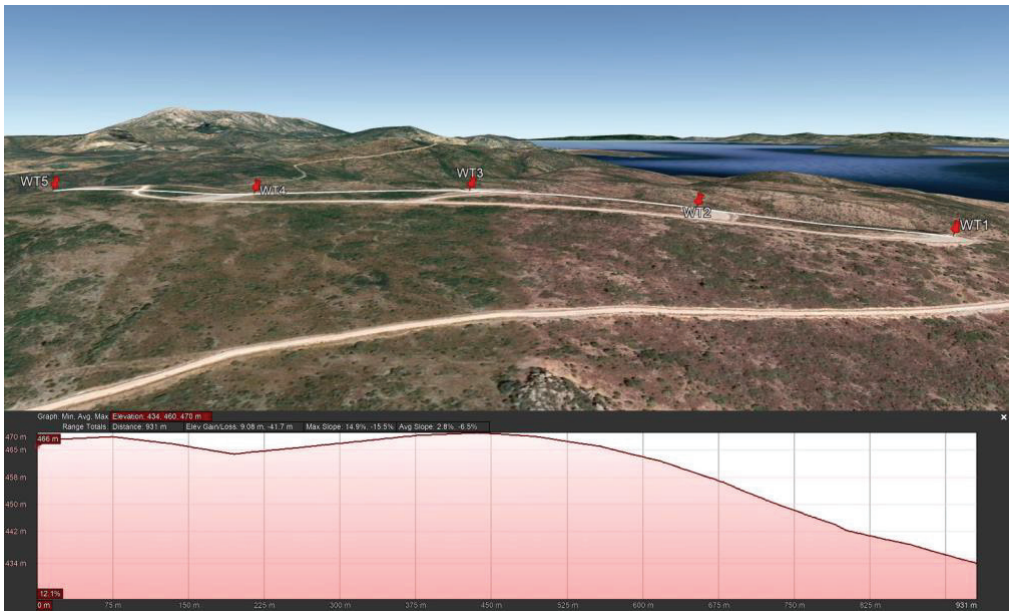

Figure 11. Elevation of the wind farm.

To understand the layout of the turbines, two different wind farm images are shown in Figure 12.

(a)

(b)

Figure 12. Urla Wind Farm (a) Near View (b) Far View.

The single-row state of the turbines in the wind farm is observed in Figure 11 and Figure 12. In addition, the front view of the turbine arrangement is in Figure 13.

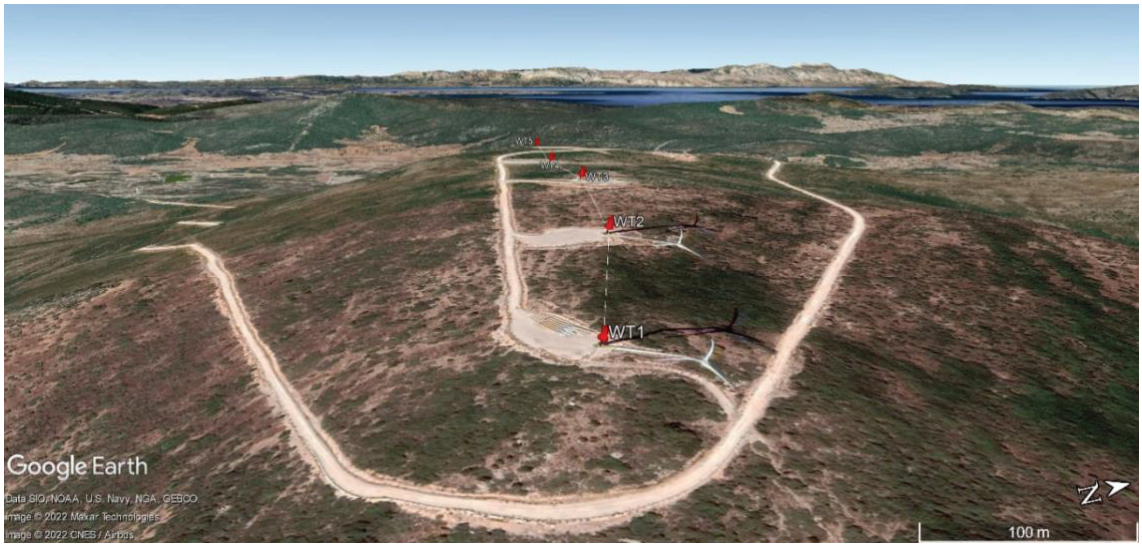

Figure 13. Single row view of the Wind Farm.

CHAPTER 4

A WIND FARM TOOL: PYWAKE

PyWake is an open-source wind farm simulation tool. It is used to create wind farms, simulate flow characteristics, calculate power production, and calculate AEP. PyWake was developed by DTU Wind Energy [21], [34].

This study uses PyWake for site description, site mapping, power production calculation, AEP calculation, wake modeling, deficit model comparison, blockage modeling, and coupled wake and blockage model creation.

It is fast thanks to its vectorial infrastructure. The general flowchart of PyWake is as follows.

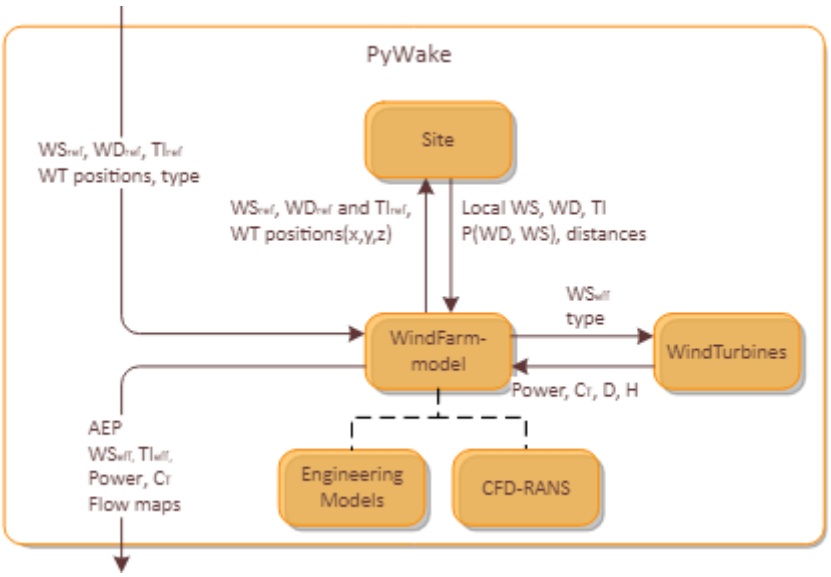

Figure 14. PyWake Flowchart [21].

As seen in Figure 14, all outputs can be obtained when reference wind speed, wind direction, turbulent intensity, wind turbine coordinates, and wind turbine specifications are input. A sample of PyWake scripts are available in Appendices.

CHAPTER 5

WIND FARM DATA VALIDATION

Real-time data is primarily required for wind farm validation. The data obtained from SCADA is raw data. Filters are applied to the raw data to get rid of error signals. Validation proceeds with the useful data.

5.1. Filtering the Data

Data filtering is a necessary process that must be carefully executed early in the study. It is crucial for the reliability of the filtering that the functions to be used have been tested in more than one study since incomplete or incorrect filtering of the data will directly affect the entire research output. Each data can have different parameters, and the important thing is that the algorithm is correct.

If data acquisition is divided into certain parts and progresses step by step, the margin of error decreases, and it becomes easier to detect and correct the error. For example, 9999 and similar erroneous data is filtered by first examining the dates—the number of data changes according to the data used. As the number of data increases, filtering becomes more complex. Also, accuracy should be checked when obtaining raw data from SCADA. The calibration of data is another crucial point. The direction perception of each turbine and the airflow coming from that direction should be equal to each other simultaneously.

The data acquisition process is explained and implemented in detail in [35].

5.2. Urla Wind Farm

After data filtering, five turbines have a total of 1313543 10-min data. This is approximately 262708 10-min data per turbine. 262708 10-min data covers about five

years. 5 years of data is reasonably sufficient for model comparison and interpretation. Even seasonal climatic changes can be observed during this period.

5.3. Wind Conditions

Wind roses are obtained from the real-time production of Urla Wind Farm to discuss the wind speed and direction on the same diagram. Each of the wind turbines has similar wind conditions. It is sufficient to confer the first and last single-row turbines that make up the wind farm.

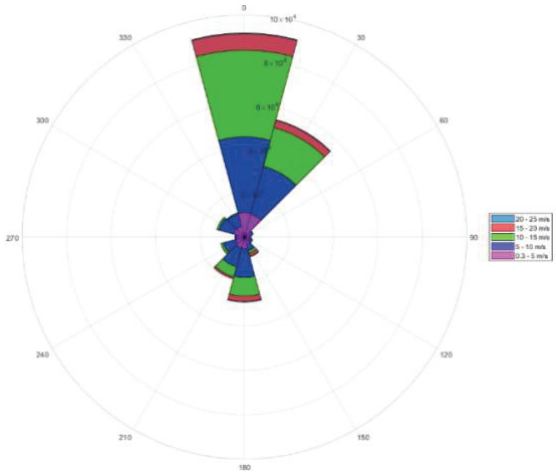

(a)

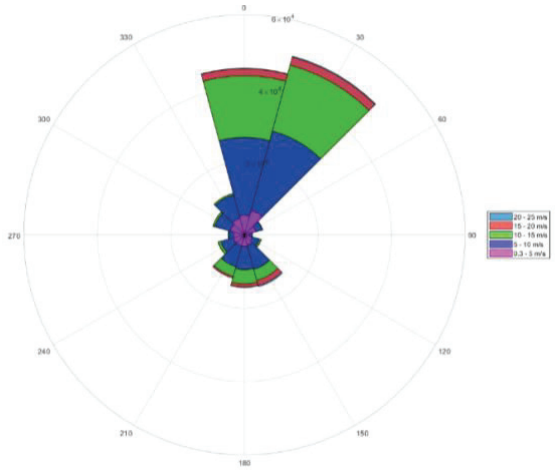

(b)

Figure 15. Wind Rose (a) WTG0, (b) WTG4.

In Figure 15, when wind roses are examined, the range of 350-60 °s wind direction is quite efficient. The AEP calculation corresponding confirms this interpretation of the wind directions.

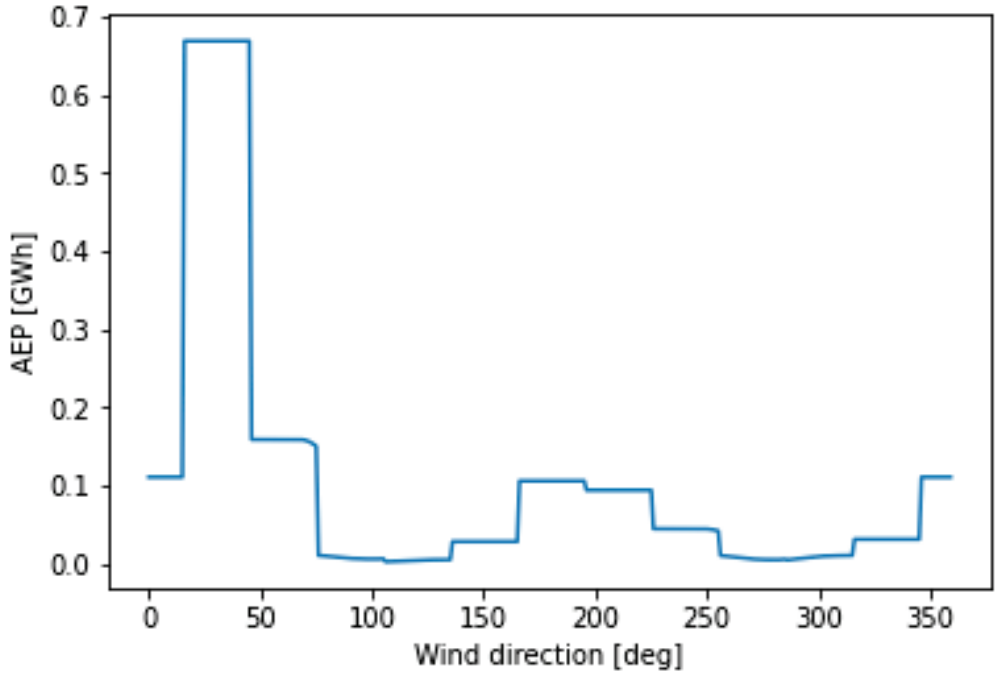

Figure 16. Urla Wind Farm AEP by wind direction.

Figure 16 represents the annual wind farm energy production distribution in each wind direction. Accordingly, the peak level of annual energy production at the 0-50° wind direction confirms the wind roses. At the same time, it is observed that the wind farm is formed in a single row, and the turbines are not under the influence of each other in the range of 0-50 °s. Hence, the 75-125 and 250-300 °s wind direction ranges, which are the bottom points of the AEP, are the scenarios where the turbines are in a single row. When all this is considered, the wind angles especially wake models, should be examined within the two ranges mentioned. Modeled AEP map of the wind farm is as in Figure 17.

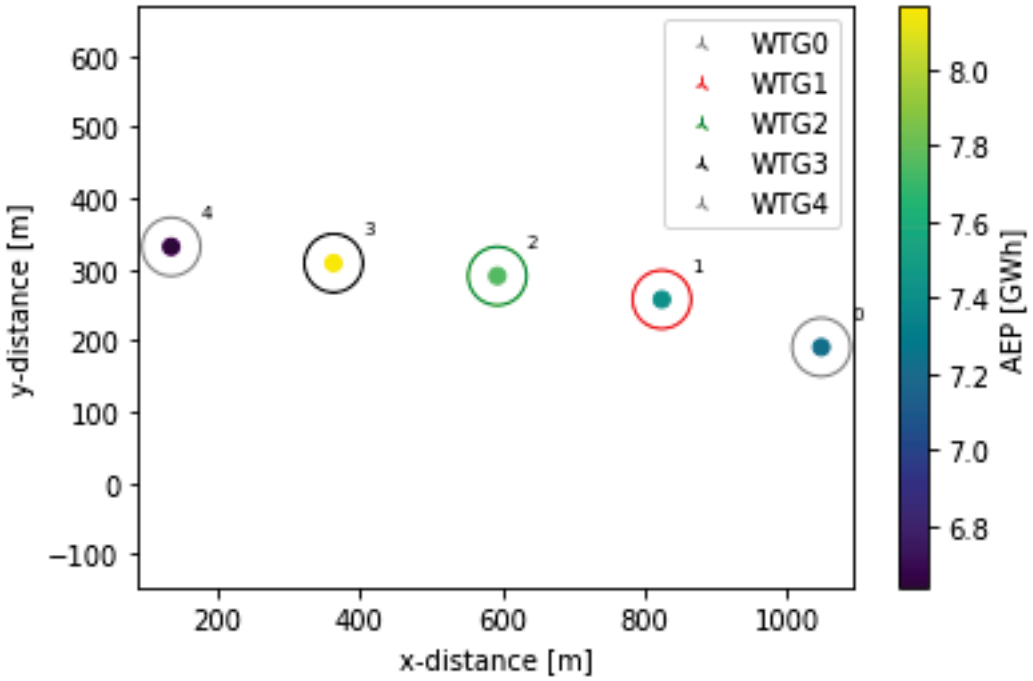

Figure 17. AEP map of Urla Wind Farm.

5.4. Power Validation in Urla Wind Farm

One of the most critical inputs required to examine the wake and blockage models is the power data of the turbines. In a way, it defines the identity of the turbine and makes it easier to predict the behavior of the turbine. Modeling with the theoretical power curve of the 3 MW wind turbine used in Urla Wind Farm is insufficient to observe the field's actual behavior. Power validation is required to obtain more precise results.

The basis of power validation is power data in wind directions where wind turbines encounter free stream airflow. Considering the positions of the turbines on the field in Figure 17, five turbines at 0-10° wind directions and 180-190° wind directions capture free stream airflow. As seen in Figure 15, since the prevailing wind direction at Urla Wind Farm is north, power-wind speed data at 0 degrees wind direction is used in this validation study.

Urla Wind Farm's real-time power generation data cannot be shared due to privacy policy. Therefore, a ratio of real-time power and the power data of the 3 MW turbine is obtained. Thanks to the validated Power Curve, real-time power production and

theoretical power data are compared and interpreted. In addition, it is aimed to improve model results by using validated power as model input in models run in the tool.

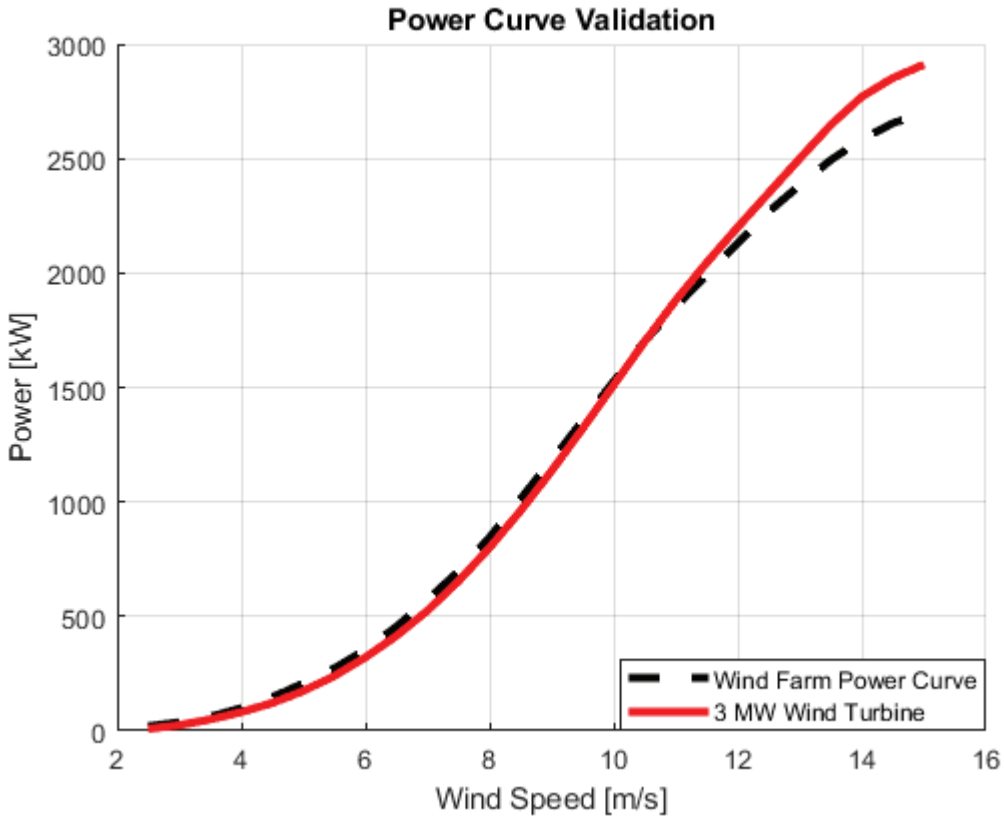

Figure 18. Power Validation in Urla Wind Farm.

As seen in Figure 18, the real-time power data of wind turbines from 7m/s wind speed is very similar to the theoretical power data of 3 MW wind turbine. The reason why wind farm power curve converges properly with the theoretical power curve of the turbine is that the field is not complex (land conditions are stable) and it consists of only one row of wind turbine. According to the positioning strategy of the wind turbines, all the turbines encounter free stream airflow at the prevailing wind direction range. This is the reason for the convergence of the wind farm power curve and the theoretical power curve of the turbine.

5.5. Model Inputs

There are several inputs which are necessary for site description of the wind farm and wake-blockage model simulations. The parameters required to create the model in the Pywake tool are in Table 1.

The wind farm's location on rough and high terrain causes a difference in air density. Air density decreases from sea level to higher [36]. In this study by Ferhat BİNGÖL, the air density under different conditions is calculated. Accordingly, considering the terrain conditions of the Urla Wind Farm, the air density can be accepted as 1.146 kg/m^3.

Table 1. Required General Inputs for the Analysis.

	Parameter	Input
Required Inputs	Wind Speed	[2.5:0.5:15]
	Power	Urla WF Validated Power Data
	Thrust Coefficient	Wind Turbine Ct Curve
	Diameter	82 m
	Hub Height	78 m
	x-coordinates	Urla WF Coordinates
	y-coordinates	Urla WF Coordinates
	z-coordinates	Urla WF Coordinates
	Air Density	1.146 kg/m³
	Weibull Parameters	A,k,f

In addition to common inputs, the inputs required for wake, blockage, and coupled models are in Table 2 the model inputs defined for the models created in the PyWake tool. The models are examined on the flow map to observe their behavior of the models. The scenarios required to explore the wake and blockage effect are the scenarios where the turbines are exposed to each other's turbulent flow and vortex. For these scenarios, the wind turbines should be in a single row. For this reason, 90° and 270° wind directions are examined on the flow map. In addition, the 0° wind direction, where the turbines capture free stream airflow, is also discussed to compare and see the blockage effect in the induction zone more clearly.

Table 2. Model Inputs for Wake, Blockage, and Coupled Models.

	Parameter	Wake Model	Blockage Model	Coupled Model
Model Inputs	Reference Wind Direction	0°,90°,270°	0°,90°,270°	0°,90°,270°
	Reference Wind Speed	10 m/s	10 m/s	10 m/s
	Wake Deficit Models	NOJ , GCL , Gaussian	-	NOJ , GCL , Gaussian
	Superposition models	LinearSum, SquaredSum(Gaussian)	LinearSum	LinearSum
	Blockage models	-	VortexCylinder, VortexDipole, SelfSimilarity, RankineHalfBody , HybridInduction	VortexCylinder, VortexDipole, SelfSimilarity, RankineHalfBody, HybridInduction

No wake interactions at 0° wind direction, as seen in Figure 19. At the 90° wind direction, the foremost turbine is WTG0, while the backmost turbine is WTG4. At the 270° wind direction, the foremost turbine is WTG4, while the backmost turbine is WTG0.

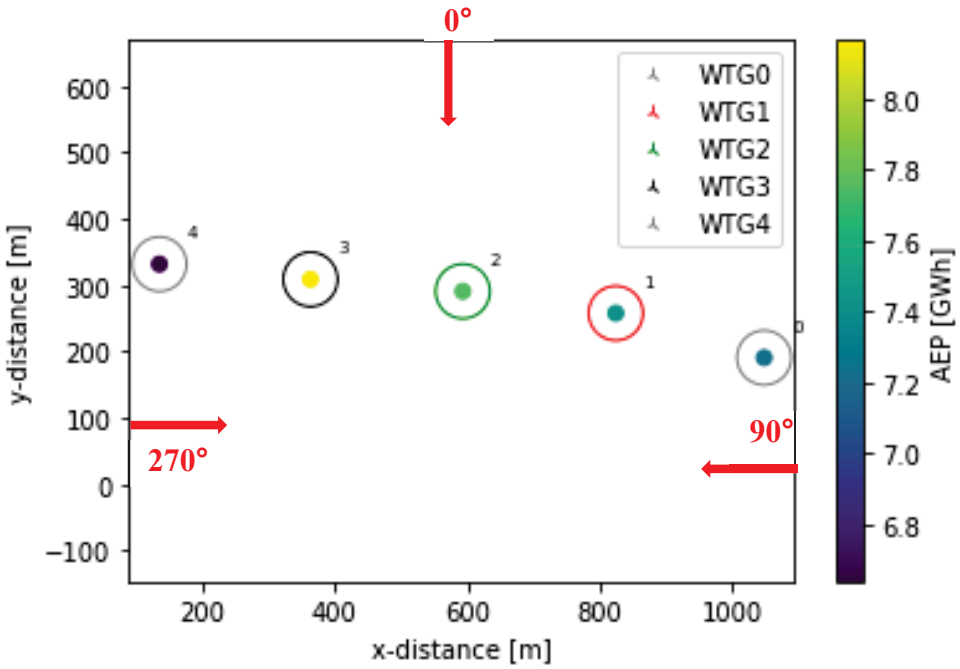

Figure 19. Wind Directions on the map.

5.6. Wake Modelling

This study examines various variations of three fundamental wake models and a total of seven wake models. These models are

- Jensen
- Jensen Local
- Turbo Jensen
- Gaussian
- Turbo Gaussian
- Larsen
- Larsen Local.

The main parameters in wake model review and comparison are wind direction, wind speed and turbulent intensity. The most effective and important parameter is wind direction. For this reason, three critical wind directions are studied at 10 m/s wind speed. All turbines encounter free stream aiflow in one of the wind directions, this direction is 0°. At the other two wind directions, the turbines are lined up in the field. Thus, it is aimed to observe the effects of the models objectively.

5.6.1. The Jensen Wake Modelling

In this part, three versions of the Jensen wake model are examined. These are Jensen, Jensen Local and Turbulence Optimized Jensen.

In Figure 20, the power data of the Jensen wake model at 0° wind direction is compared with the wind farm power curve. The fact that all five turbines in the field encounter free stream airflow in this wind direction explains the convergence of the model outputs with the wind farm power curve. Because the results belong to the wake model and there is no wake interaction in this scenario. In contrast, a deviation is observed in WTG4. While there are many possibilities why the WTG4 is different from other turbines, it is likely to be a common calibration error or maintenance issue. The validated power data, different for the five turbines, is used in all subsequent models.

Figure 21 shows the flowmap of the Jensen wake model at 0° wind direction. The turbines are not under wake effect. Wake spreading in the downstream area, a high decrease in wind speed is observed in the near wake area. In this model, the wake area is defined by sharp demarcation lines. It spreads in a narrow lateral area, but the low wind speed persists over a long distance.

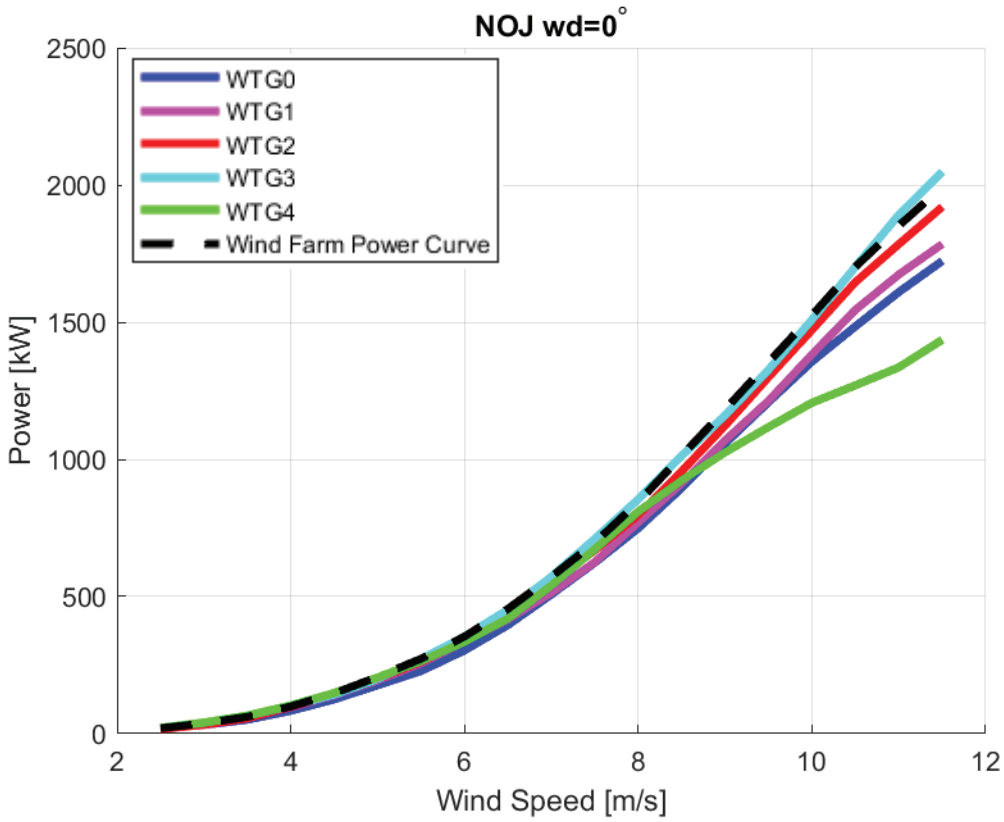

Figure 20. Power Curve of Jensen Wake Model at 0° wind direction.

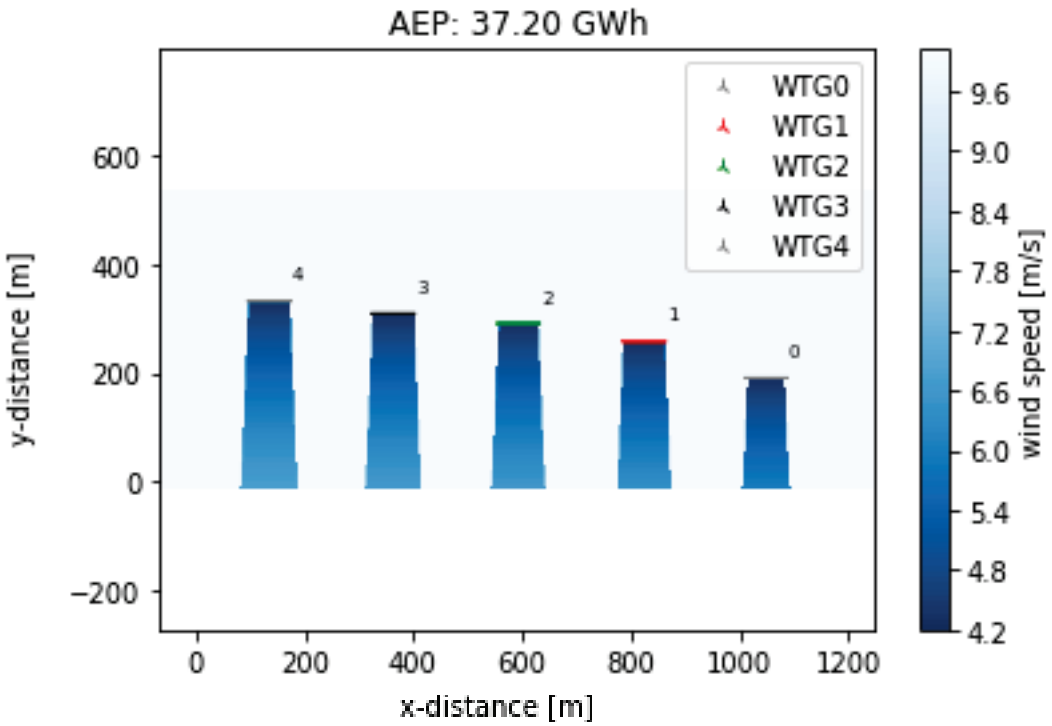

Figure 21. Flow map of Jensen Wake Model at 0° wind direction.

Since the wind direction is 90° in Figure 22, the wind farm power curve is validated with the turbine (WTG0) at the front at 90°. As seen in the figure, validated wind farm power curve at 0deg converges with WTG0. The power values of the other turbines decrease in the order of succession. This explains the wake effect.

In the flowmap seen in Figure 23, especially in the wake area of WTG3 and WTG4, the wind speed is very low.

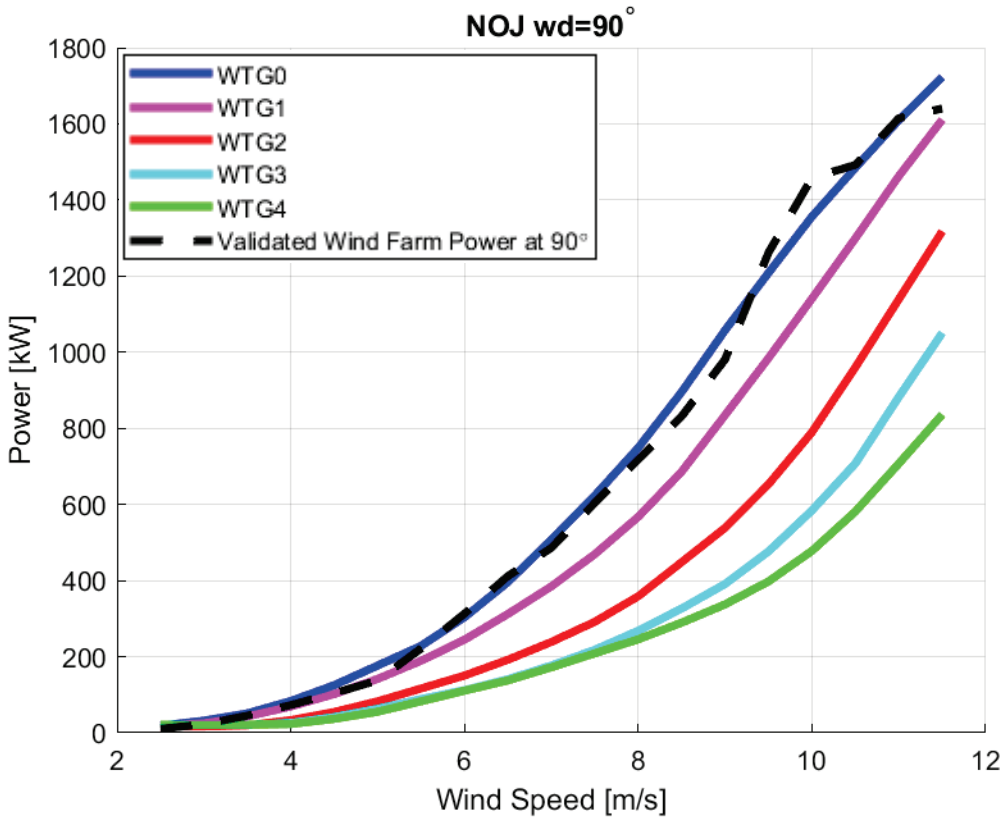

Figure 22. Power Curve of Jensen Wake Model at 90° wind direction.

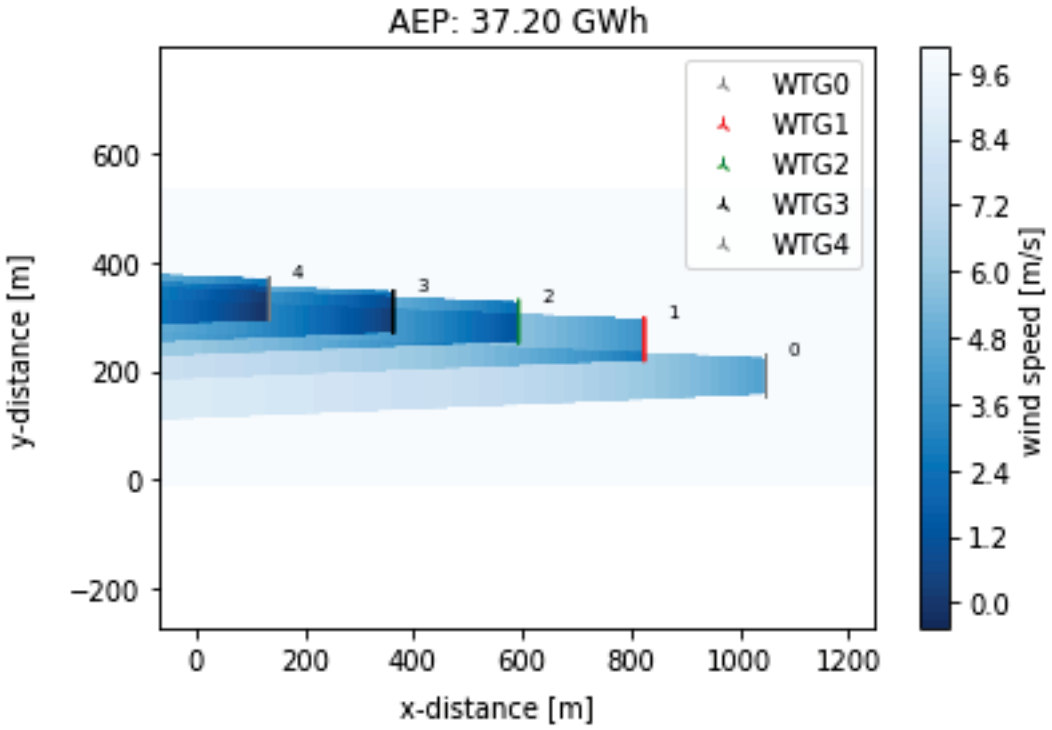

Figure 23. Flow map of Jensen Wake Model at 90° wind direction.

In Figure 24, WTG4 is the foremost turbine. The special case of WTG4 due to calibration error or maintenance issue prevents convergence with validated wind farm power at 270°. However, considering the wake effect, the power data of the other turbines are as they should be.

As seen in Figure 25, although WTG0 is the rearmost turbine, it is partially waked at the 270° wind direction due to its location. For this reason, their power values are higher than other turbines.

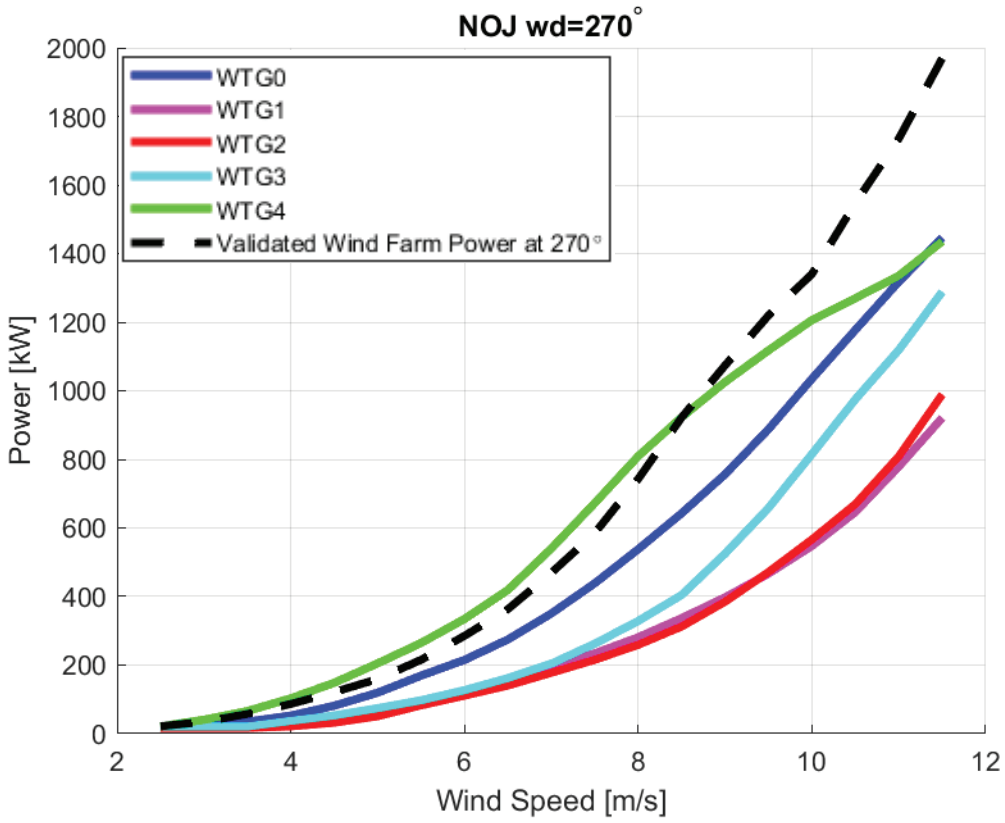

Figure 24. Power Curve of Jensen Wake Model at 270° wind direction.

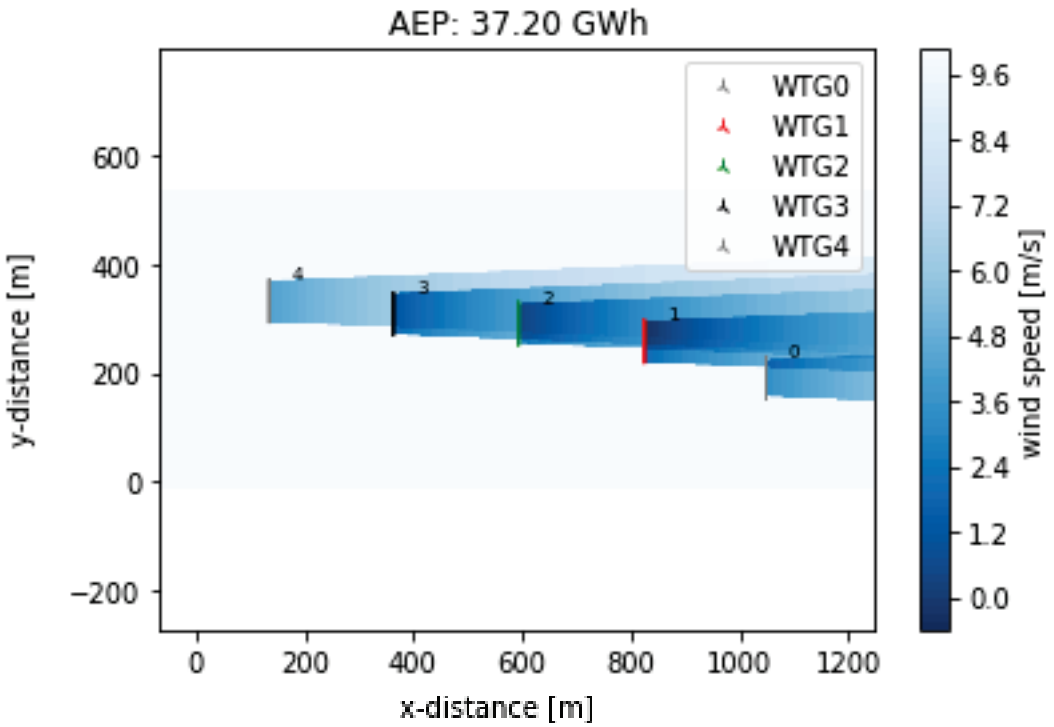

Figure 25. Flow map of Jensen Wake Model at 270° wind direction.

Although Jensen Local results for three different wind directions are similar to Jensen model results, Jensen Local wake spread is wider in the lateral area compared to Jensen as seen in Figure 29-31-33. wake field lines are less clear compared to Jensen. As the distance increases, the decrease in wind speed decreases, but spreads over a larger lateral area

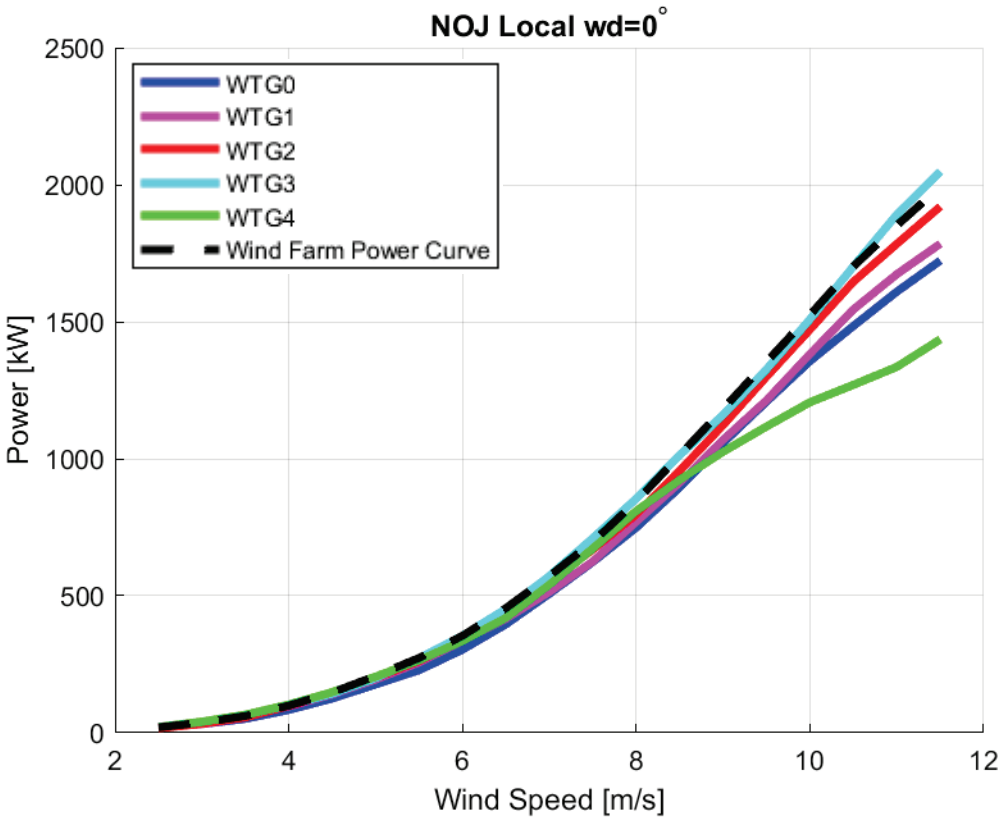

Figure 26. Power Curve of Jensen Local Wake Model at 0° wind direction.

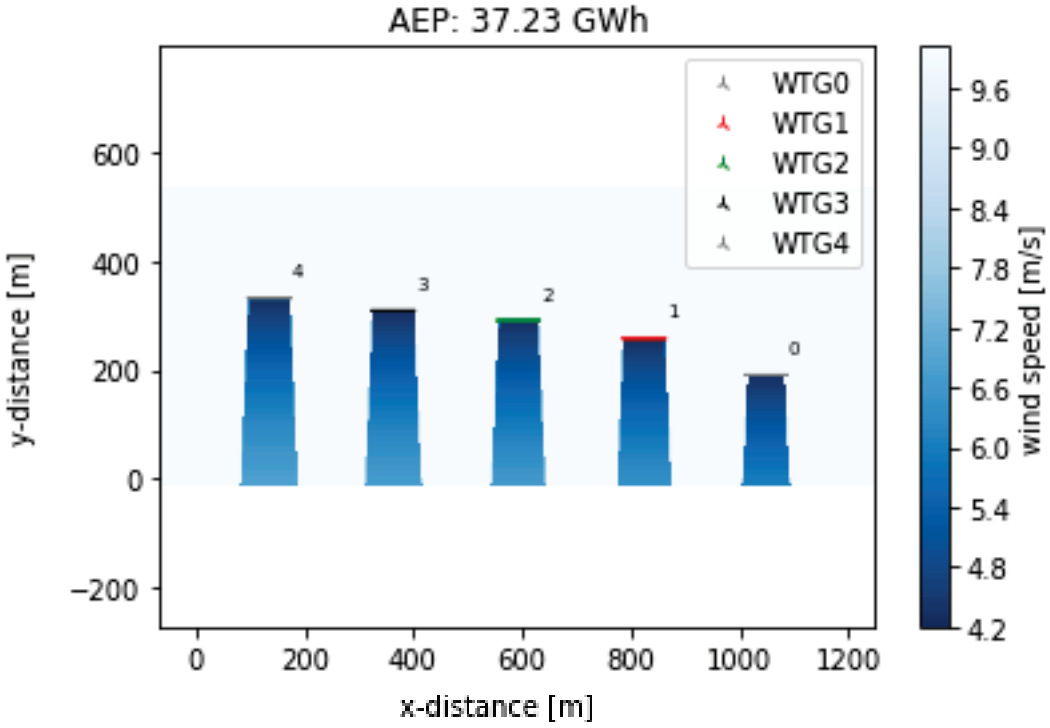

Figure 27. Flow map of Jensen Local Wake Model at 0° wind direction.

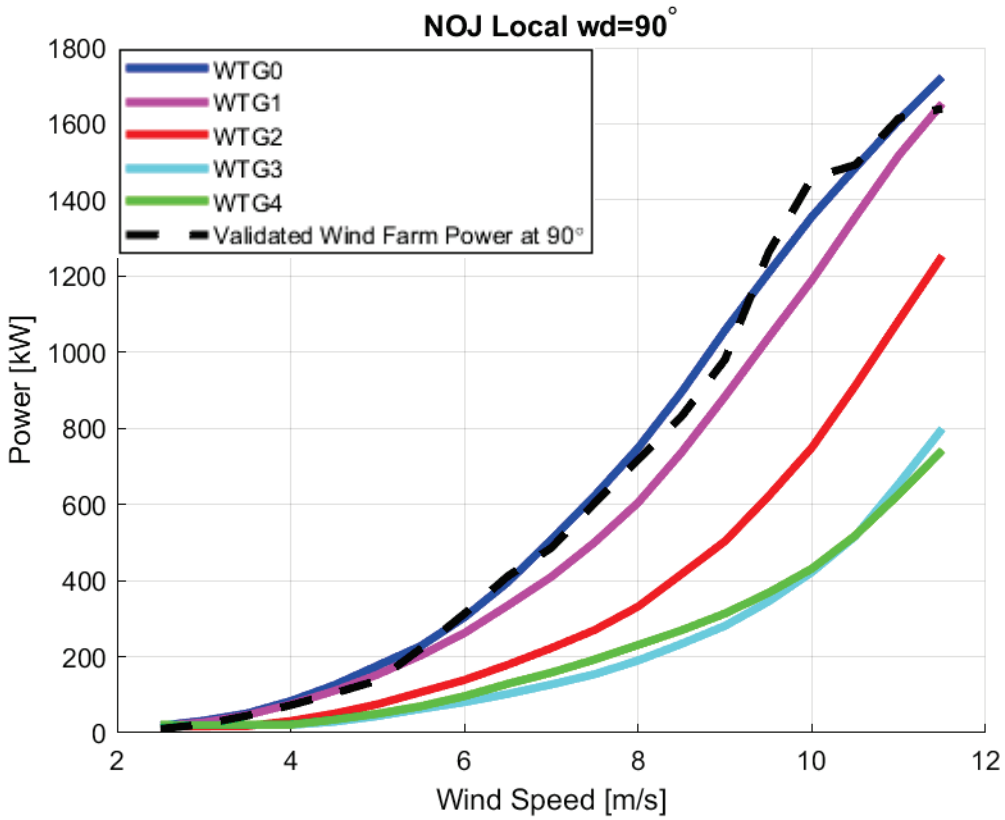

Figure 28. Power Curve of Jensen Local Wake Model at 90° wind direction.

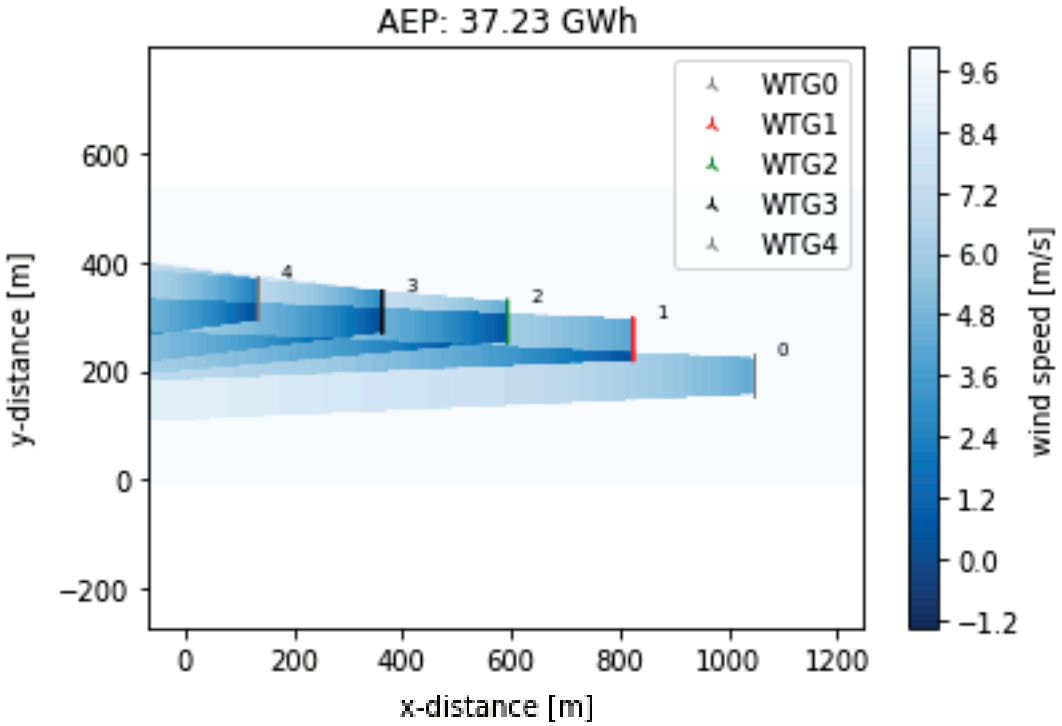

Figure 29. Flow map of Jensen Local Wake Model at 90° wind direction.

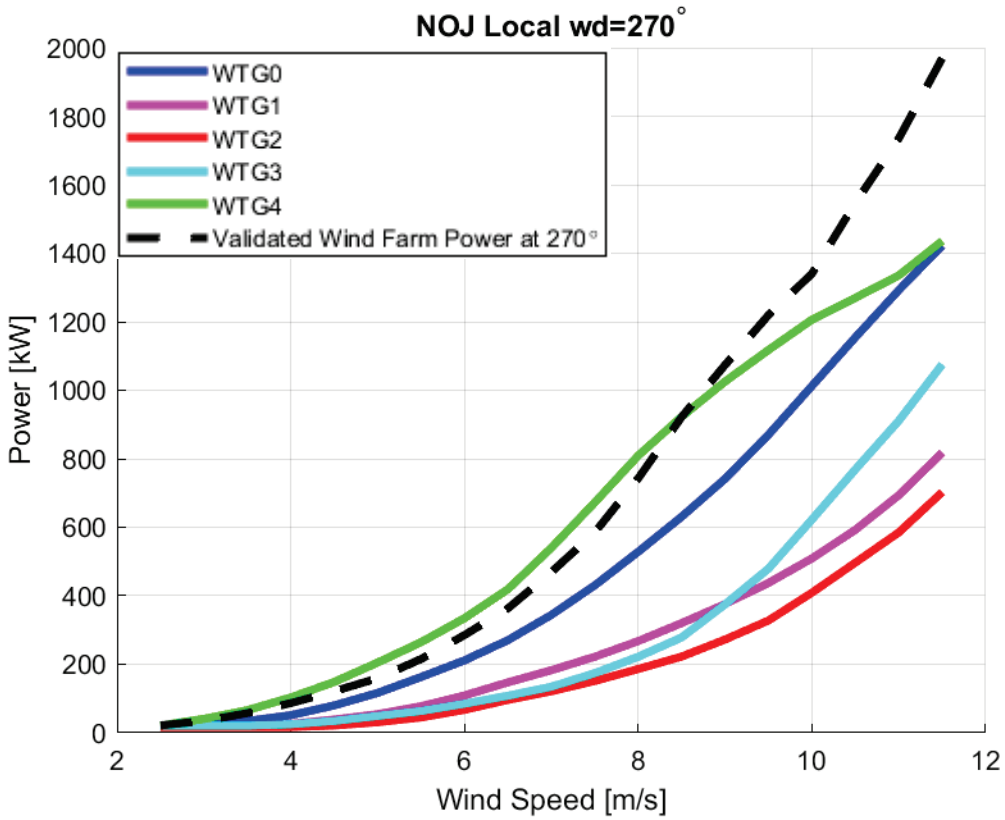

Figure 30. Power Curve of Jensen Local Wake Model at 270° wind direction.

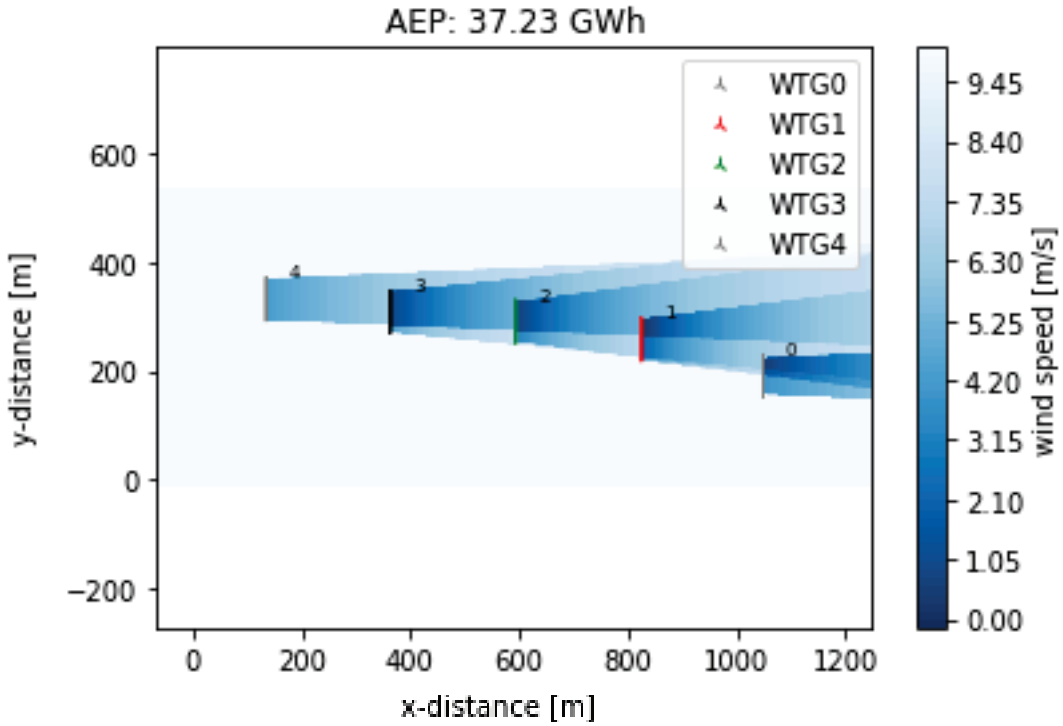

Figure 31. Flow map of Jensen Local Wake Model at 270° wind direction.

Turbulence optimized Jensen model results are as in Figure 32-34-36. In addition to the expected results, the problem with WTG4 is also observed in this model.

The change in wake characteristic is clearly seen in the flowmaps in Figure 33-35-37. The area where the wake spreads is more convex, the wind speed is higher in the far area and the spreading boundaries are less clear.

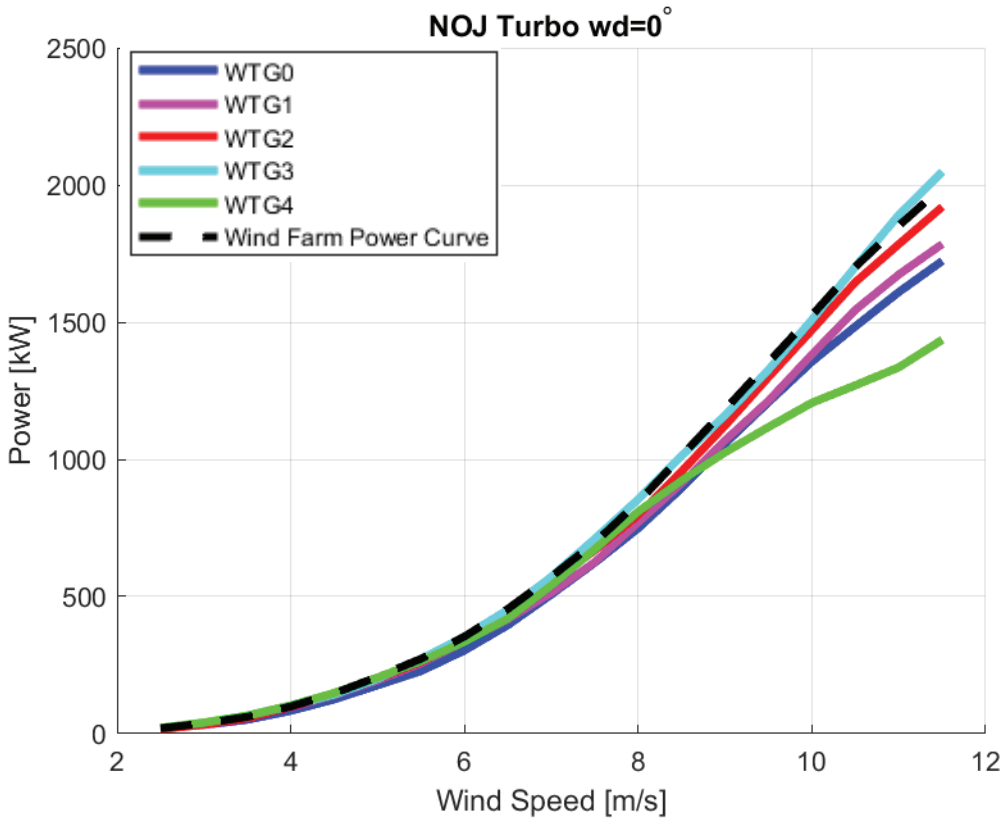

Figure 32. Power Curve of Turbo Jensen Wake Model at 0° wind direction.

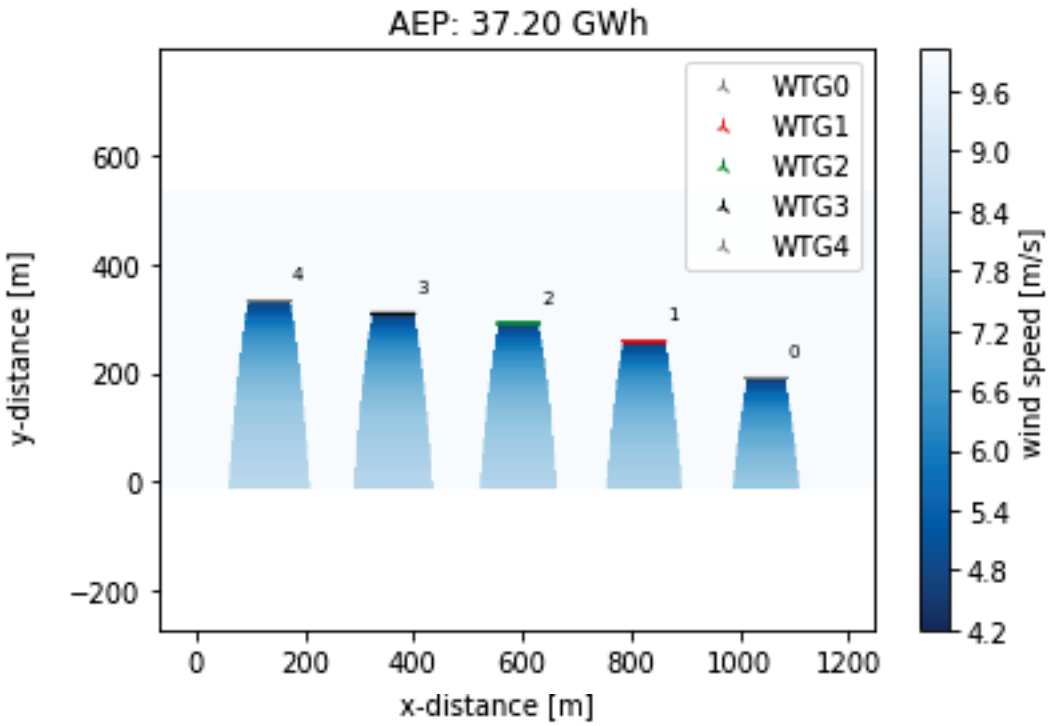

Figure 33. Flow map of Turbo Jensen Wake Model at 0° wind direction.

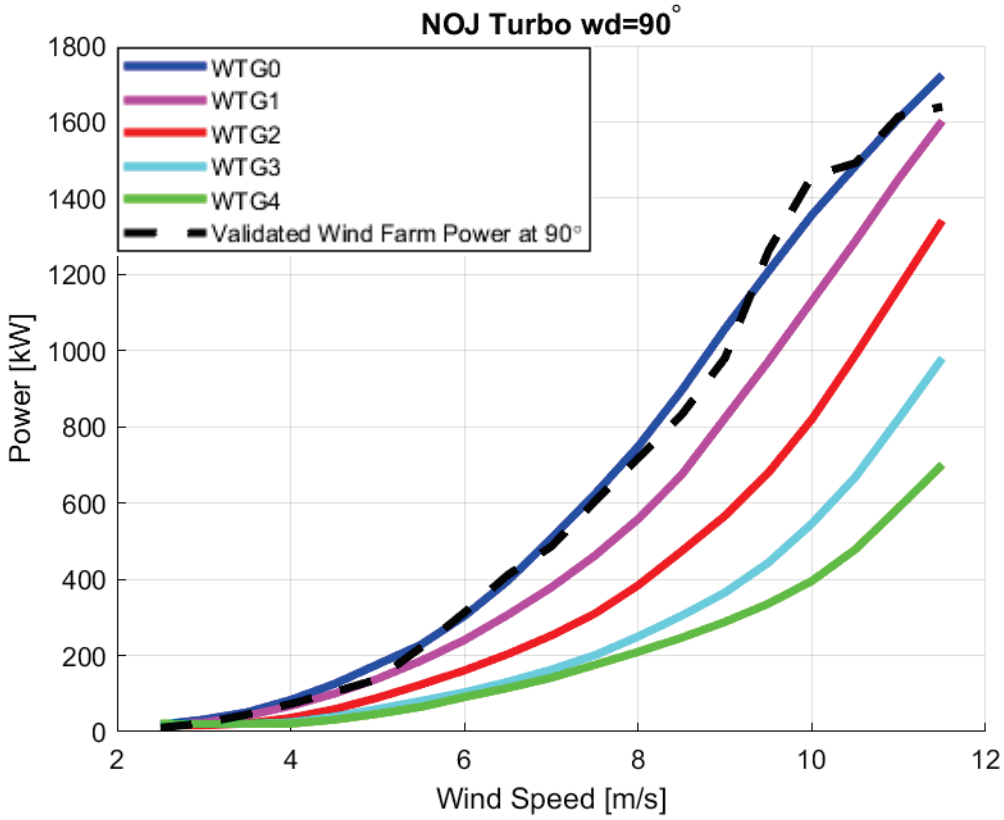

Figure 34. Power Curve of Turbo Jensen Wake Model at 90° wind direction.

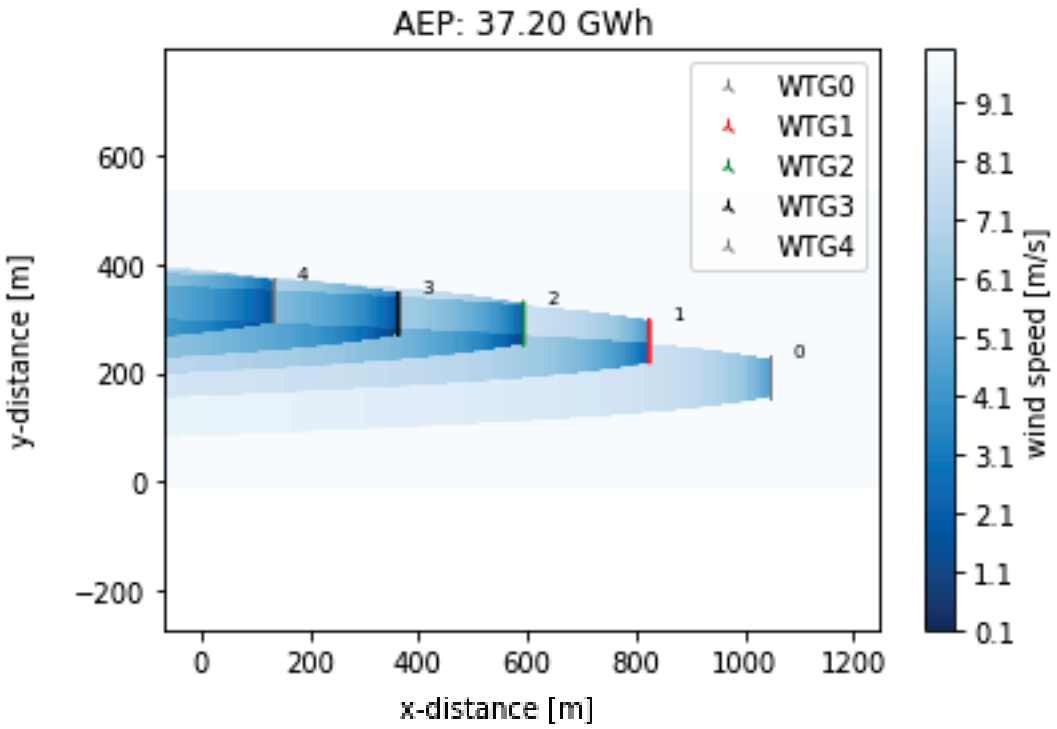

Figure 35. Flow map of Turbo Jensen Wake Model at 90° wind direction.

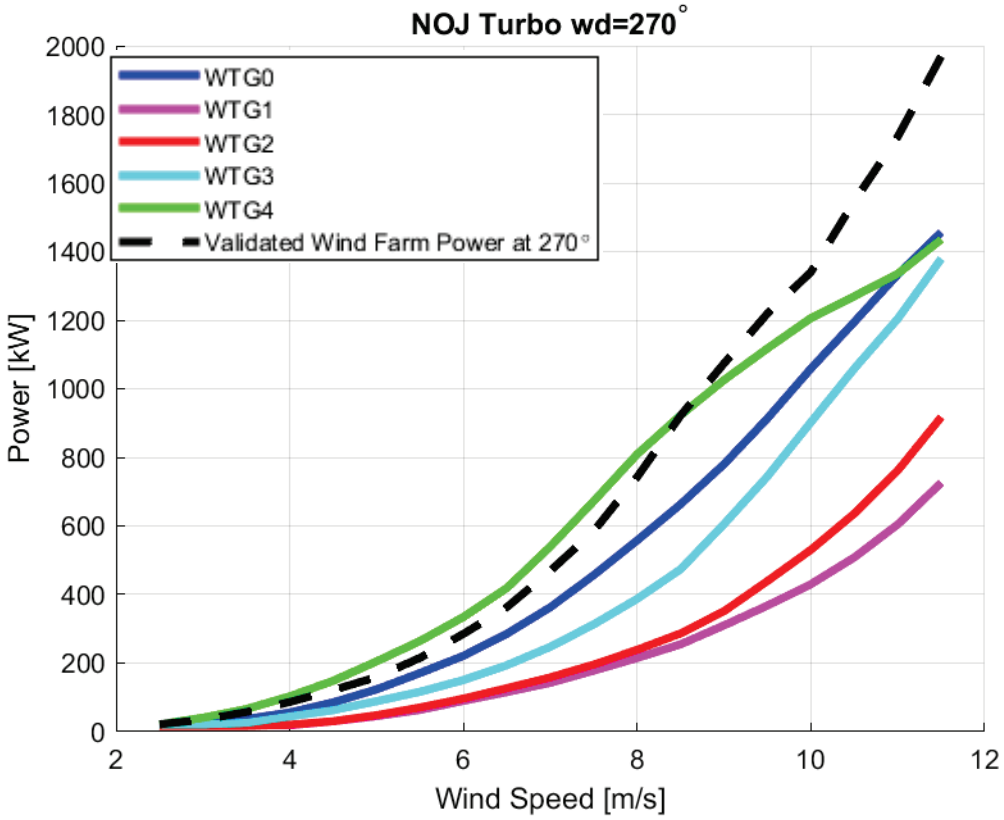

Figure 36. Power Curve of Turbo Jensen Wake Model at 270° wind direction.

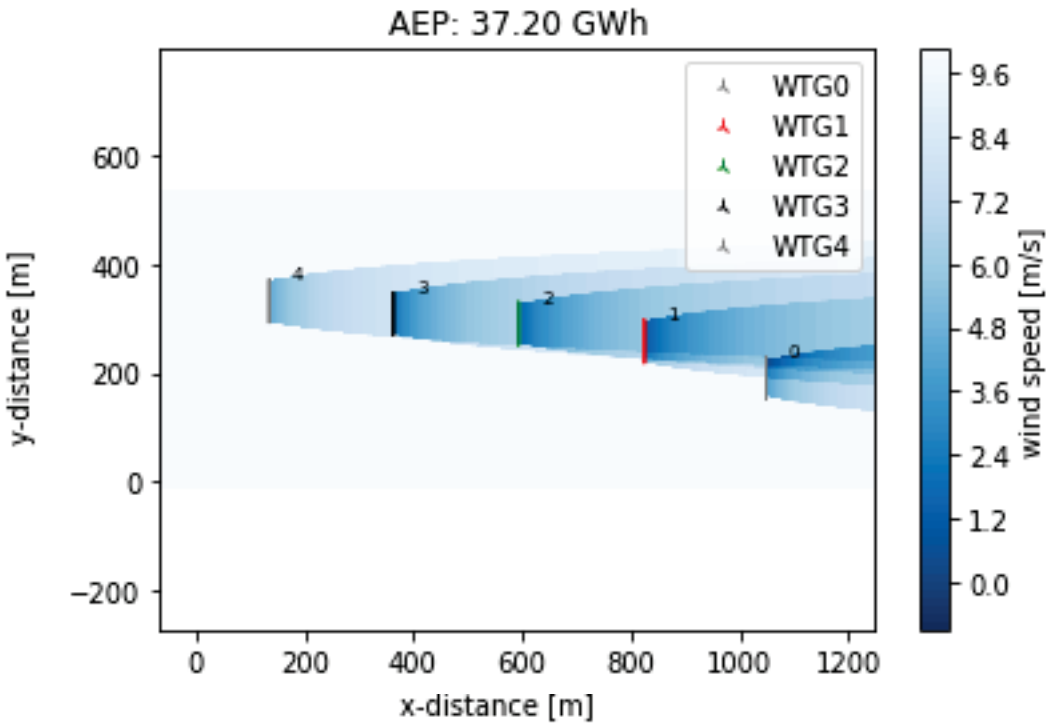

Figure 37. Flow map of Turbo Jensen Wake Model at 270° wind direction.

5.6.2. The Larsen Wake Modelling

In this study, two versions of the Larsen wake model are examined. These are Larsen and Larsen Local. Although the difference between the Jensen wake model and the further developed versions of Jensen is clearly visible, the wake characteristic of those models is similar. The fact that the field is not complex is the reason why the difference between the power results of the wake models is small. So, inferences about power results in Jensen models are valid here as well. While analyzing Larsen and Larsen Local wake models in this section, the difference between Larsen and Jensen models can be clearly observed. Although the power data is quite similar to other models, the wake's propagation strategy in the flowmap in Figure 39-41-43 is quite different from Jensen models. In a straight line just behind the turbines, the wind speed is very low. However, the wind speed drop in the lateral area is negligible. The limits of spread are almost indeterminate. The waked area, which continues along a straight and thin line behind the turbine, is the general feature of Larsen wake models. In the Larsen local model, the lateral span increases, but the span area boundary lines are still nearly invisible.

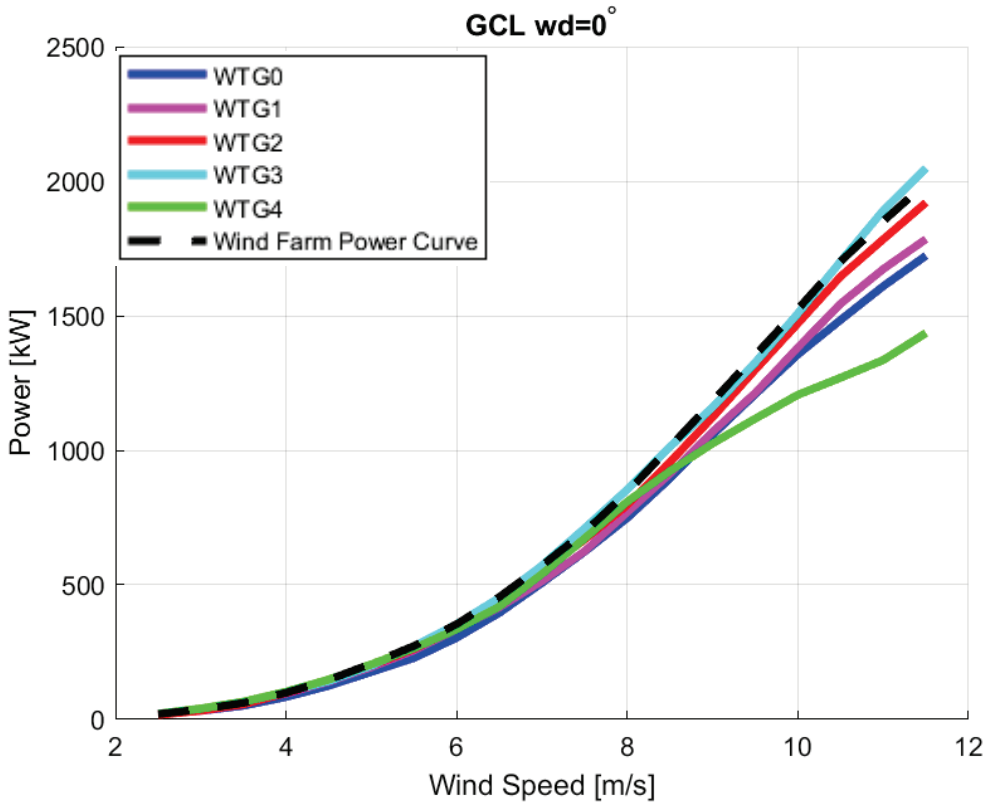

Figure 38. Power Curve of Larsen Wake Model at 0° wind direction.

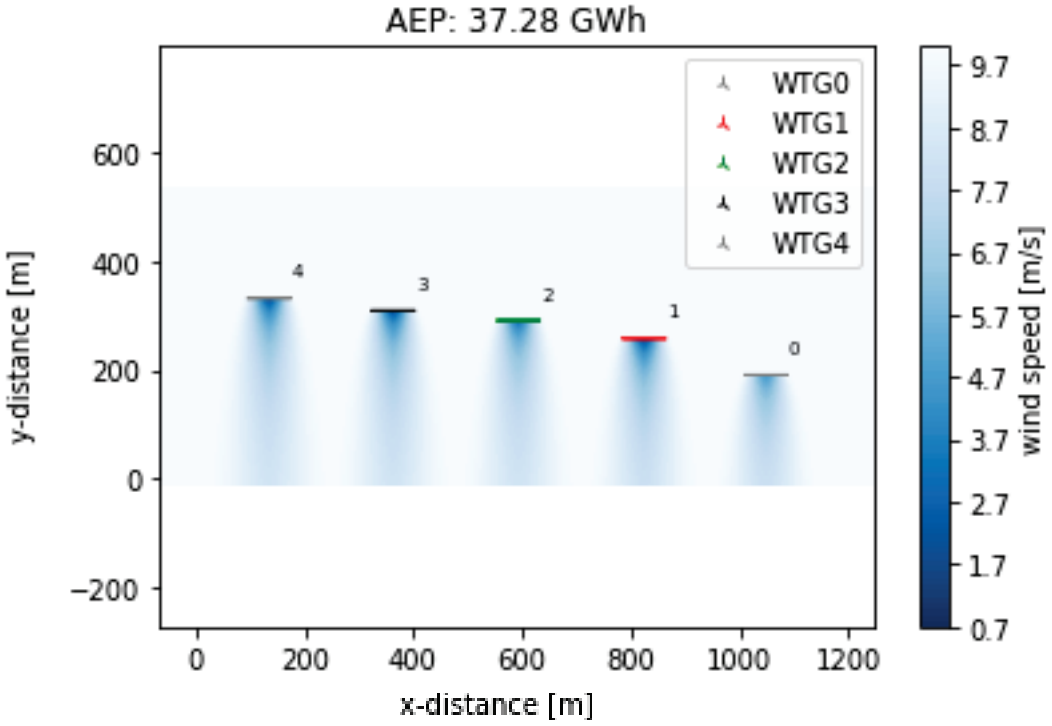

Figure 39. Flow map of Larsen Wake Model at 0° wind direction.

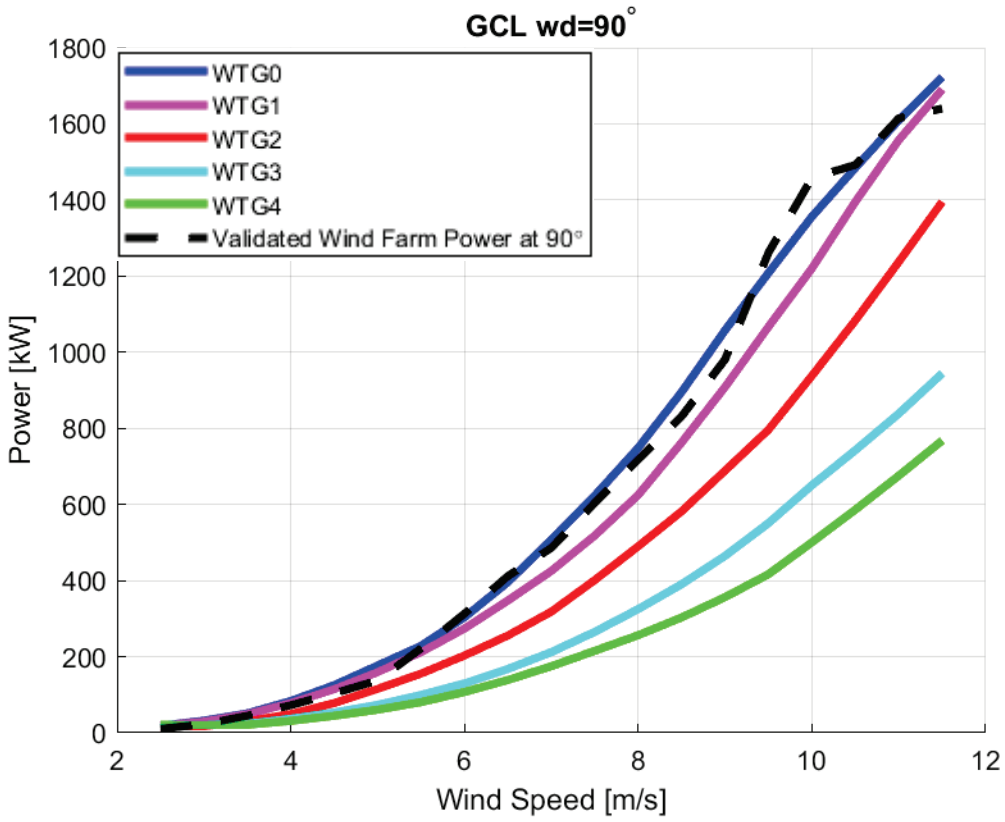

Figure 40. Power Curve of Larsen Wake Model at 90° wind direction.

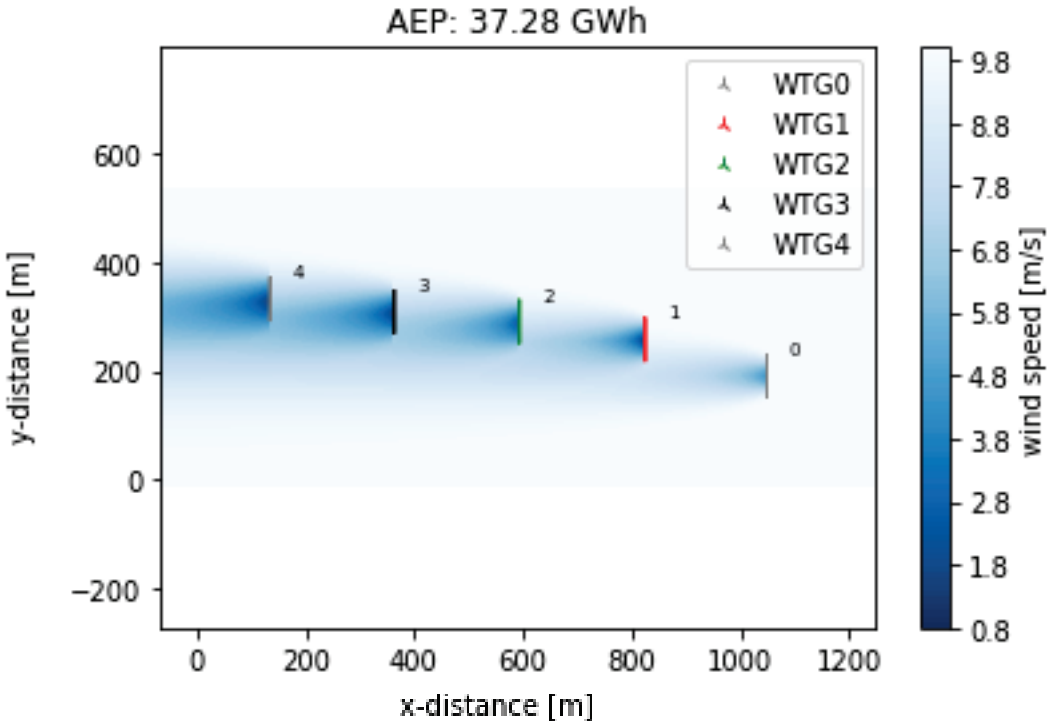

Figure 41. Flow map of Larsen Wake Model at 90° wind direction.

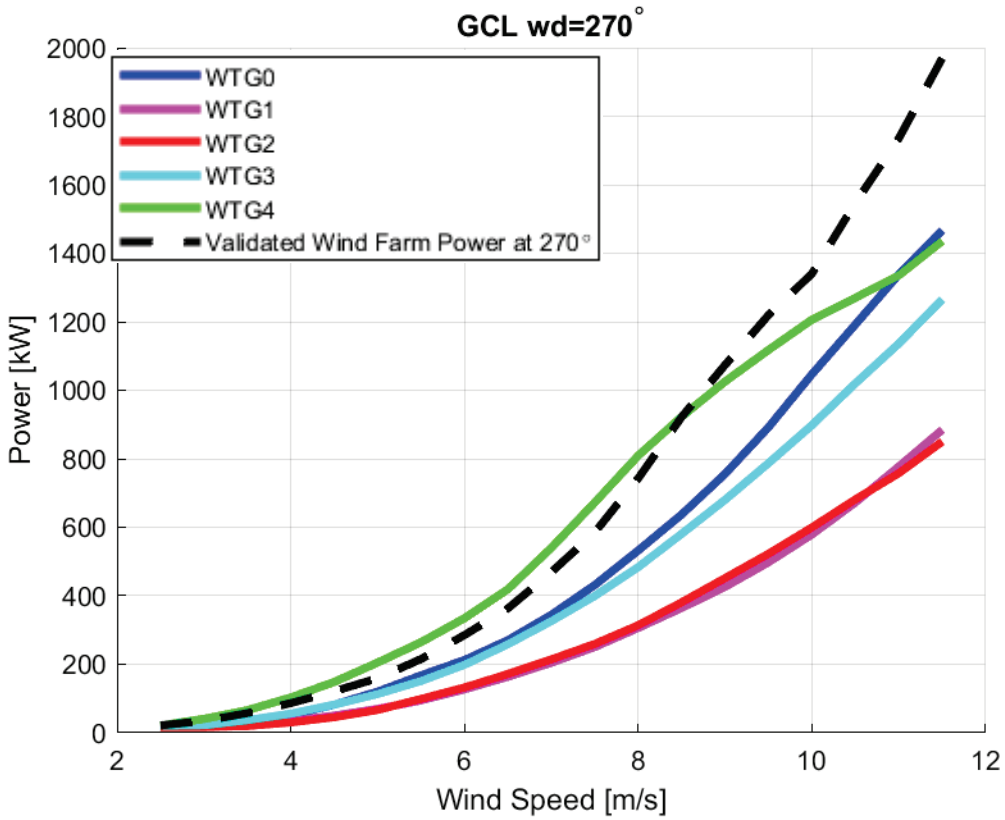

Figure 42. Power Curve of Larsen Wake Model at 270° wind direction.

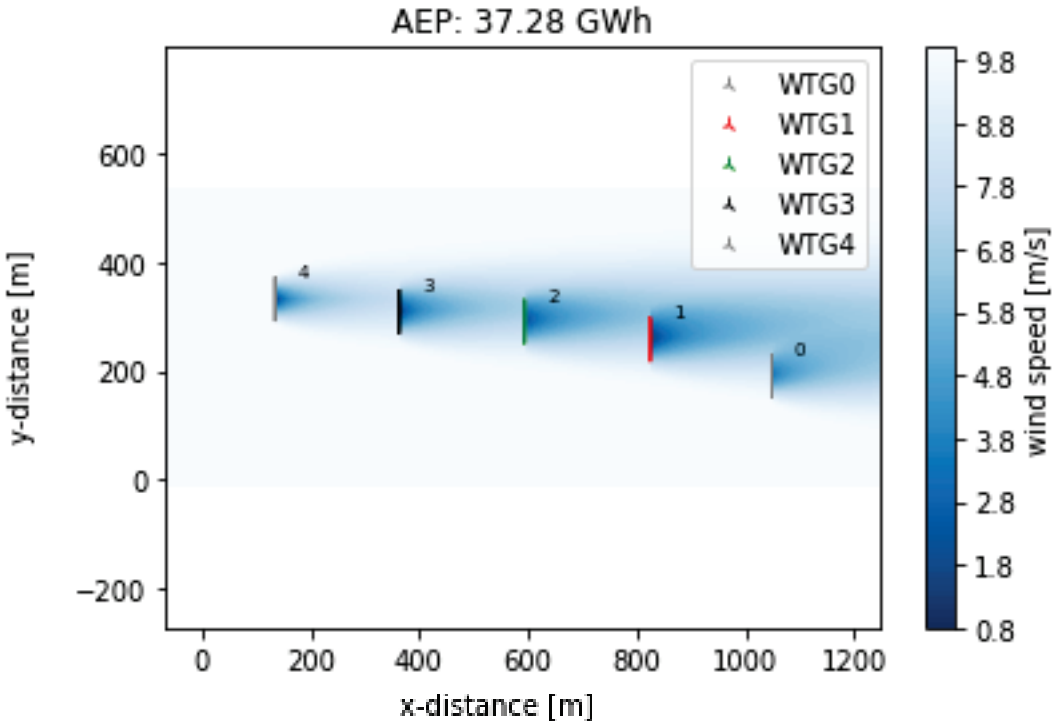

Figure 43. Flow map of Larsen Wake Model at 270° wind direction.

As seen in Figure 44-46-48, turbine results in Larsen Local model are close to each other compared to other models. This situation can be explained by the high wind speed in the flowmap in Figure 45-47-49.

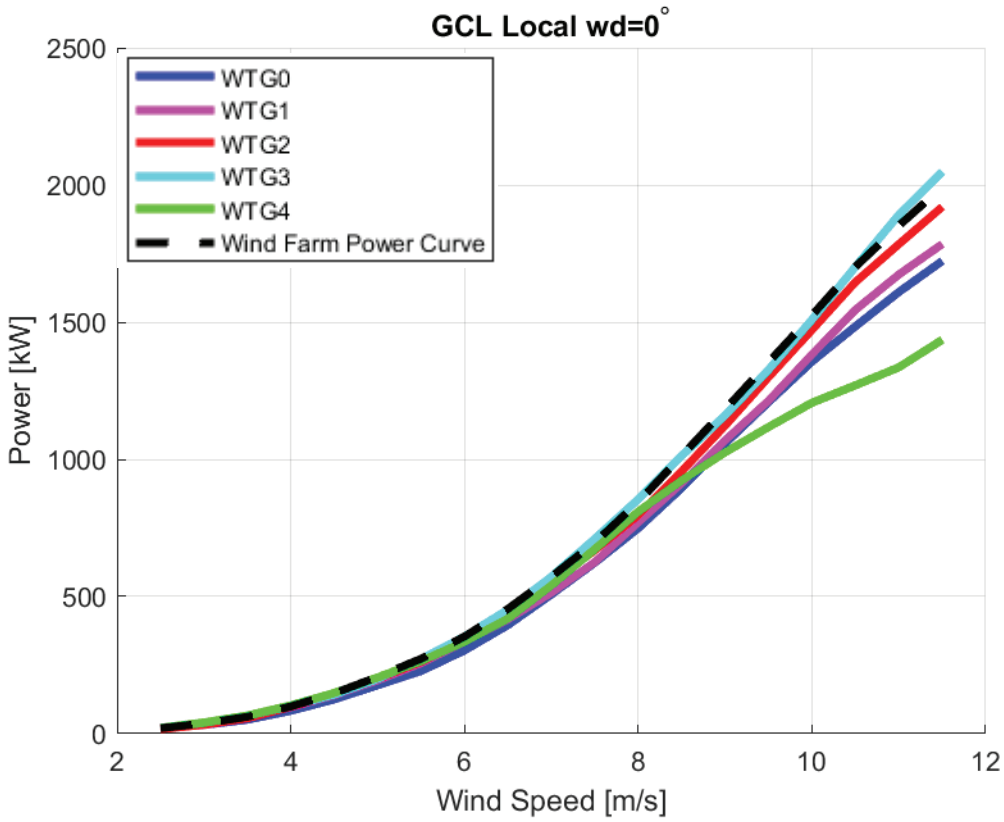

Figure 44. Power Curve of Larsen Local Wake Model at 0° wind direction.

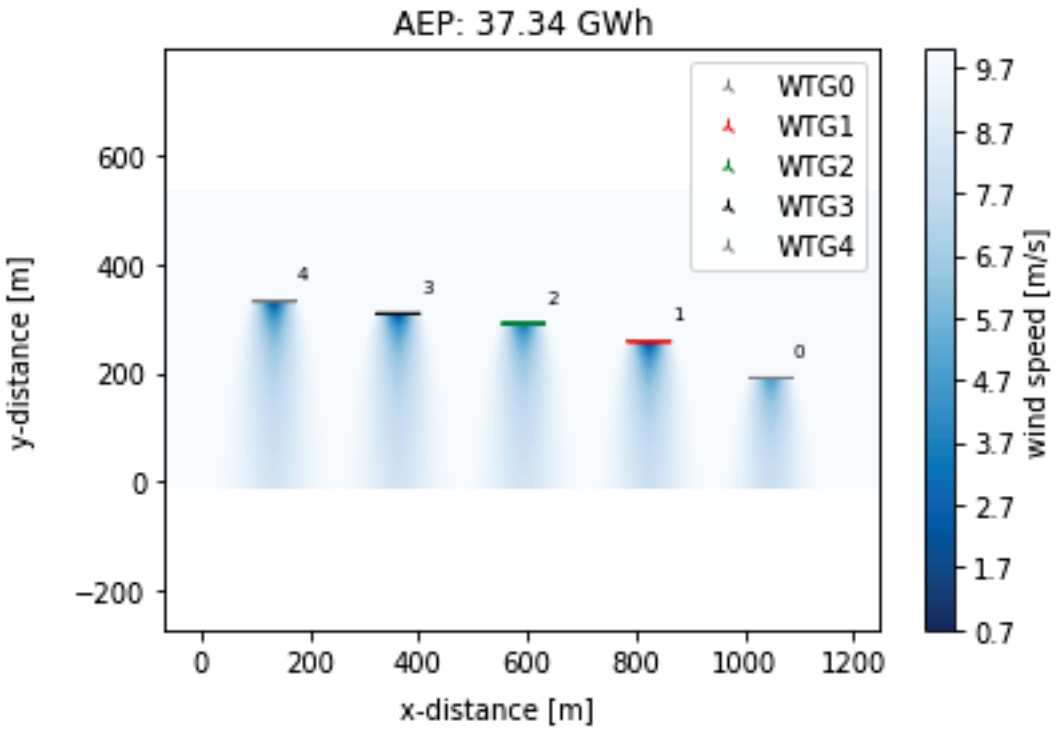

Figure 45. Flow map of Larsen Local Wake Model at 0° wind direction.

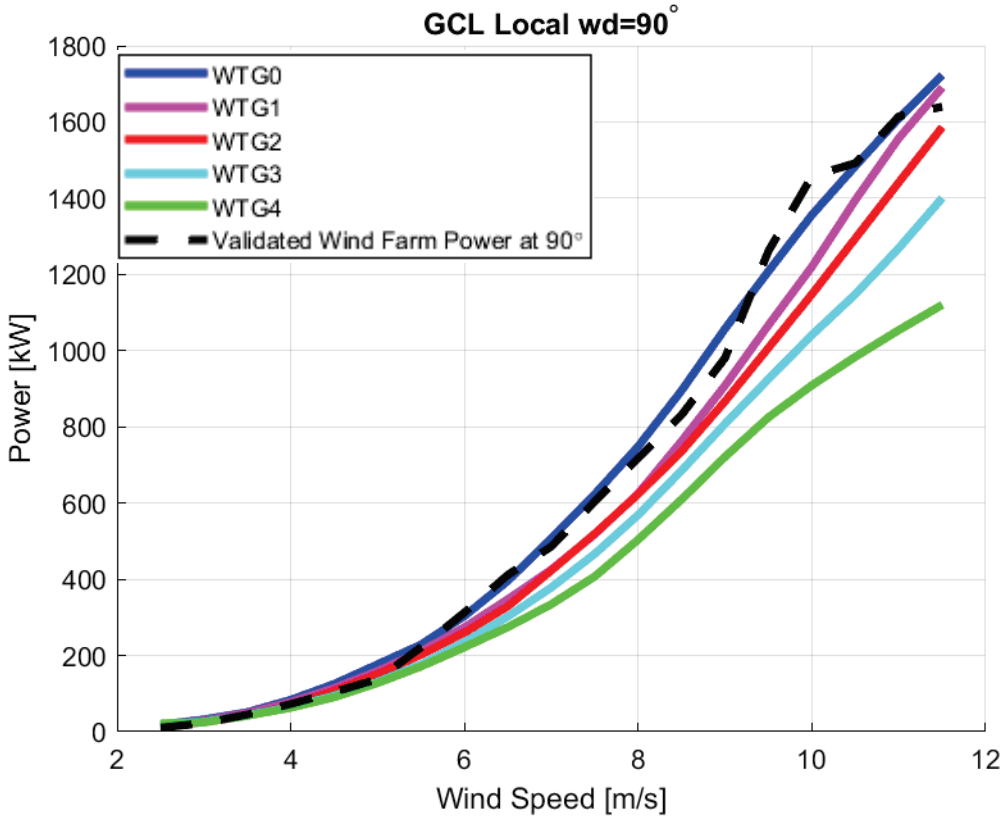

Figure 46. Power Curve of Larsen Local Wake Model at 90° wind direction.

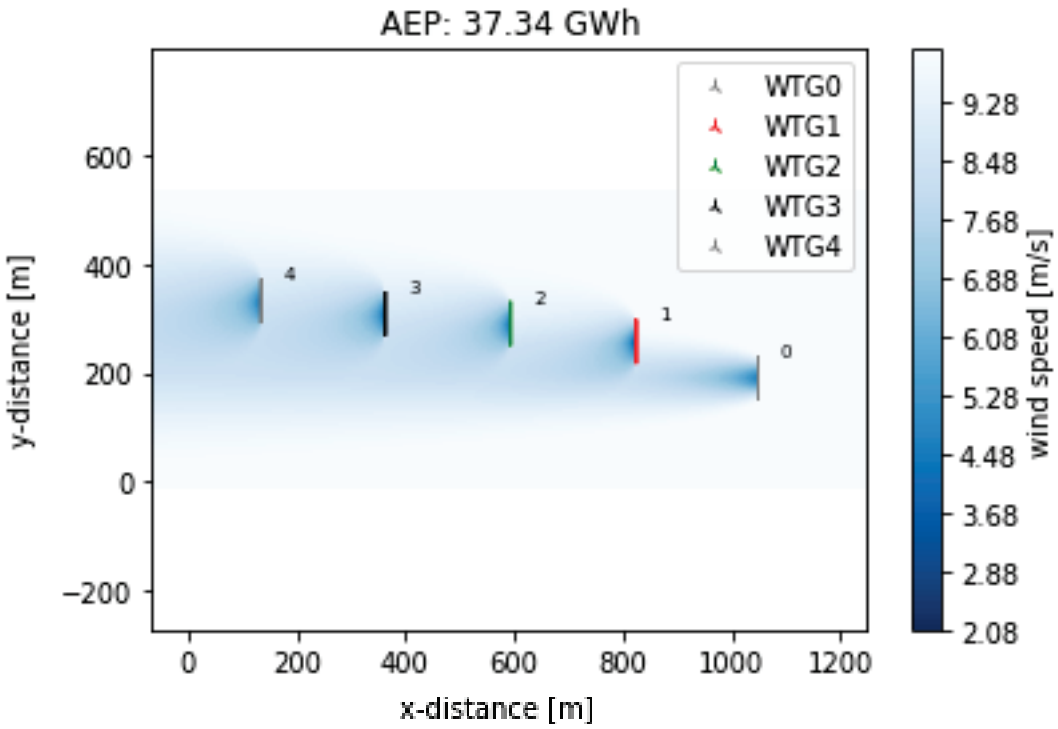

Figure 47. Flow map of Larsen Local Wake Model at 90° wind direction.

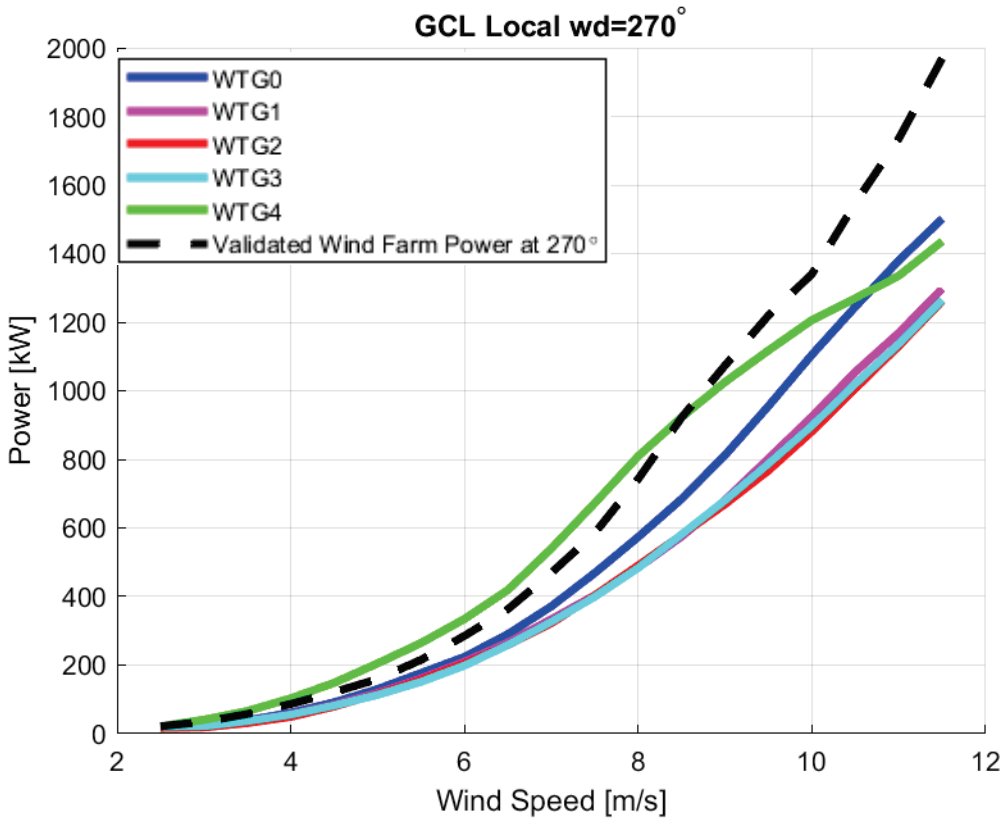

Figure 48. Power Curve of Larsen Local Wake Model at 270° wind direction.

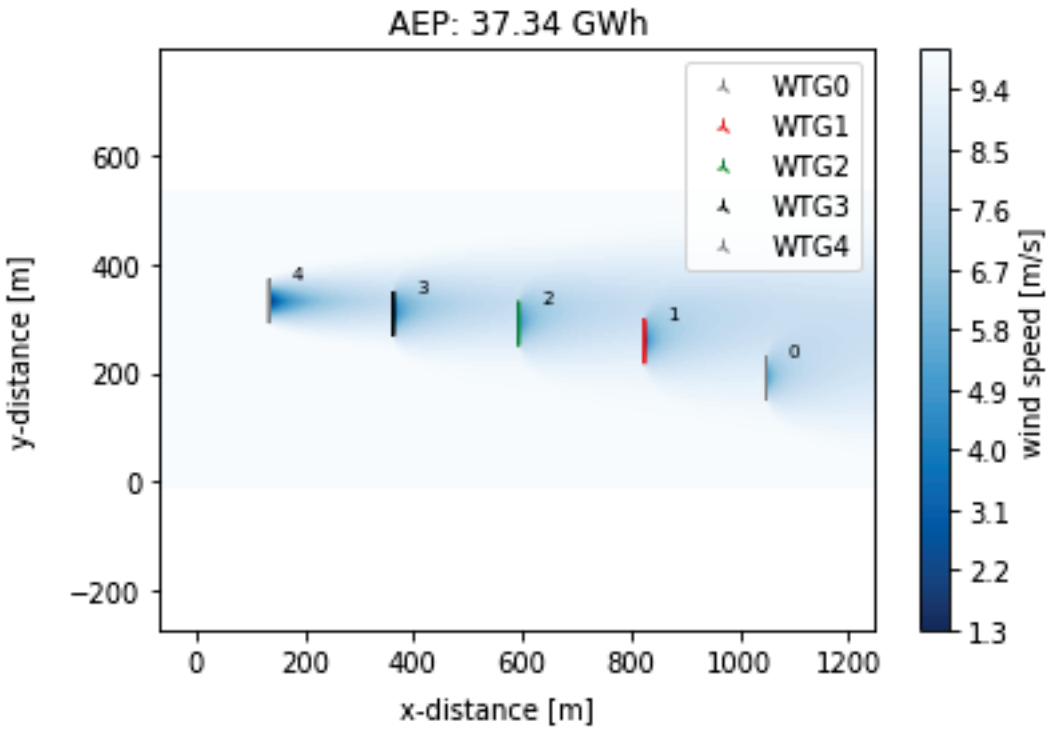

Figure 49. Flow map of Larsen Local Wake Model at 270° wind direction.

5.6.3. The Gaussian Wake Modelling

In this part, two versions of the Gaussian wake model are examined. These are Gaussian and Turbulence Optimized Gaussian.

Gaussian models are models that have different results on turbine basis compared to other models. Different behavior of WTG4 is also observed in these models, there are also minor differences between other turbines in 0° wind direction. With this feature, Gaussian models are different from other wake models. The straight-line wake behind the turbine, observed in Larsen models, appears larger and wider in Gaussian model. The straight-line wake behind the turbine, observed in Larsen models, appears larger and wider in Gaussian models.

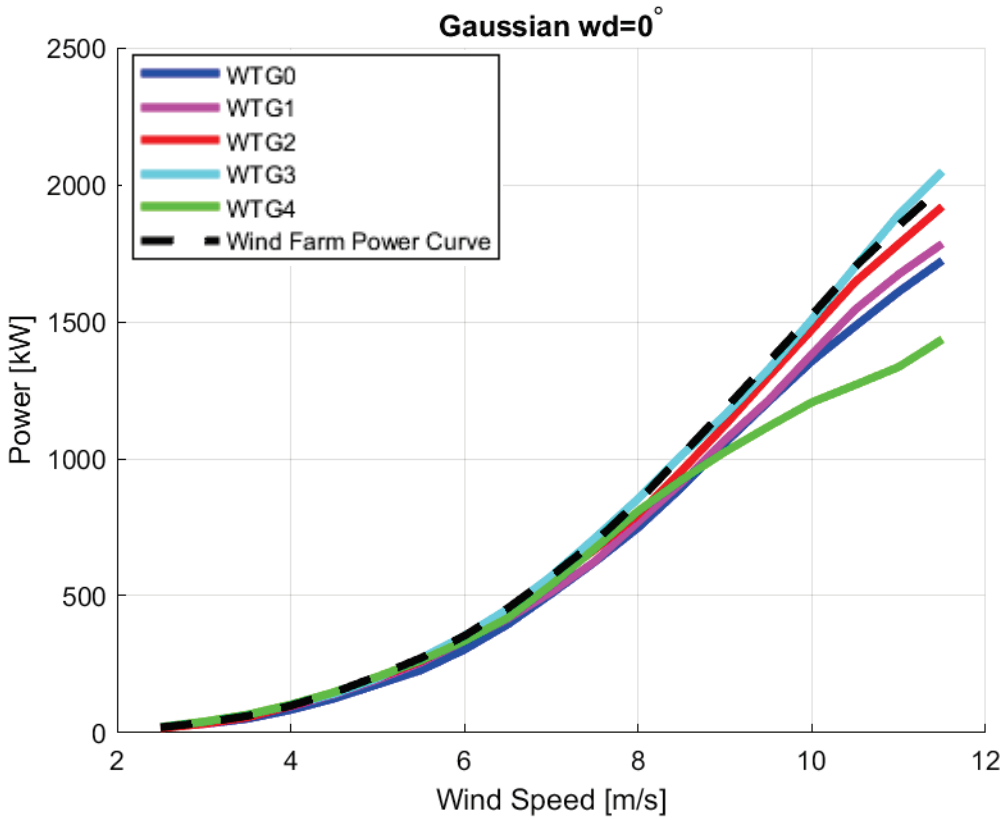

Figure 50. Power Curve of Gaussian Wake Model at 0° wind direction.

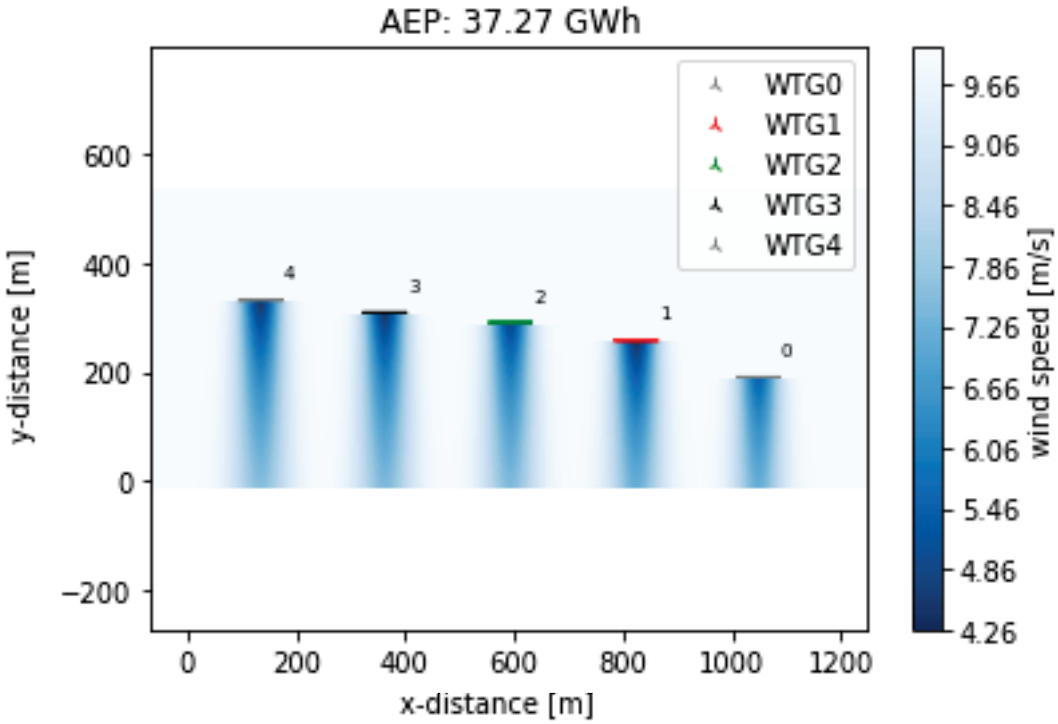

Figure 51. Flow map of Gaussian Wake Model at 0° wind direction.

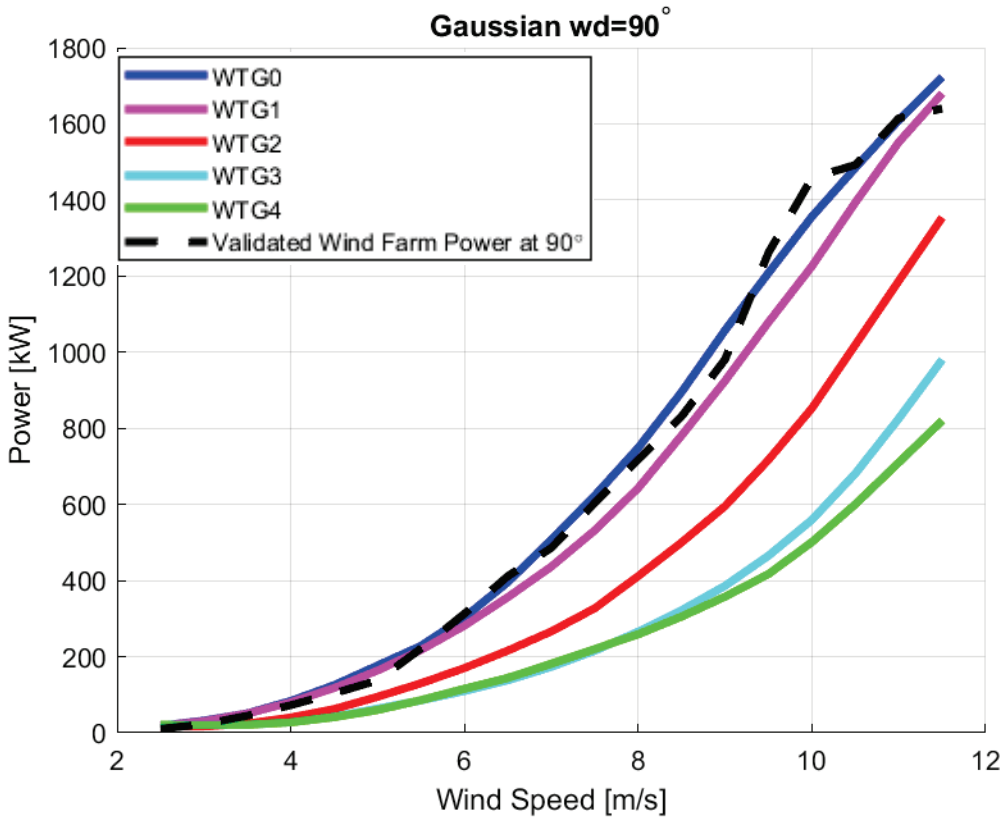

Figure 52. Power Curve of Gaussian Wake Model at 90° wind direction.

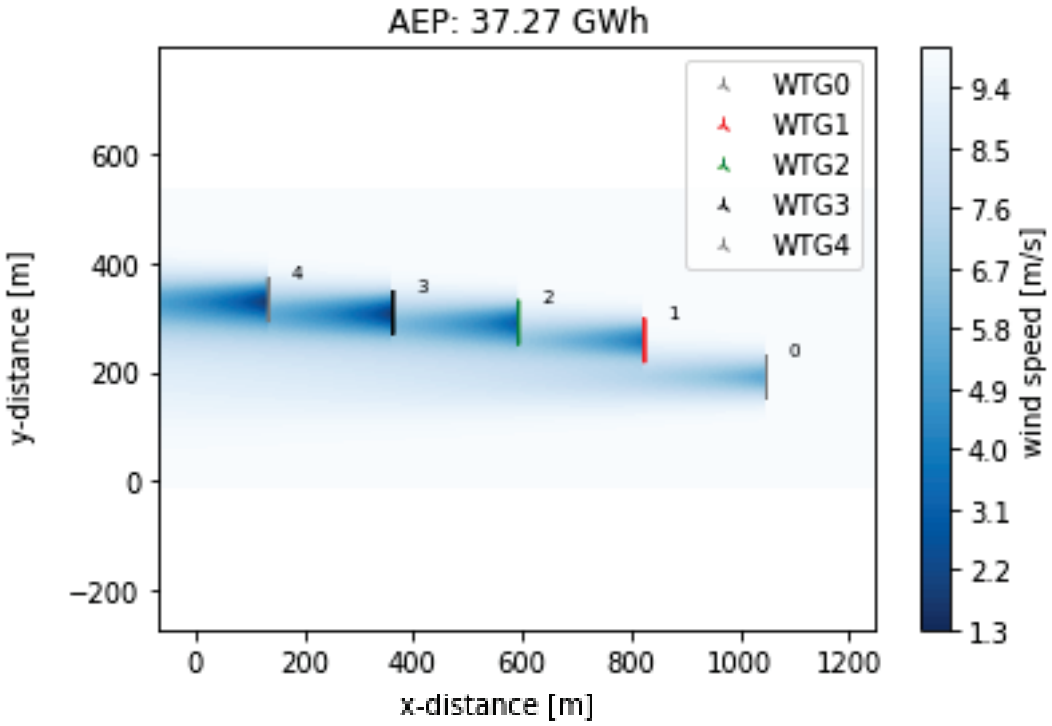

Figure 53. Flow map of Gaussian Wake Model at 90° wind direction.

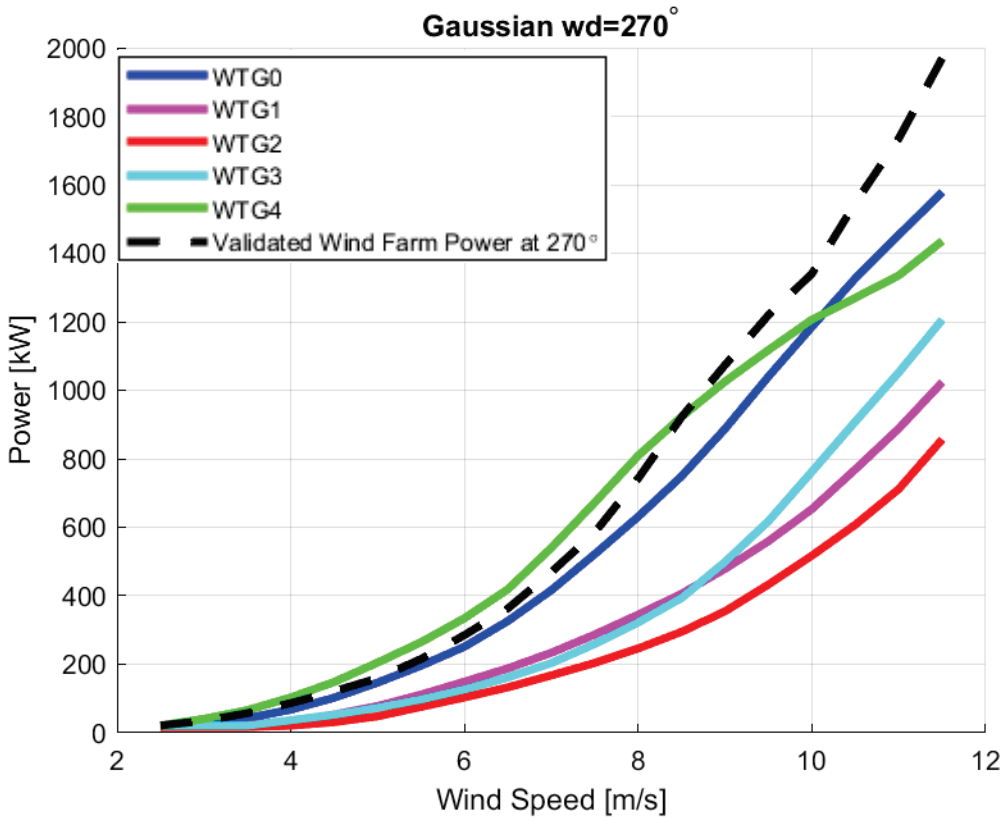

Figure 54. Power Curve of Gaussian Wake Model at 270° wind direction.

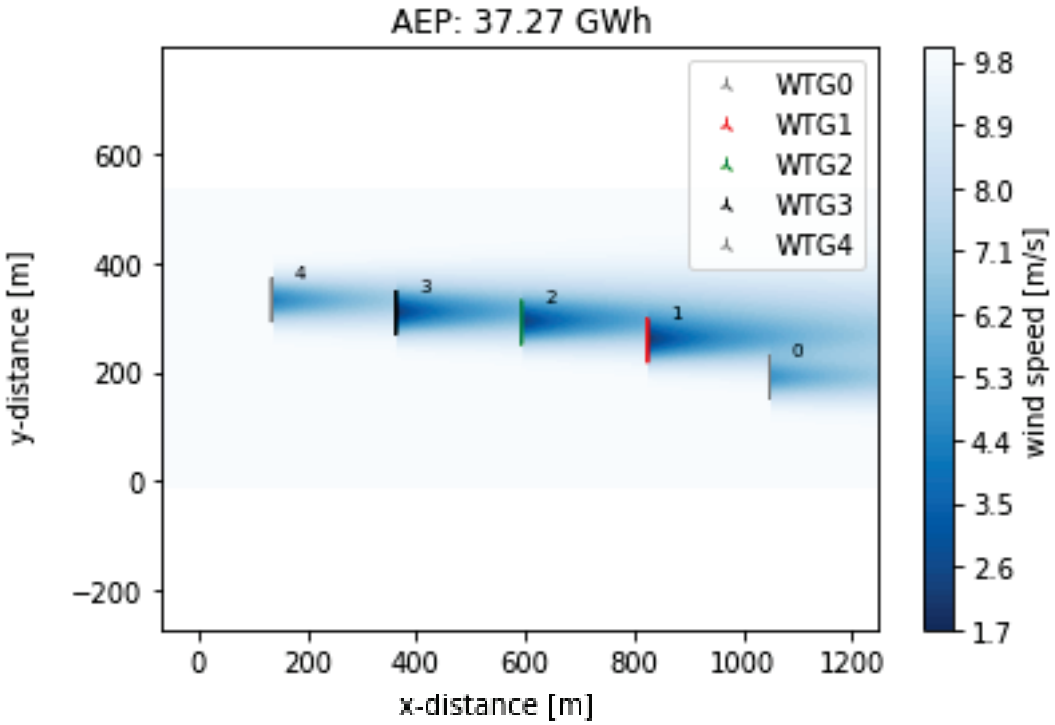

Figure 55. Flow map of Gaussian Wake Model at 270° wind direction.

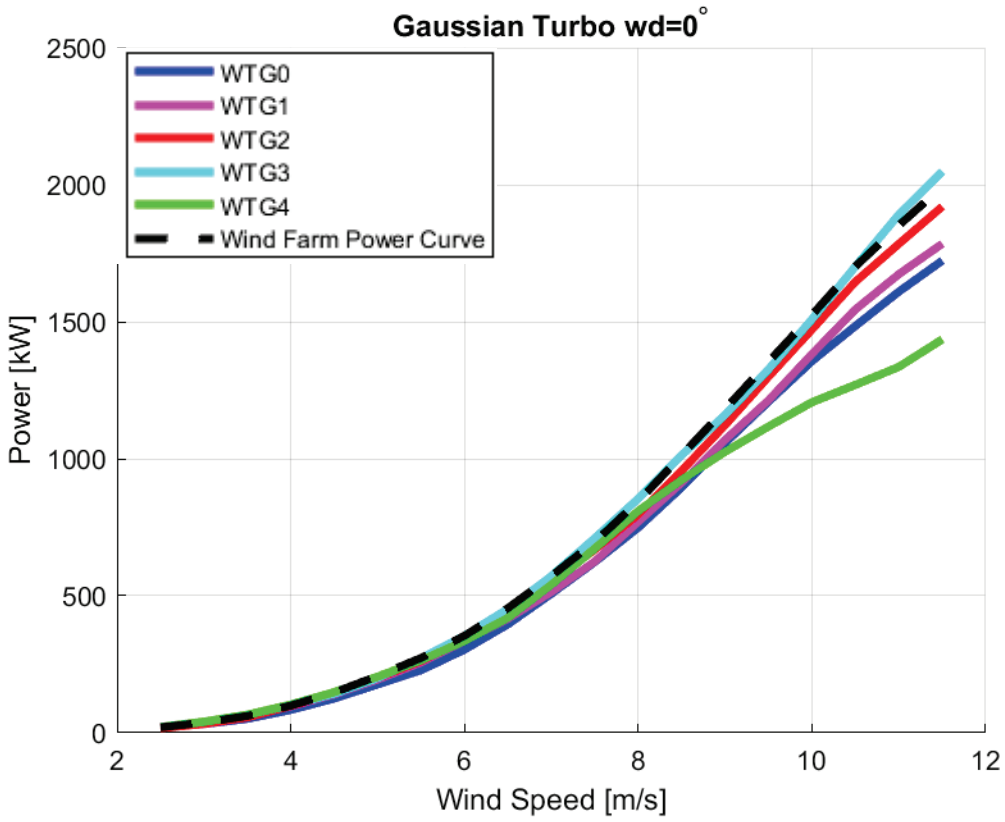

Figure 56. Power Curve of Turbo Gaussian Wake Model at 0° wind direction.

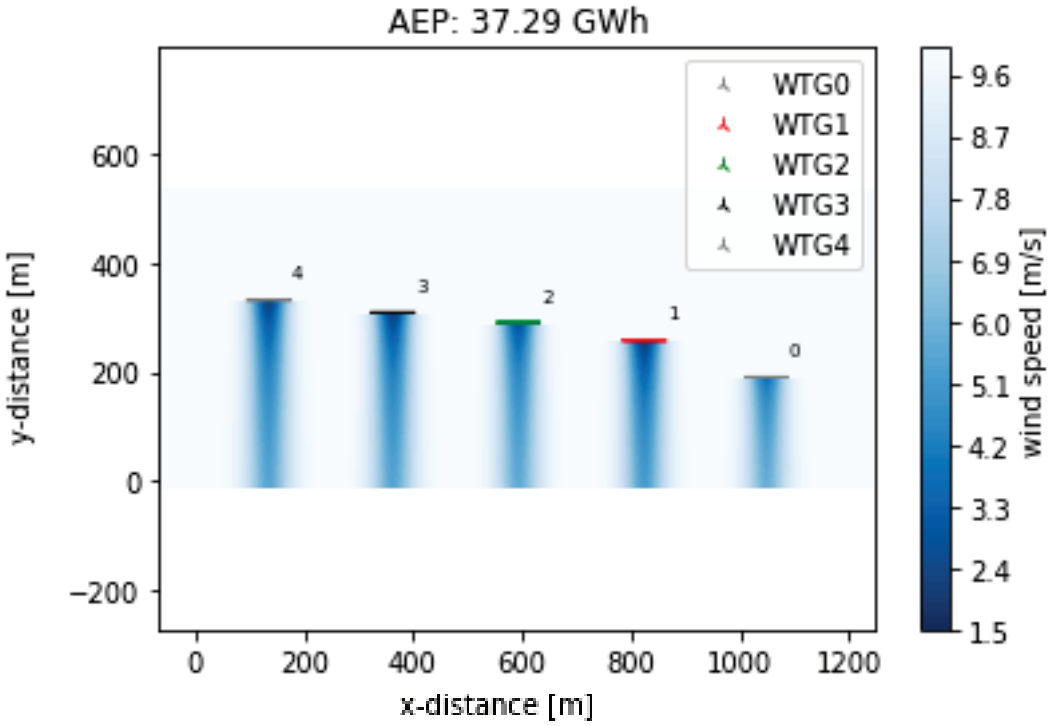

Figure 57. Flow map of Turbo Gaussian Wake Model at 0° wind direction.

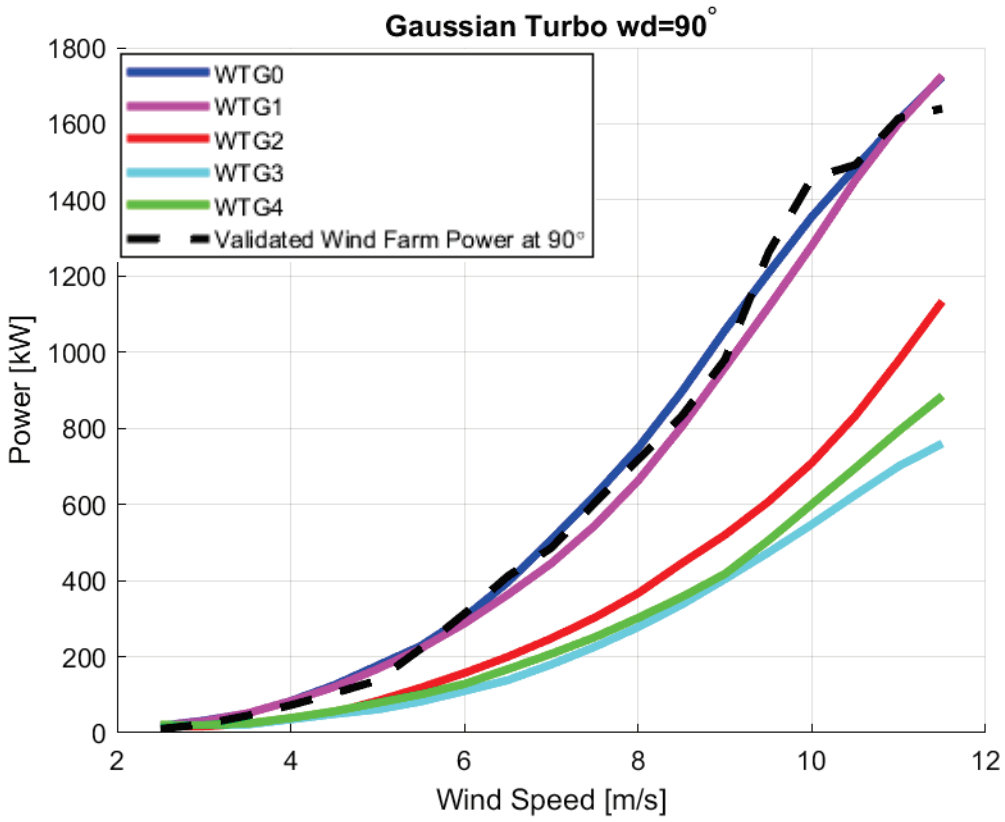

Figure 58. Power Curve of Turbo Gaussian Wake Model at 90° wind direction.

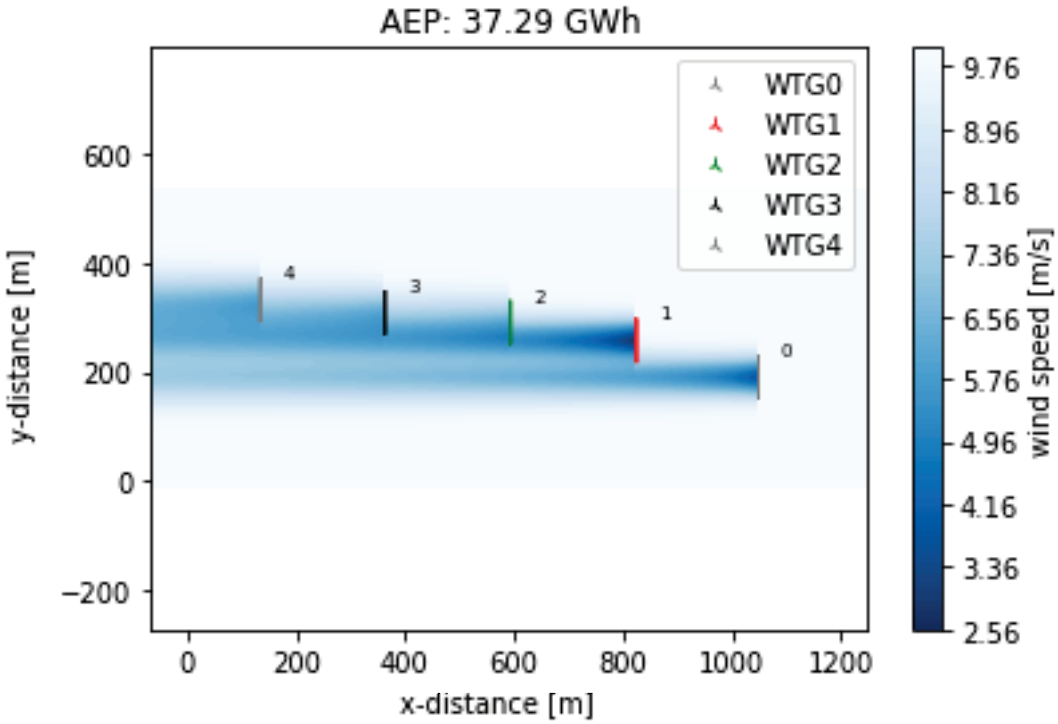

Figure 59. Flow map of Turbo Gaussian Wake Model at 90° wind direction.

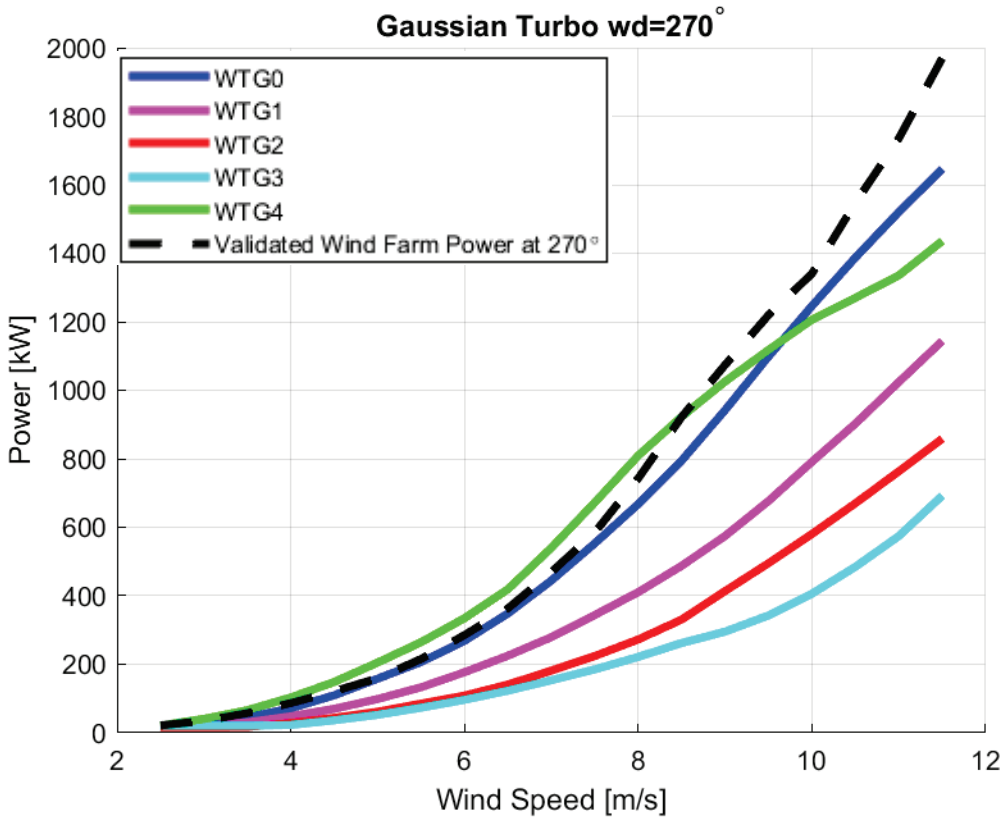

Figure 60. Power Curve of Turbo Gaussian Wake Model at 270° wind direction.

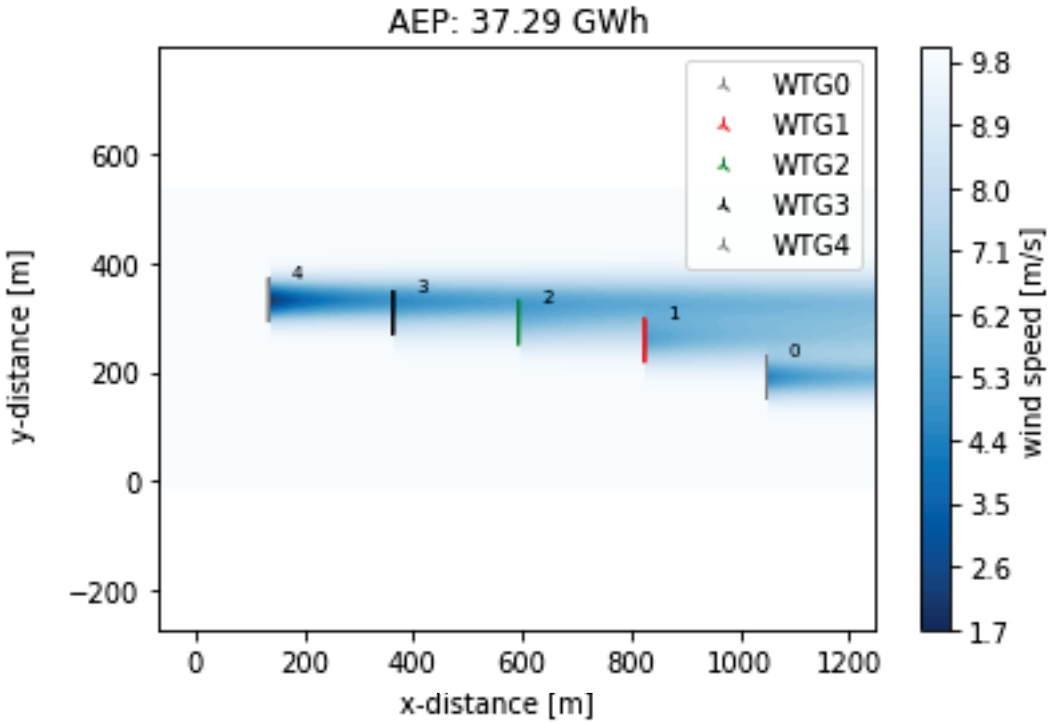

Figure 61. Flow map of Turbo Gaussian Wake Model at 270° wind direction.

When comparing the wake models, considering the wind direction, the turbine (WTG0 at WD90 and WTG4 at WD270) converges with the wake models at the front of the line. This proves that the models work correctly and that the wake effect is not observed when not in the downstream area of another turbine.

On the other hand, when WTG0 at WD270 and WTG4 at WD90, which are the last turbines in the line, are examined.

The general features of the wake models are similar. The features of the models that can be analyzed on the flowmap (such as propagation boundaries or propagation strategy) are compared.

5.7. Blockage Modelling

In this study, six different blockage models are examined. These models are

- Hybrid Induction
- Rankine Half Body
- Vortex Cylinder
- Vortex Dipole
- Self Similarity
- Self Similarity 2020.

For blockage model review and comparison, three critical wind directions are investigated at 10 m/s wind speed. Since the blockage effect is observed in the induction zone, the upstream area is examined in the flowmaps.

5.7.1. Hybrid Induction Blockage Modelling

The fact that the results do not converge in the scenario with free stream airflow seen in Figure 62 proves that the blockage occurs in the upstream area.

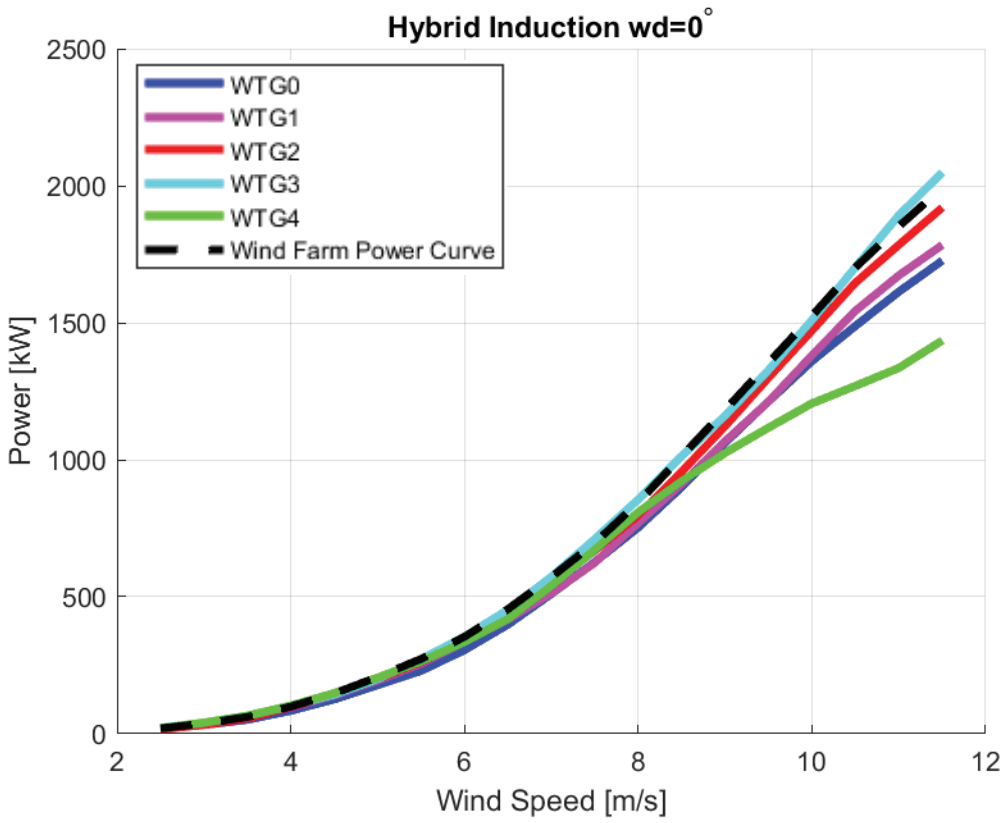

Figure 62. Power Curve of Hybrid Induction Blockage Model at 0° wind direction.

As seen in Figure 63-65-67, the hybrid induction flow characteristic is circular and gathered at the middle point.

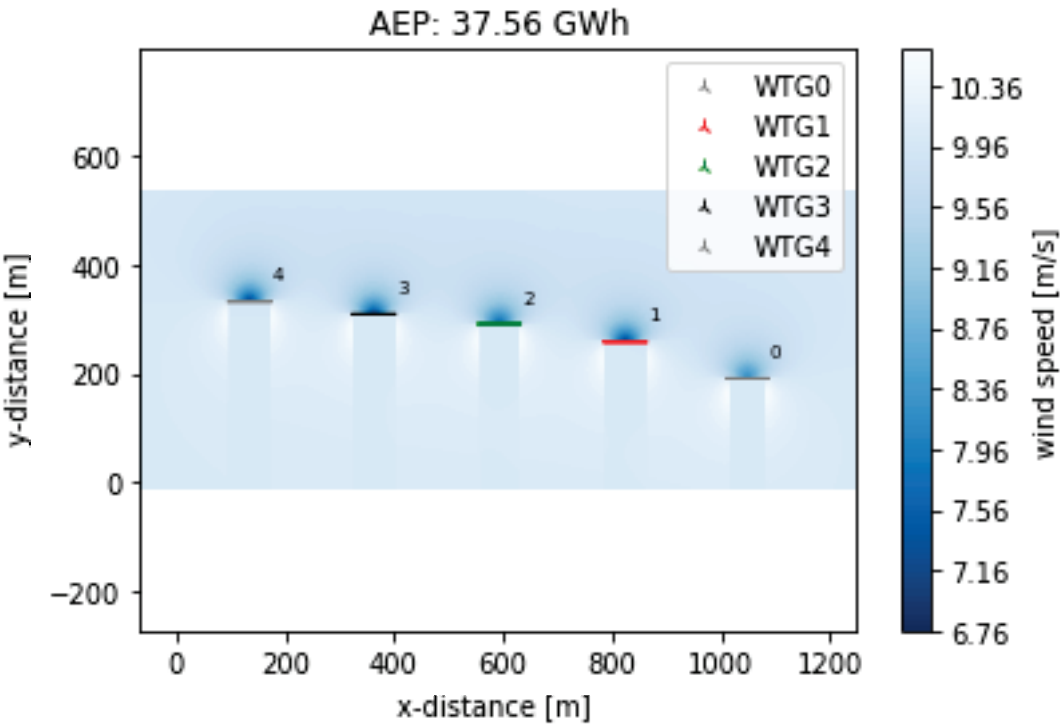

Figure 63. Flow map of Hybrid Induction Blockage Model at 0° wind direction.

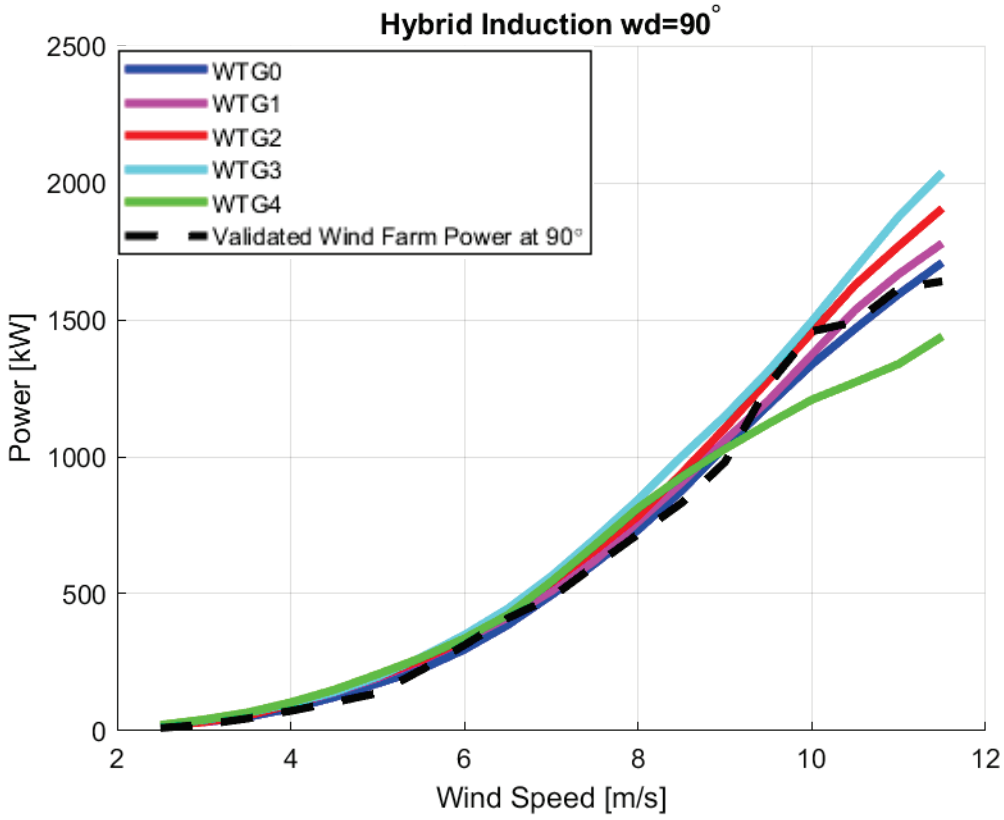

Figure 64. Power Curve of Hybrid Induction Blockage Model at 90° wind direction.

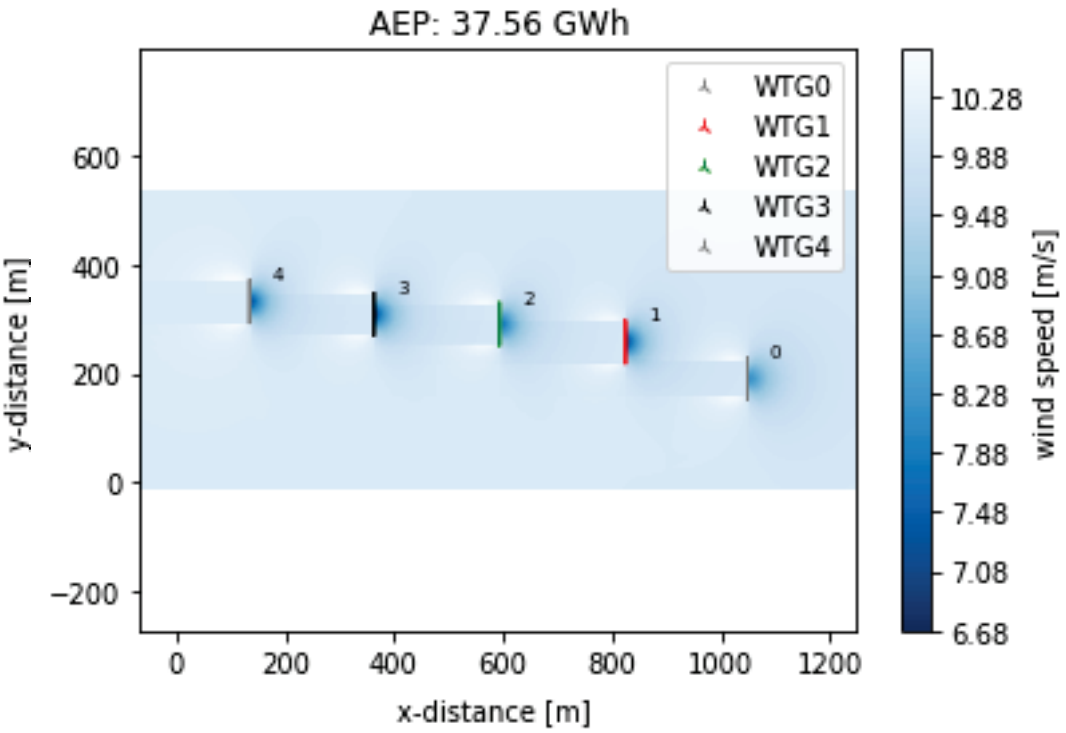

Figure 65. Flow map of Hybrid Induction Blockage Model at 90° wind direction.

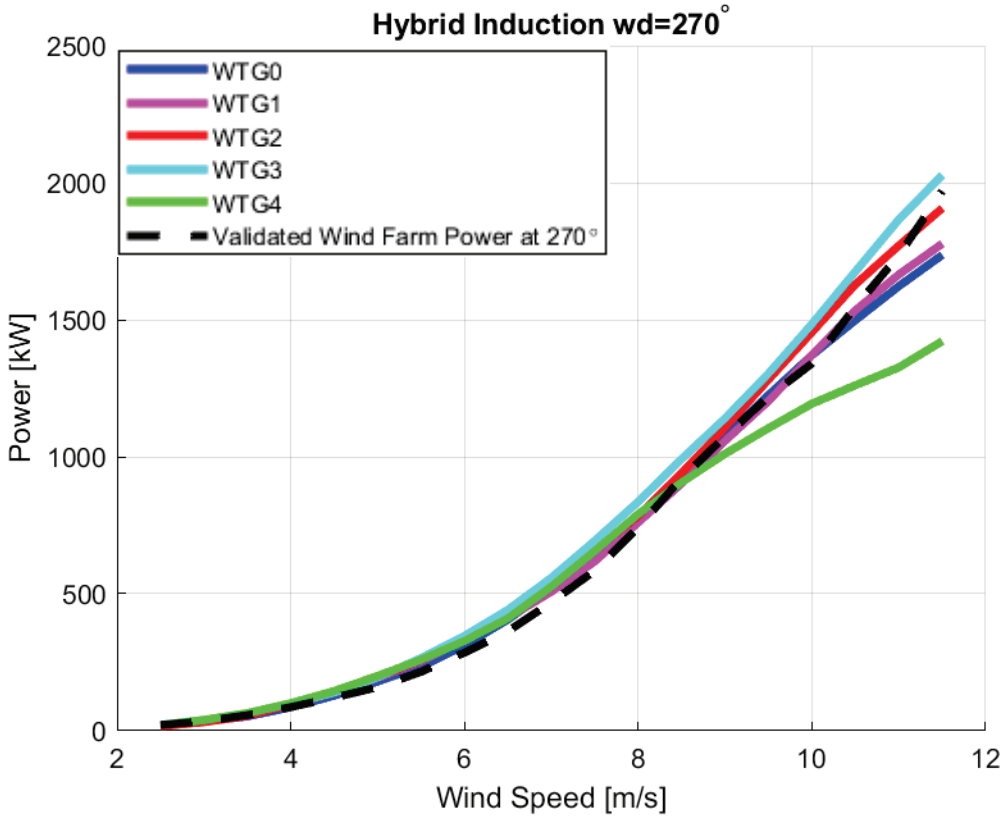

Figure 66. Power Curve of Hybrid Induction Blockage Model at 270° wind direction.

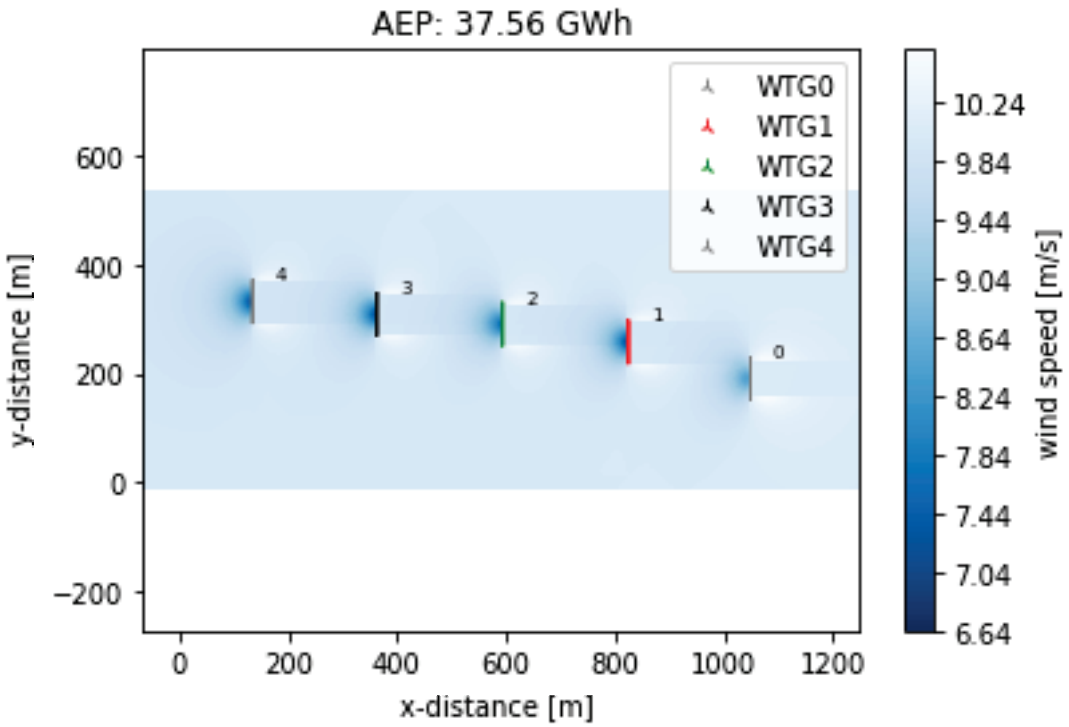

Figure 67. Flow map of Hybrid Induction Blockage Model at 270° wind direction.

5.7.2. Rankine Half Body Blockage Modelling

The difference between the power results of the wake models is even small, while the difference between the blockage models is negligible. Blockage is a smaller effect than wake. The Rankine half body model has a larger area. As seen in Figure 69-71-73, the circular area at the midpoint of the turbines has lower wind speed. The decrease in wind speed is clear.

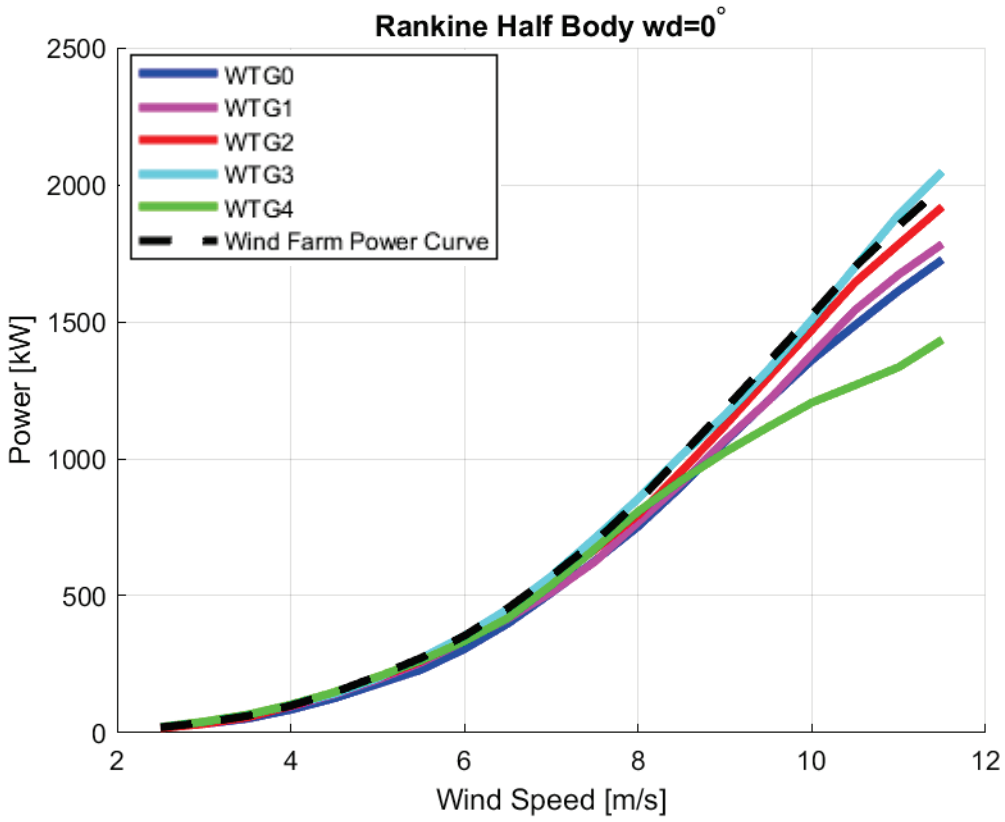

Figure 68. Power Curve of Rankine Half Body Blockage Model at 0° wind direction.

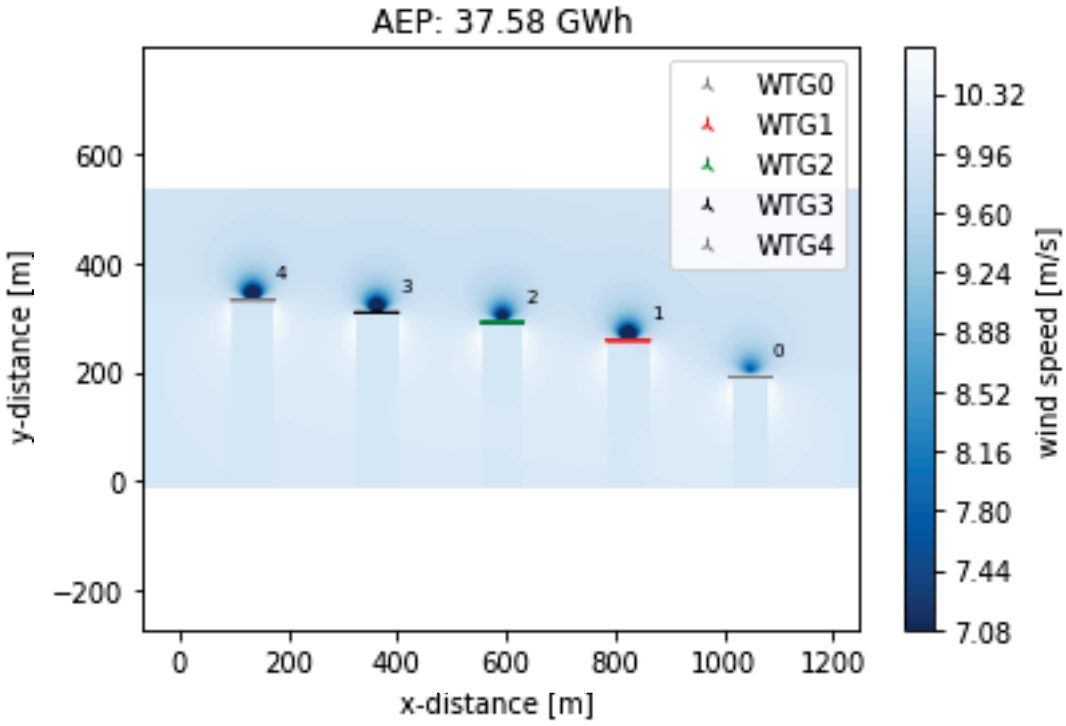

Figure 69. Flow map of Rankine Half Body Blockage Model at 0° wind direction.

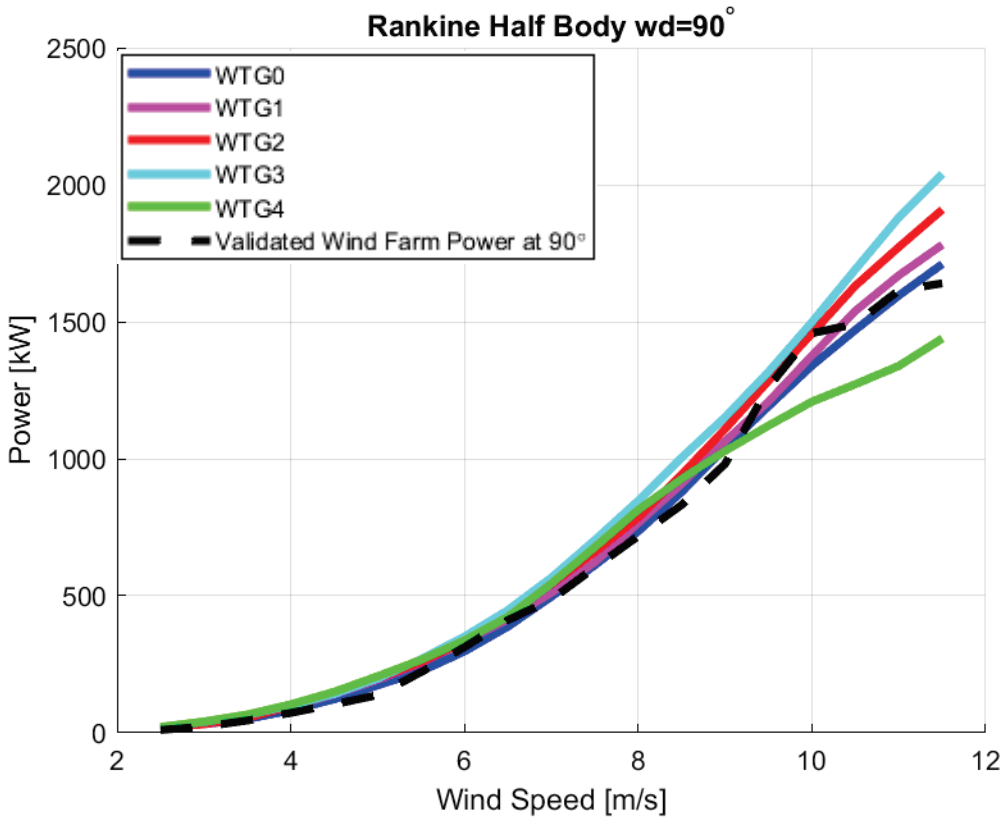

Figure 70. Power Curve of Rankine Half Body Blockage Model at 90° wind direction.

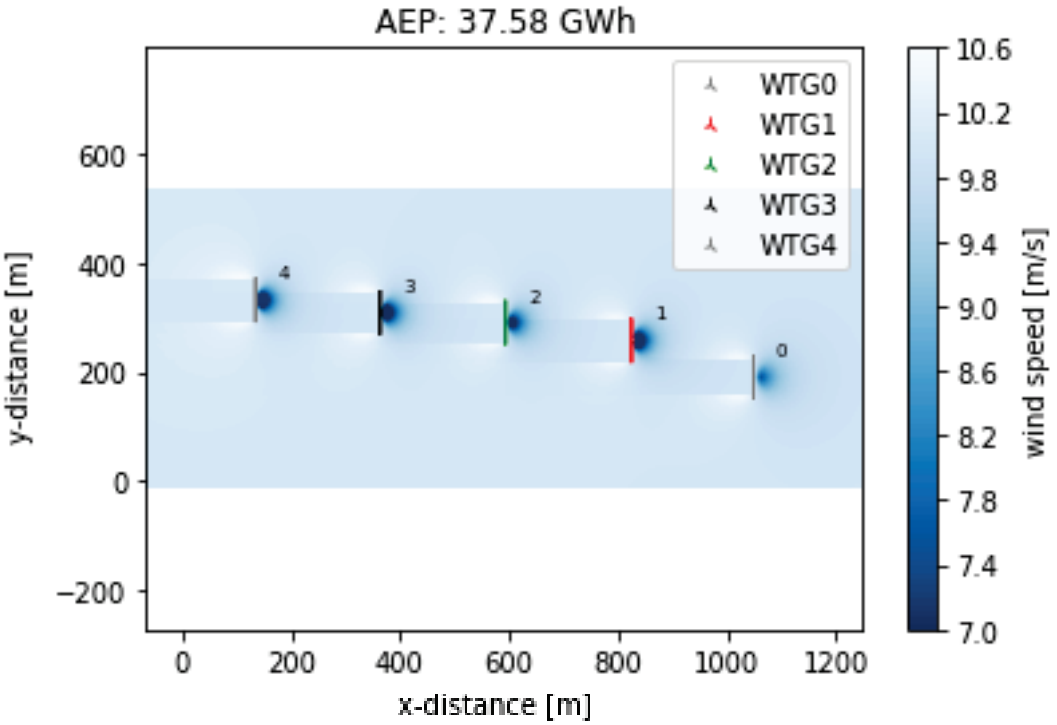

Figure 71. Flow map of Rankine Half Body Blockage Model at 90° wind direction.

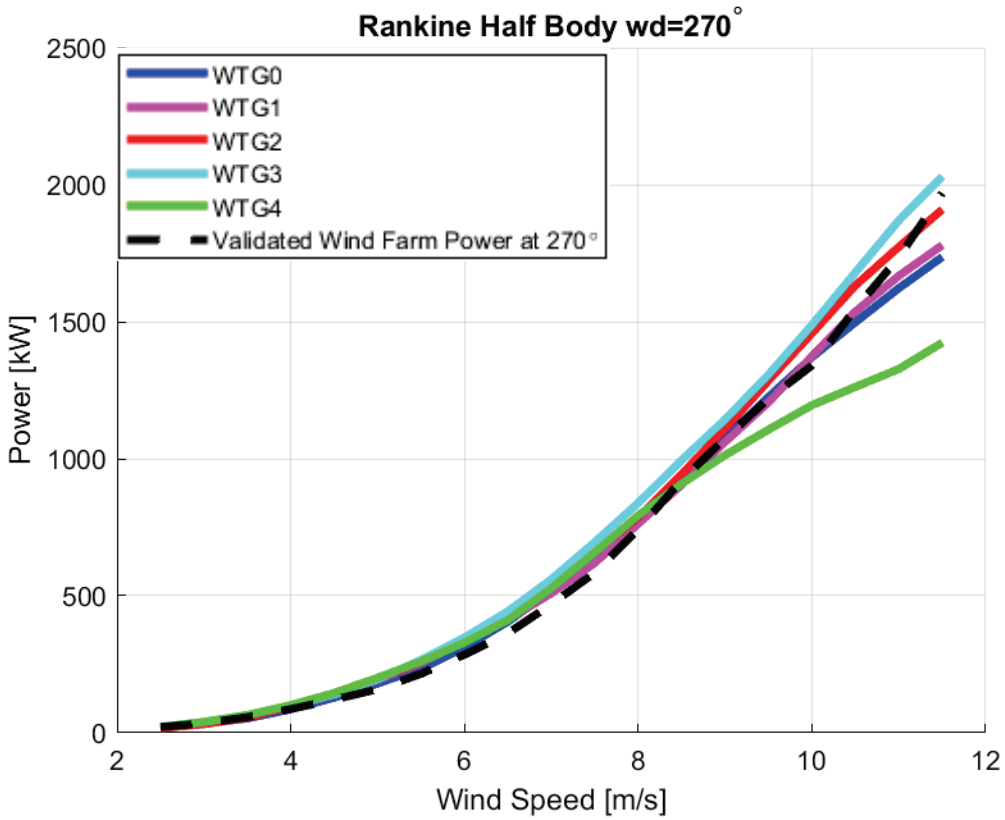

Figure 72. Power Curve of Rankine Half Body Blockage Model at 270° wind direction.

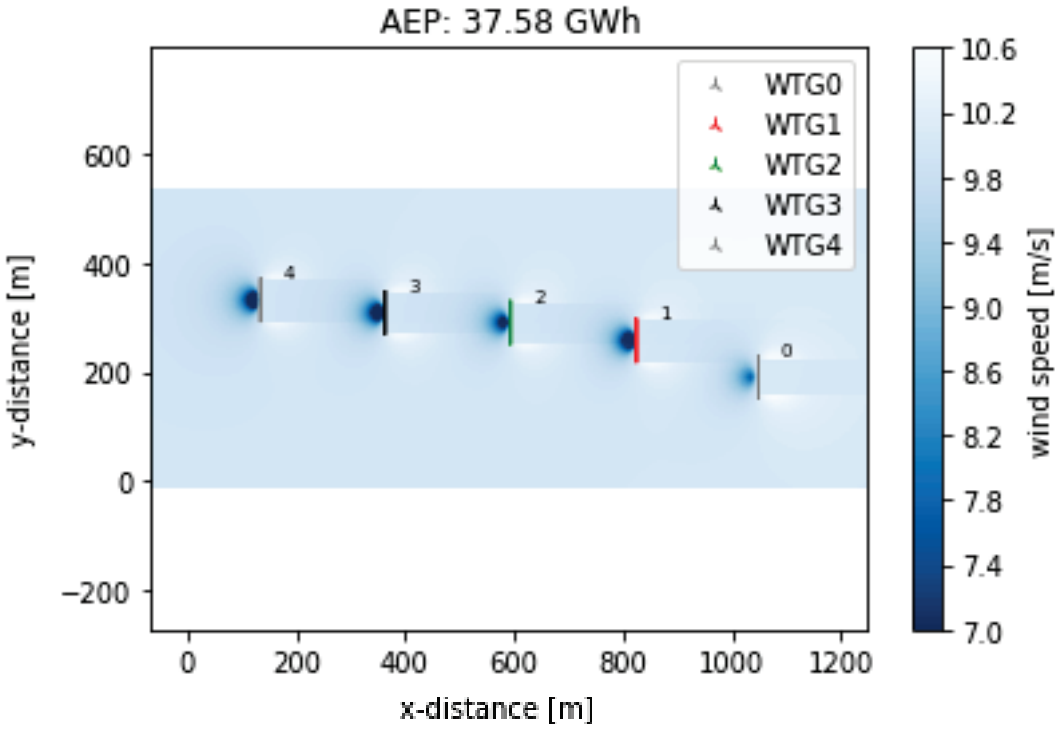

Figure 73. Flow map of Rankine Half Body Blockage Model at 270° wind direction.

5.7.3. Vortex Cylinder Blockage Modelling

Hybrid induction and rankine half body have circular span, while vortex cylinder spans linearly. The lowest wind speed is not in the middle of the turbine, but spread over the entire area in front of the turbine.

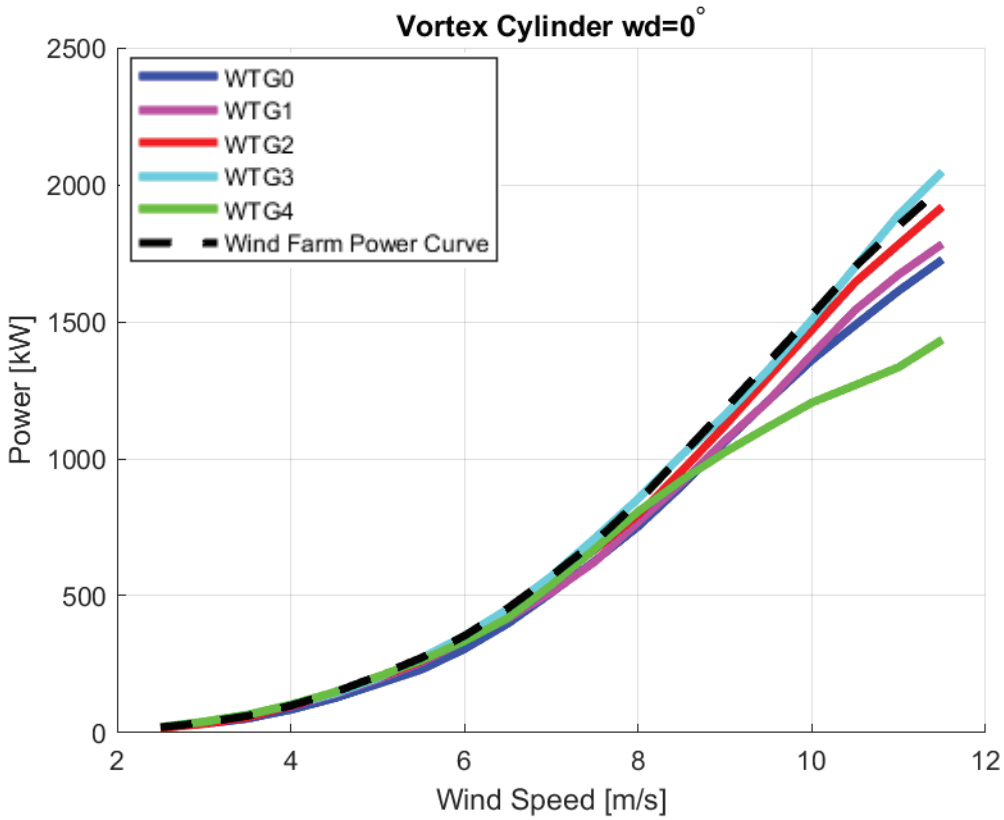

Figure 74. Power Curve of Vortex Cylinder Blockage Model at 0° wind direction.

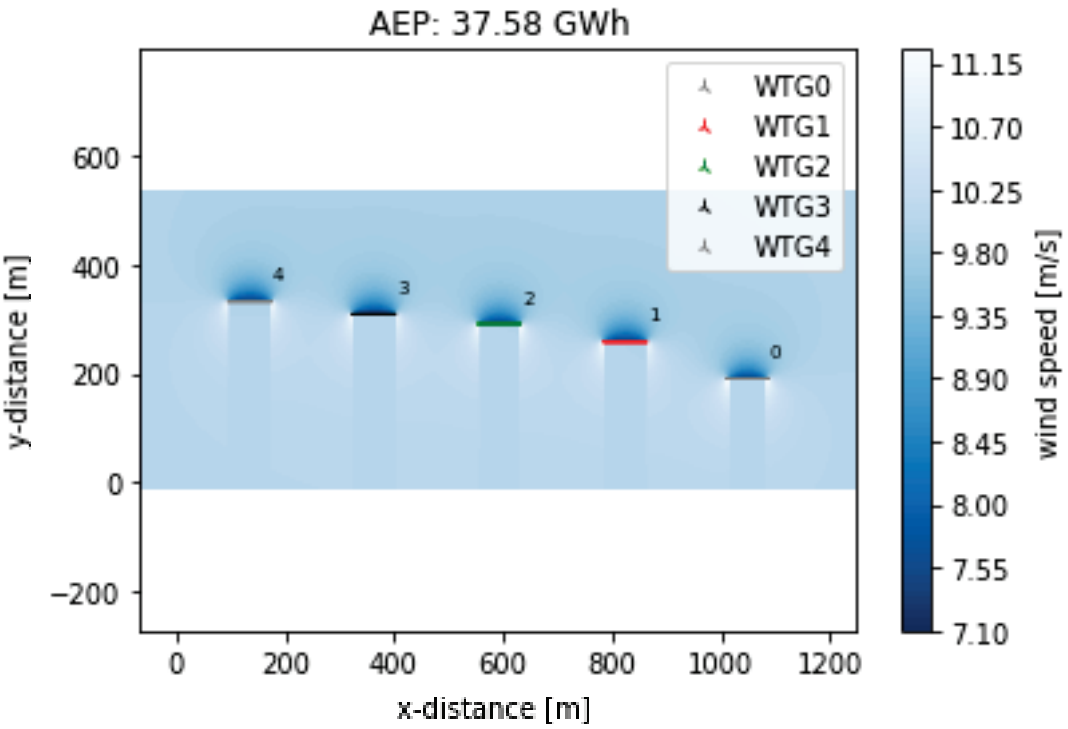

Figure 75. Flow map of Vortex Cylinder Blockage Model at 0° wind direction.

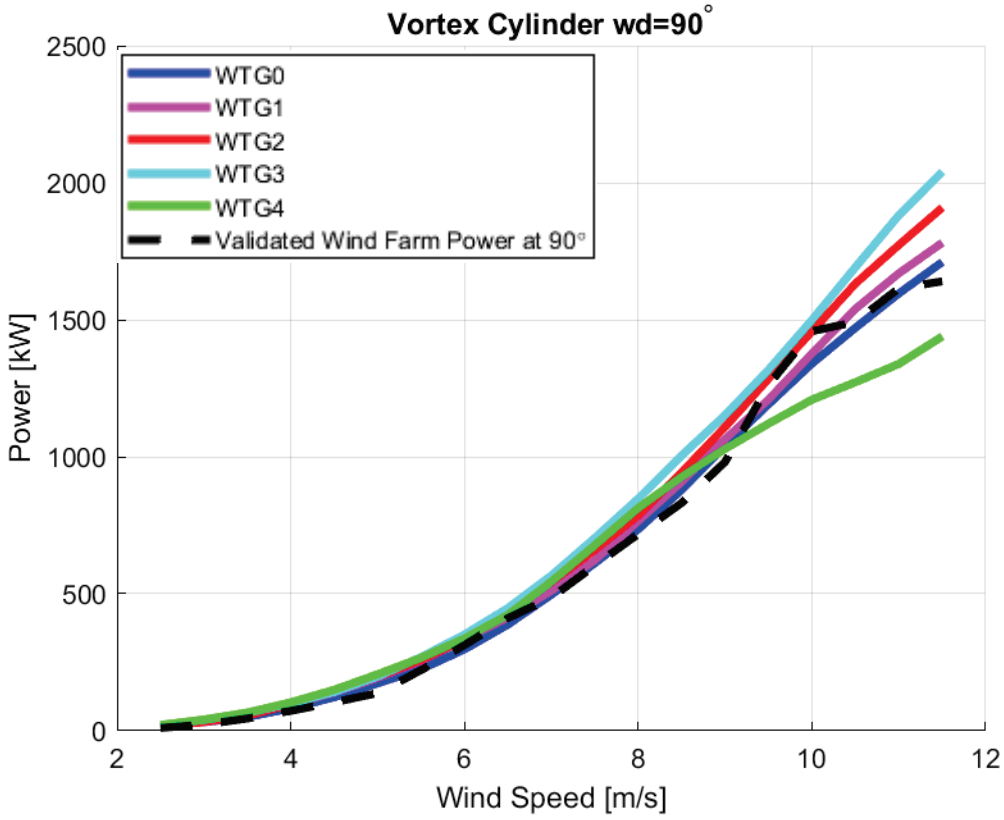

Figure 76. Power Curve of Vortex Cylinder Blockage Model at 90° wind direction.

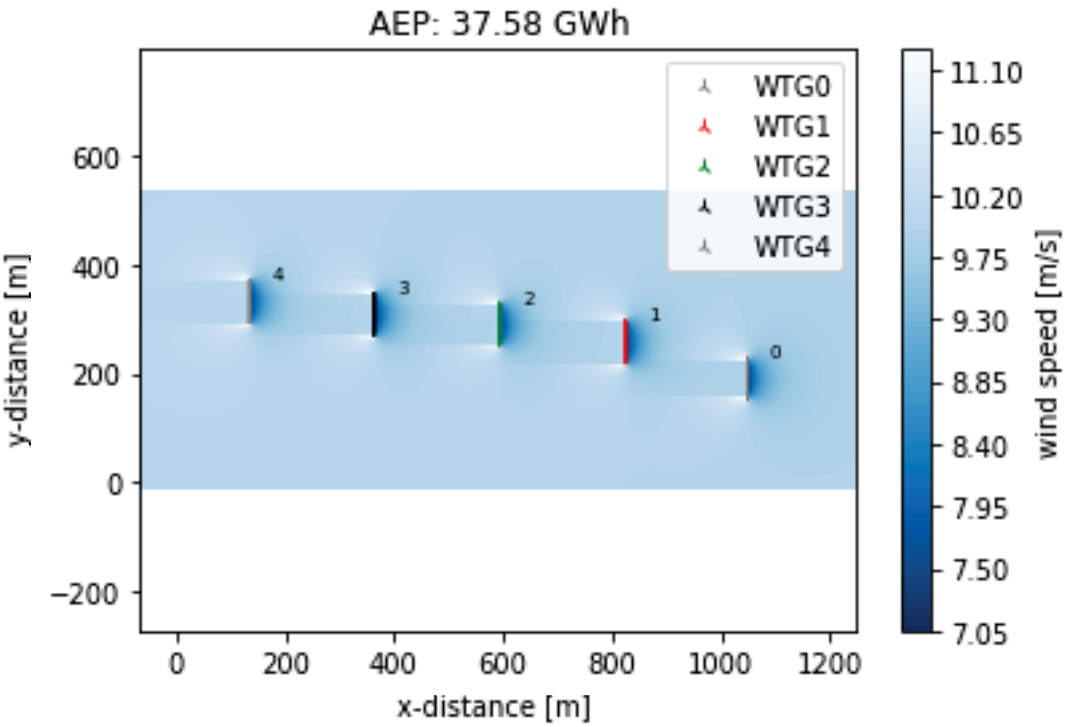

Figure 77. Flow map of Vortex Cylinder Blockage Model at 90° wind direction.

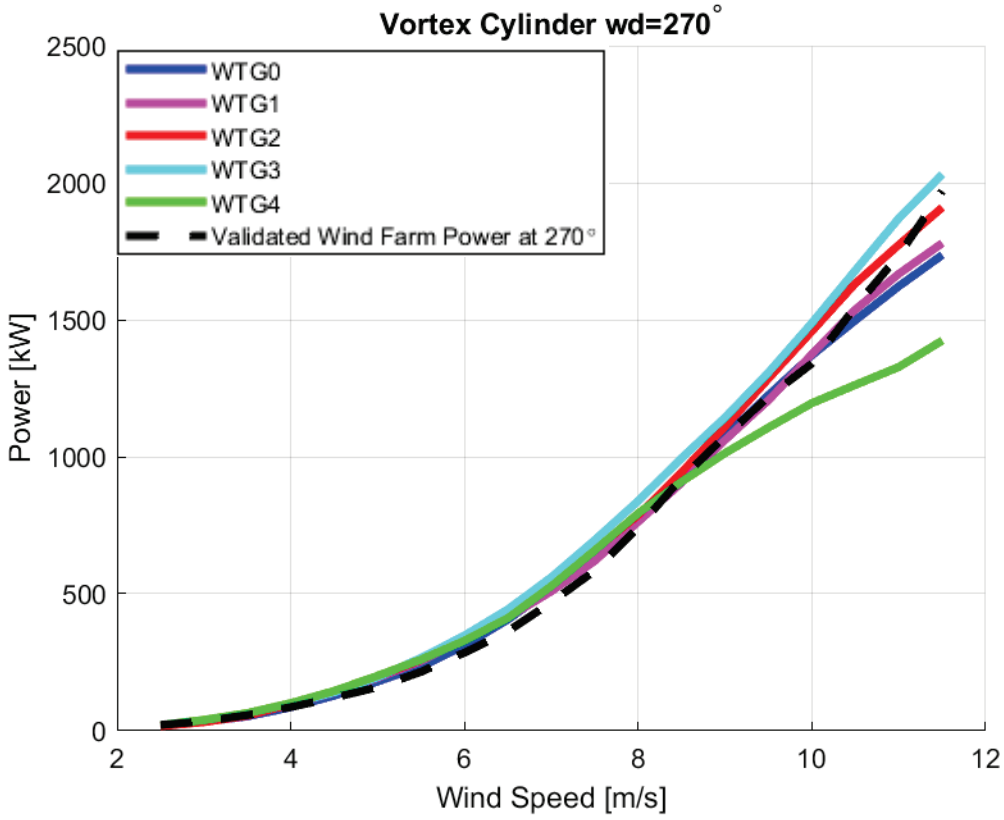

Figure 78. Power Curve of Vortex Cylinder Blockage Model at 270° wind direction.

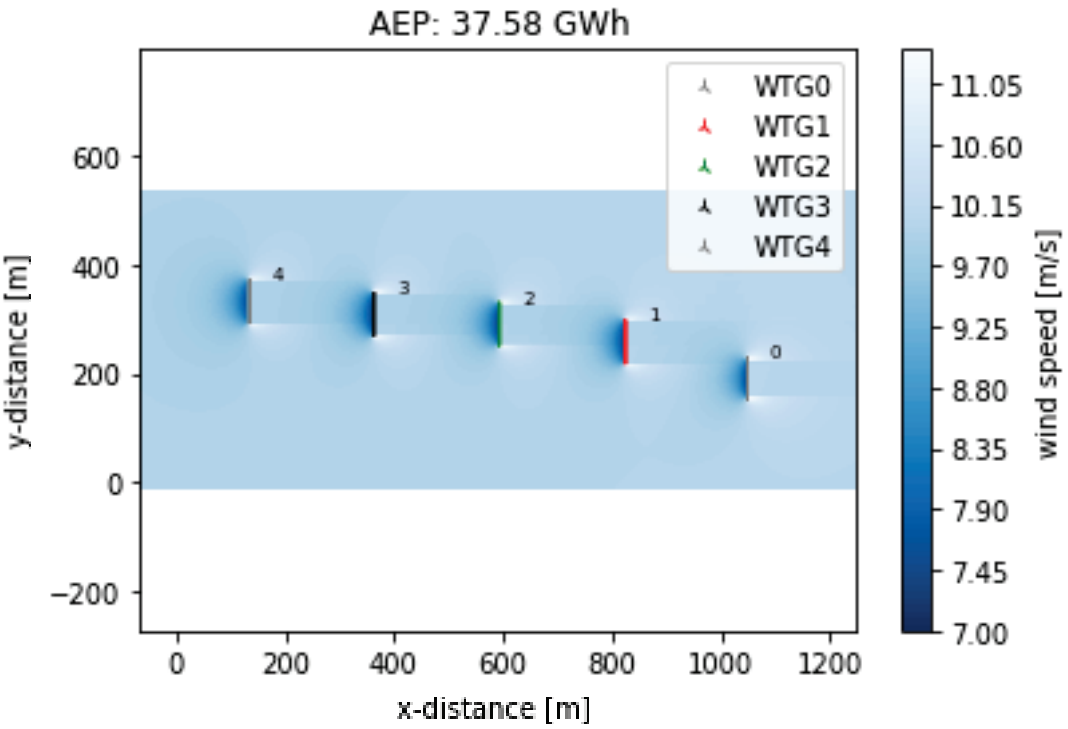

Figure 79. Flow map of Vortex Cylinder Blockage Model at 270° wind direction.

5.7.4. Vortex Dipole Blockage Modelling

Vortex dipole also spreads circularly just like hybdid induction and rankine half body. While the front-side parts of the turbine have high wind speeds, the wind speed at the center of the turbine is very low.

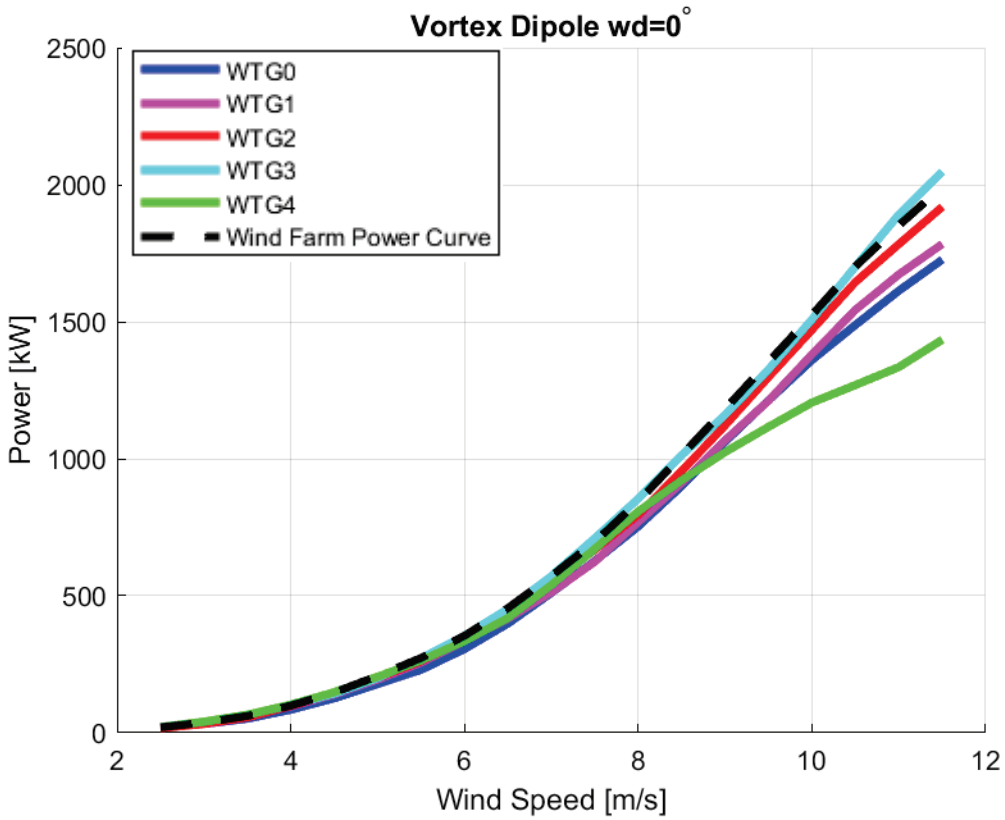

Figure 80. Power Curve of Vortex Dipole Blockage Model at 0° wind direction.

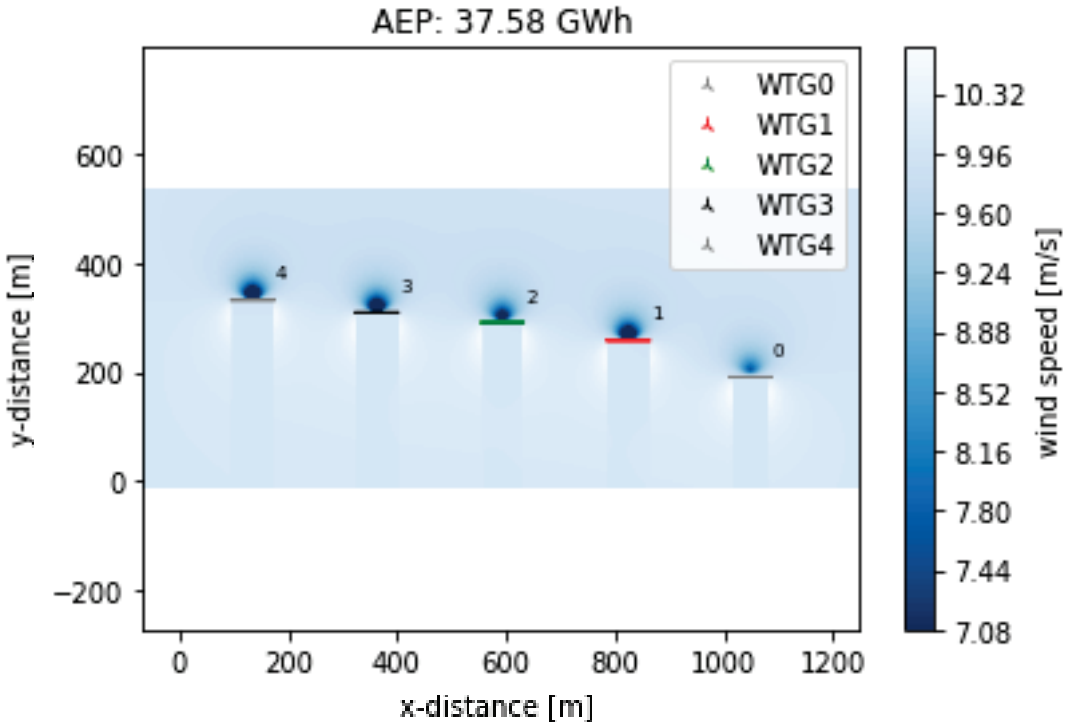

Figure 81. Flow map of Vortex Dipole Blockage Model at 0° wind direction.

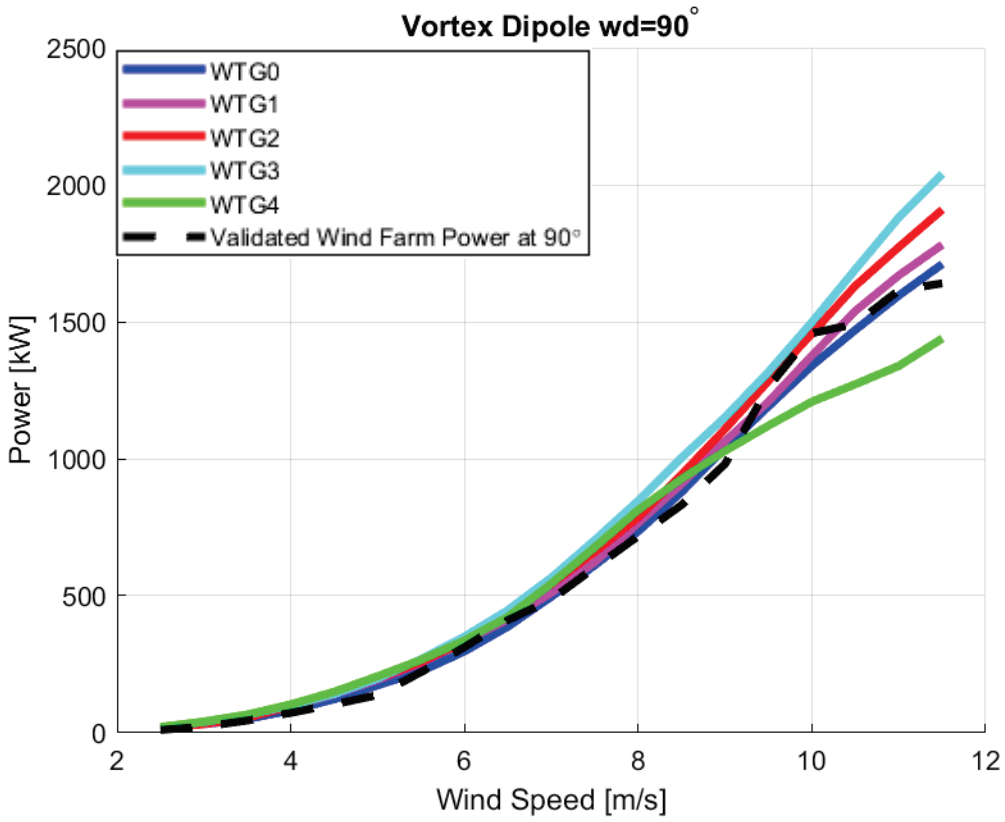

Figure 82. Power Curve of Vortex Dipole Blockage Model at 90° wind direction.

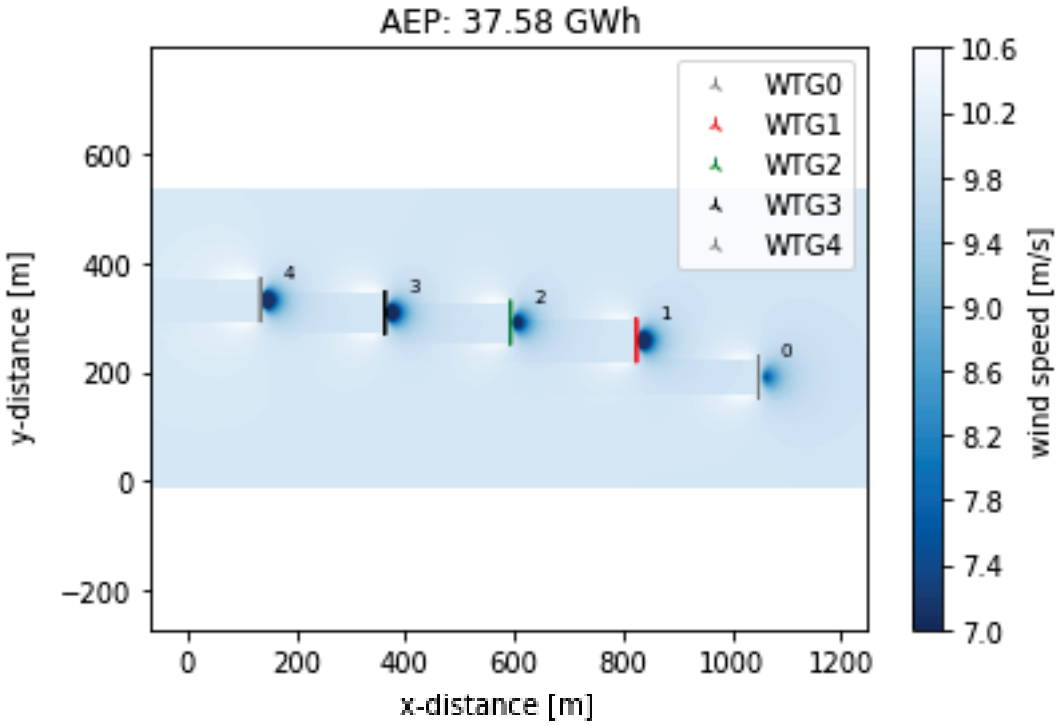

Figure 83. Flow map of Vortex Dipole Blockage Model at 90° wind direction.

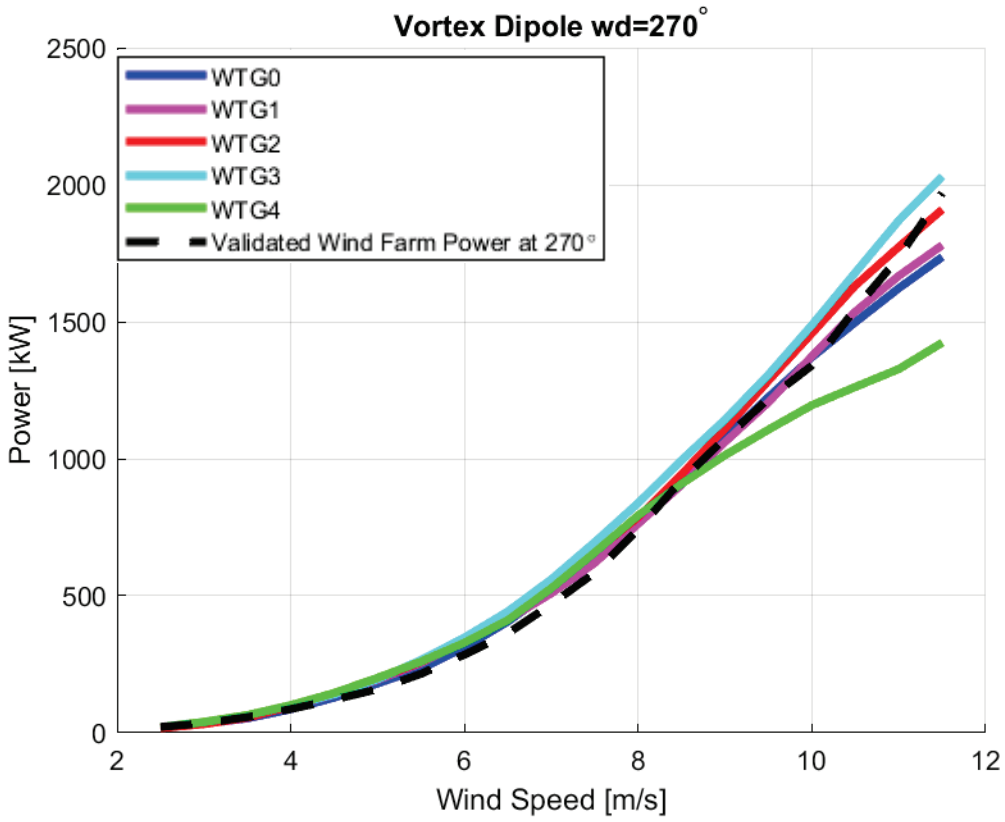

Figure 84. Power Curve of Vortex Dipole Blockage Model at 270° wind direction.

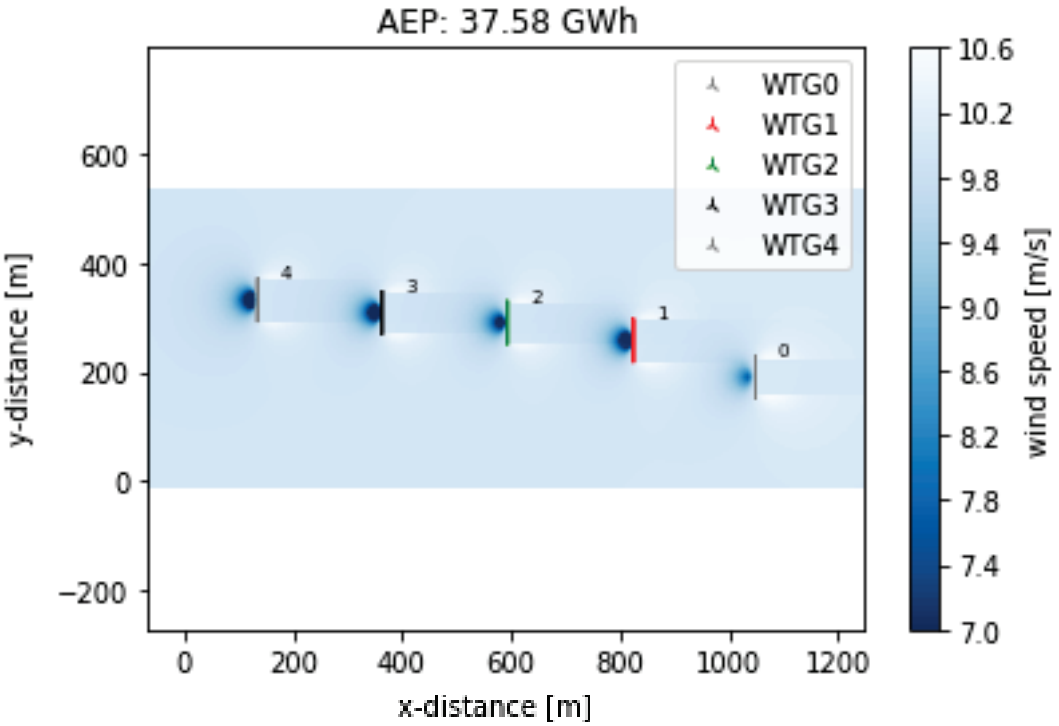

Figure 85. Flow map of Vortex Dipole Blockage Model at 270° wind direction.

5.7.5. Self Similarity Blockage Modelling

The self similarity model spreads more linearly compared to other models. Power results are similar as expected. The self similarity model spreads more linearly compared to other models. Power results are similar as expected. Unlike other models, a higher wind speed drop is observed in the front-side area.

The self similarity model spreads more linearly compared to other models. Power results are similar as expected. Unlike other models, a higher wind speed drop is observed in the front-side area. In addition to the progress of the blockage effect in the lateral area, it is observed that the spreading movement is circular.

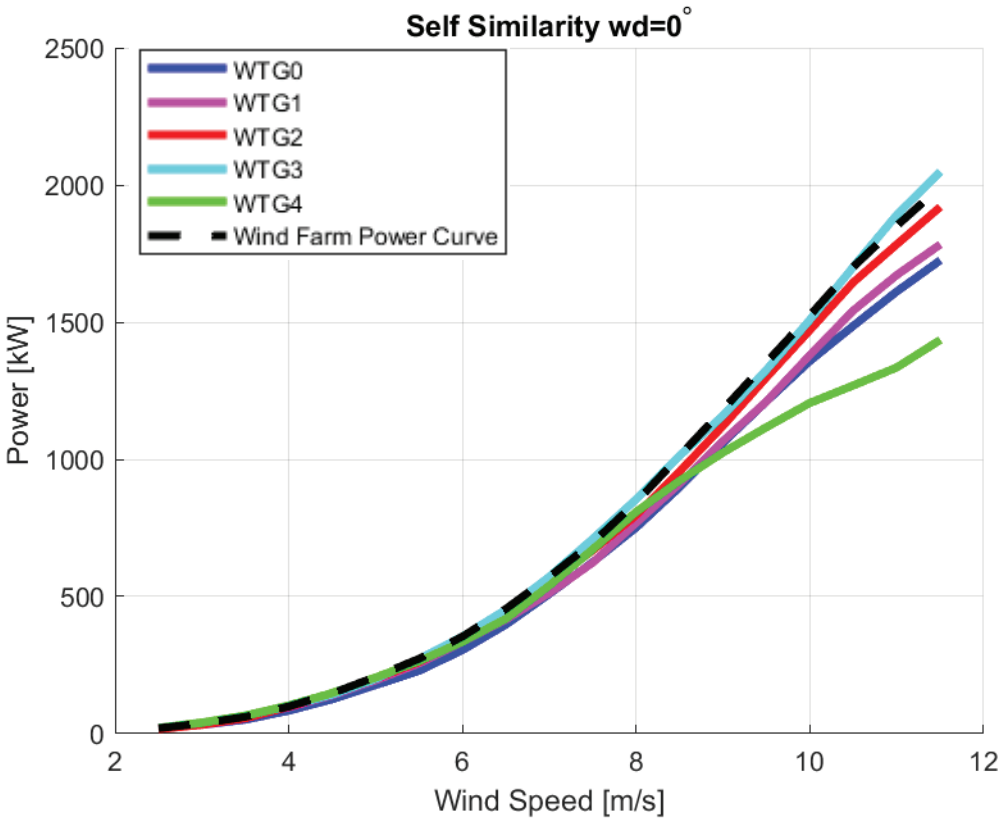

Figure 86. Power Curve of Self Similarity Blockage Model at 0° wind direction.

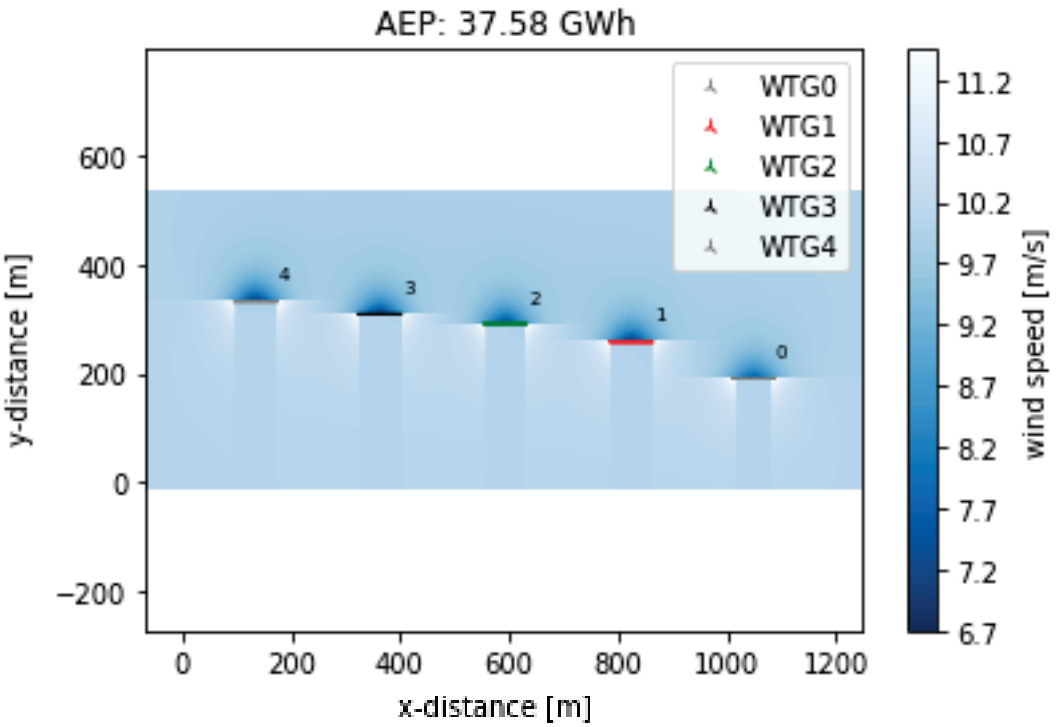

Figure 87. Flow map of Self Similarity Blockage Model at 0° wind direction.

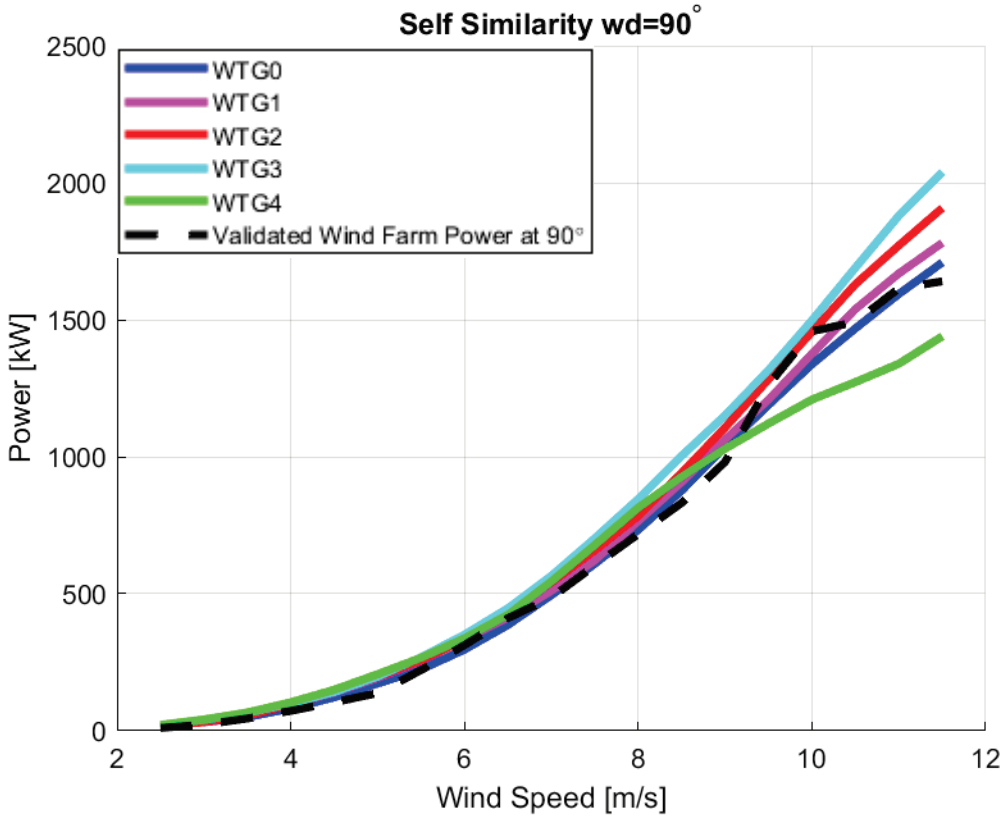

Figure 88. Power Curve of Self Similarity Blockage Model at 90° wind direction.

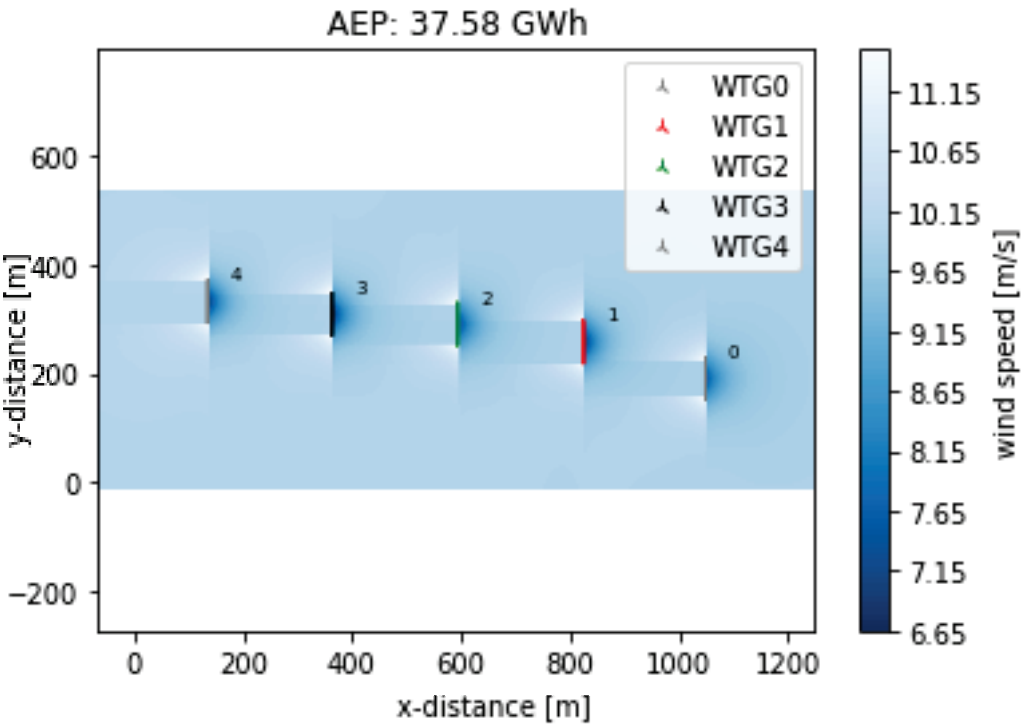

Figure 89. Flow map of Self Similarity Blockage Model at 90° wind direction.

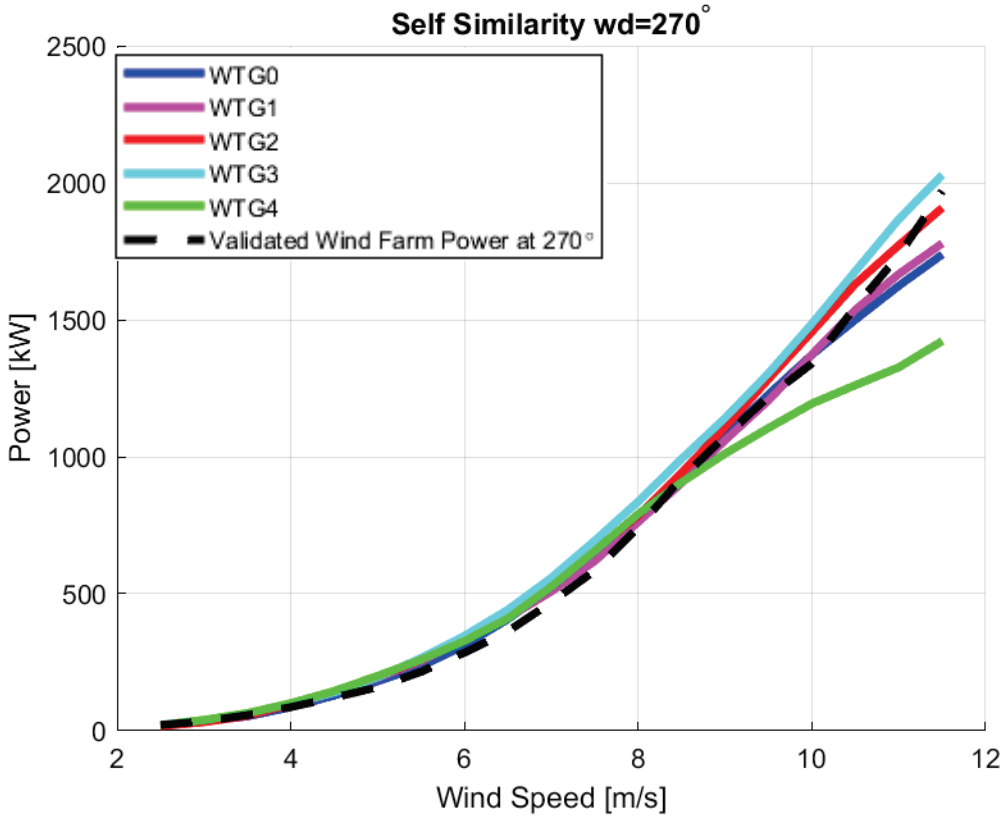

Figure 90. Power Curve of Self Similarity Blockage Model at 270° wind direction.

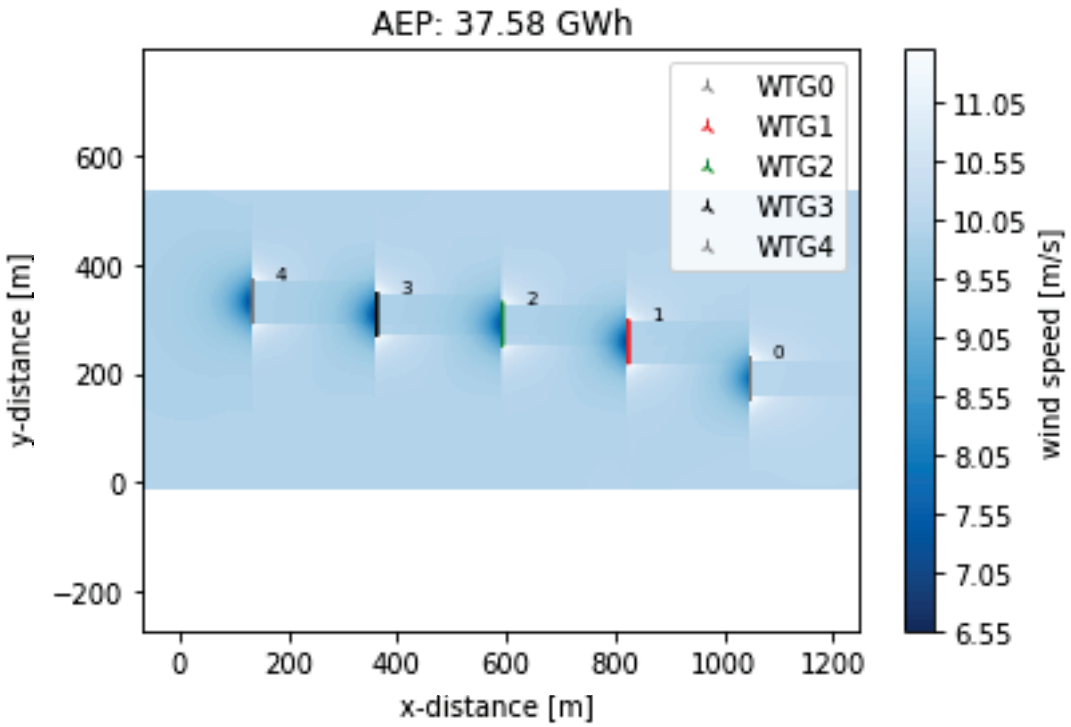

Figure 91. Flow map of Self Similarity Blockage Model at 270° wind direction.

5.7.6. Self Similarity 2020 Blockage Modelling

Self Similarity 2020 is quite similar to Self similarity. There is no other difference except that the spreading movement is more circular.

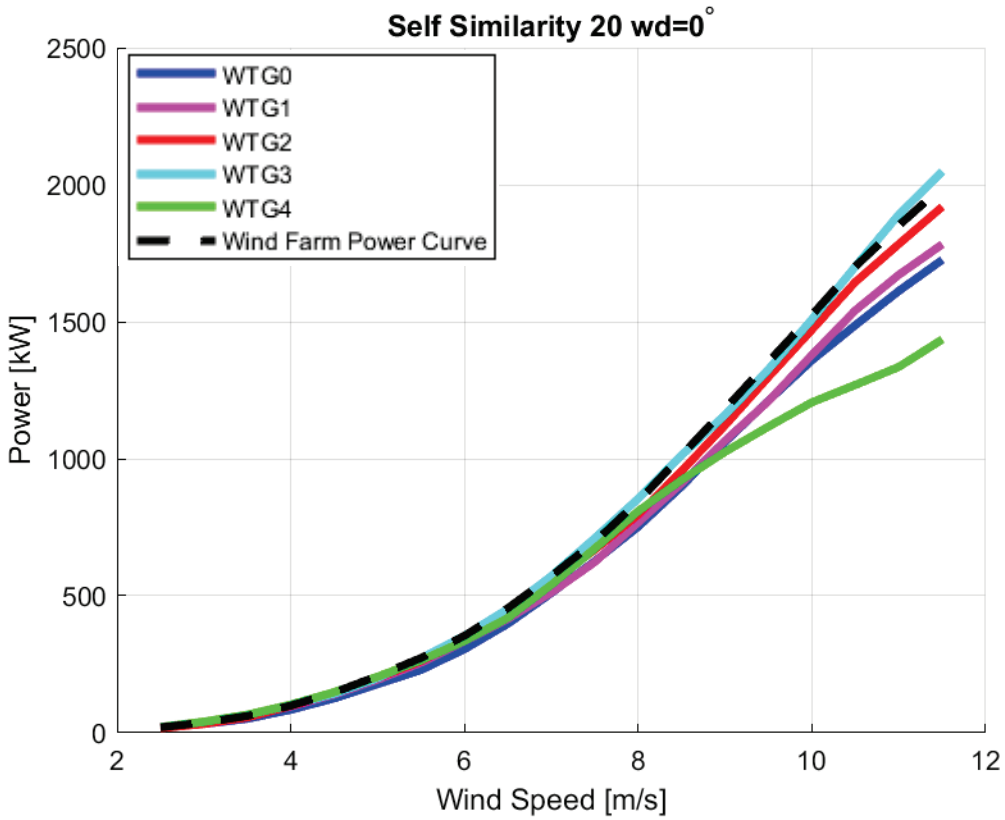

Figure 92. Power Curve of Self Similarity 2020 Blockage Model at 0° wind direction.

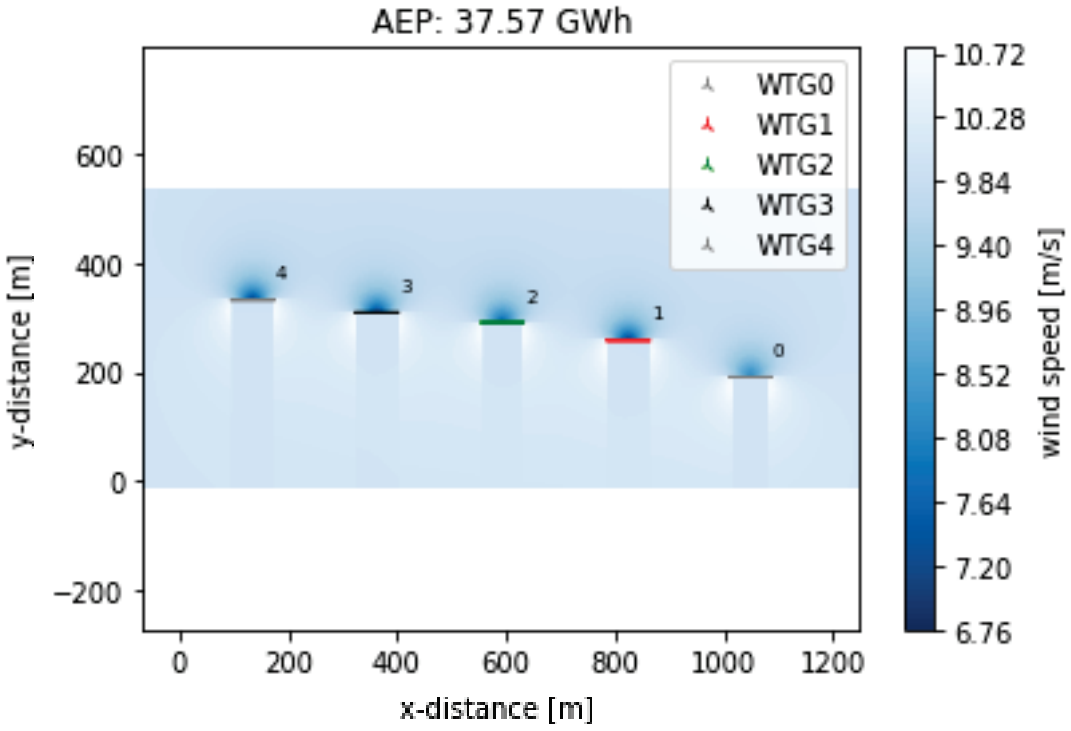

Figure 93. Flow map of Self Similarity 2020 Blockage Model at 0° wind direction.

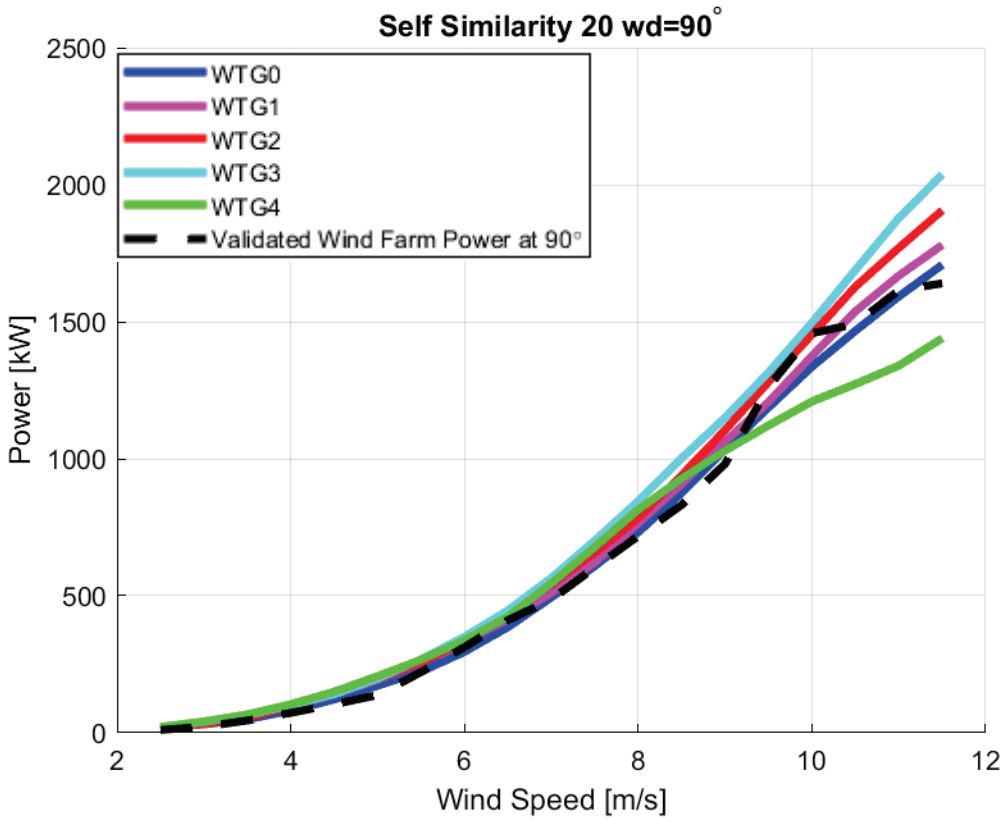

Figure 94. Power Curve of Self Similarity 2020 Blockage Model at 90° wind direction.

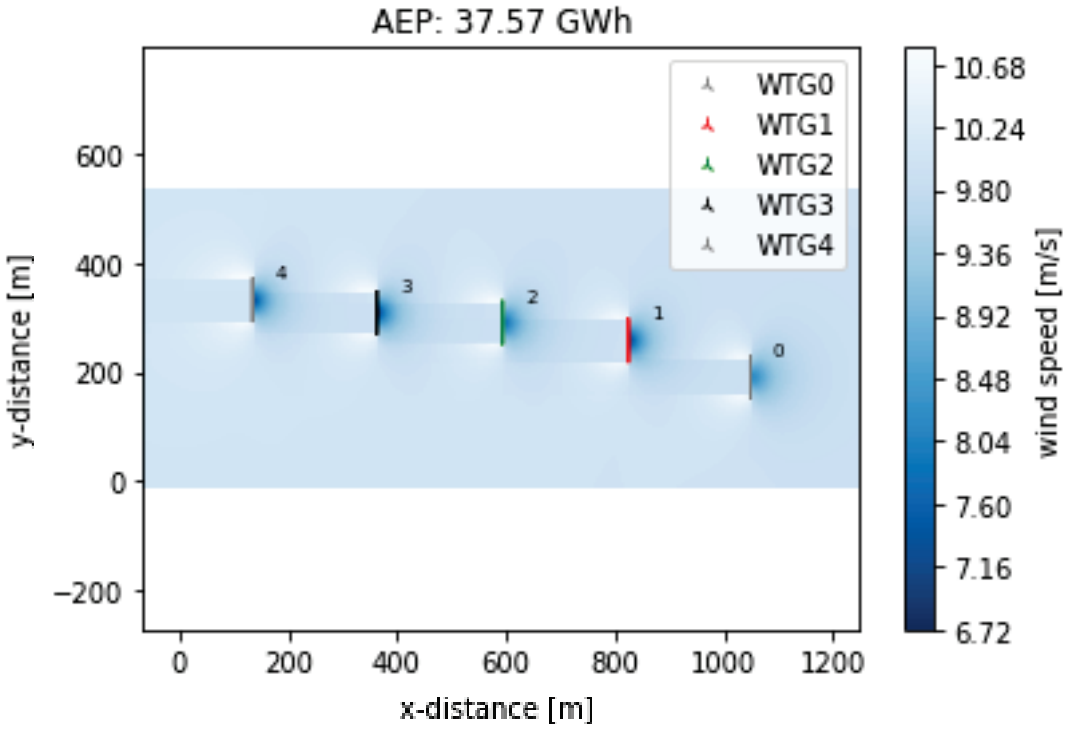

Figure 95. Flow map of Self Similarity 2020 Blockage Model at 90° wind direction.

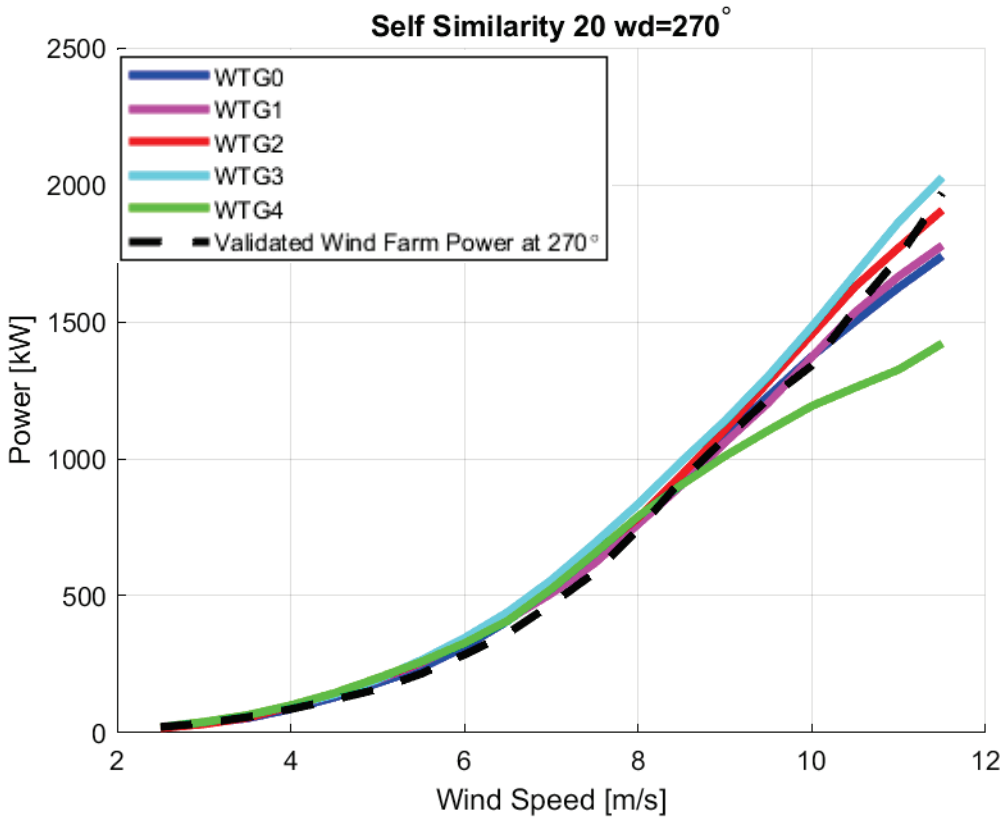

Figure 96. Power Curve of Self Similarity 2020 Blockage Model at 270° wind direction.

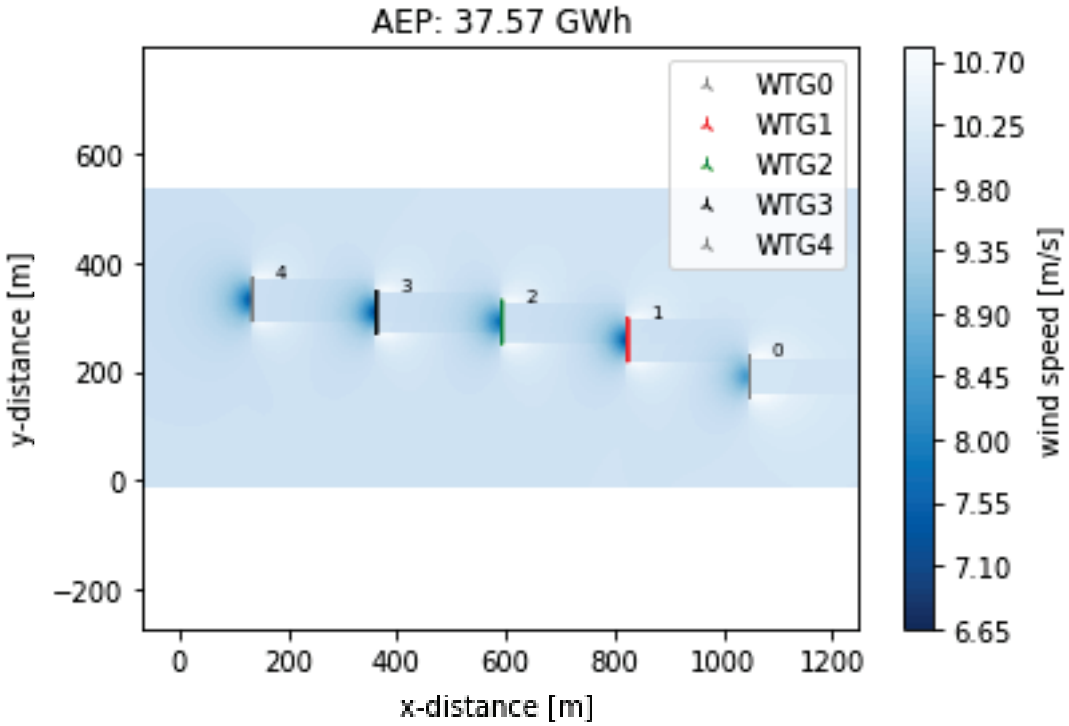

Figure 97. Flow map of Self Similarity 2020 Blockage Model at 270° wind direction.

In contrast to wake models, blockage models are the effect that the front row turbine will observe. As seen in the figures, the blockage models are pretty close to each other. This may be because the blockage effect is smaller than the wake effect, and the models are still in the development stage.

Therefore, easy and fast computation is the priority when deciding on the blockage model.

5.8. Wake & Blockage Results and Coupled Model Decision

The wake and blockage model results are examined to decide the wake and blockage models used in the coupled model. The wind farm has a single row of turbines. Therefore, two different wind directions are sufficient for wake and blockage analysis. The turbine with free stream wind conditions at 90° wind direction is WTG0. The turbine with free stream wind conditions at 270° wind direction is WTG4. The percentage relationship between models and SCADA data is examined when comparing models. The foremost and rearmost turbines (WTG0-WTG4) of the wind farm in two different wind directions are inspected in four cases.

As can be seen in Table 3, the results are generally very close to each other. As seen in the previous figures, an unexpected power loss is observed in WTG4. This may be because the turbine is over-maintained due to unforeseen malfunctions.

Since the difference between the models is minimal, Turbo Gaussian, which gives the closest results to SCADA data, and Jensen and Larsen, the most common models, are selected to create the coupled model. Among the Blockage models, Vortex Cylinder is the closest model to SCADA data, while Self Similarity 20 is the farthest model. Since the distance between the other models was less than 0.3%, it was unnecessary to examine.

Table 3. Wake and Blockage Model Results

Models	WTG0 wd=90	WTG4 wd=90	WTG0 wd=270	WTG4 wd=270
			(%)	
NOJ	**0.22**	**-64.69**	**-23.53**	**-10.88**
NOJ Local	0.22	-68.11	-25.18	-10.88
NOJ Turbo	0.22	-70.77	-21.75	-10.88
GCL	**0.22**	**-63.01**	**-22.66**	**-10.88**
GCL Local	0.22	-32.83	-18.35	-10.88
Gaussian	0.22	-62.97	-12.42	-10.88
Gaussian Turbo	**0.22**	**-55.60**	**-7.92**	**-10.88**
Hybrid Induction	-1.20	-10.71	1.28	-11.79
Rankine Half Body	-0.99	-10.71	1.28	-11.66
Vortex Cylinder	**-0.97**	**-10.71**	**1.26**	**-11.64**
Vortex Dipole	-0.99	-10.71	1.28	-11.66
Self Similarity	-1.15	-10.69	1.42	-11.76
Self Similarity 20	**-1.29**	**-10.66**	**1.54**	**-11.86**

The results in percentages seen in Table 3 are calculated with the validated wind farm power curve of the models results. The results in percentages seen in Table 3 are calculated with the validated wind farm power curve of the models results. The results in the table are obtained by dividing the model outputs by the wind farm power curve. These small numbers represent the difference between models and SCADA data.

5.9. Coupled Wake and Blockage Modelling

This study uses three different wake and three blockage models for the coupled model. Wake Models are

- Jensen
- Larsen
- Turbo Gaussian

Blockage Models are

- Vortex Cylinder
- Self Similarity 2020.

Figure 98. Coupling of the vortex cylinder induction model with the wake model. Left: one turbine. Right: two turbines(WT1 and WT2). The"+" sign indicates that velocity fields are added, whereas"x" indicates a flow field merging [31].

The most obvious interpretation that can be made in this case is the excess power production decrease in the lateral region. Since the blockage models are the same, to compare the wake model, while the power production decrease in the lateral area is regular in the Larsen wake model, there is only a decrease in the far-wake region in the Jensen wake model. The idea of coupling the wake and blockage models is not a common topic in the literature. To couple these two models, it is necessary to establish a connection between them: the thrust coefficient. According to Nygaard's study, the input value of blockage models is the thrust coefficient. In addition, the blockage (solid body blockage) caused by the presence of turbines changes the wind speed. Therefore, the model's output creates an input value for another turbine. This problem is solved for all wind speeds and directions [6]. The wake model is calculated from upwind to downwind. Thus, different ct values are used for each turbine.

5.9.1. Jensen-Vortex Cylinder Coupled Model

In coupled model analysis, there is interaction in both the upstream and downstream areas. When examining two areas, it is clearly seen that the wake effect is more dominant. As seen in Figure 99-101-103, the power results are very similar to the results of the wake models. The wind speed drop in the wake model is quite large compared to blockage model. For this reason, the blockage effect is observed less in the flowmaps in Figure 100-102-104.

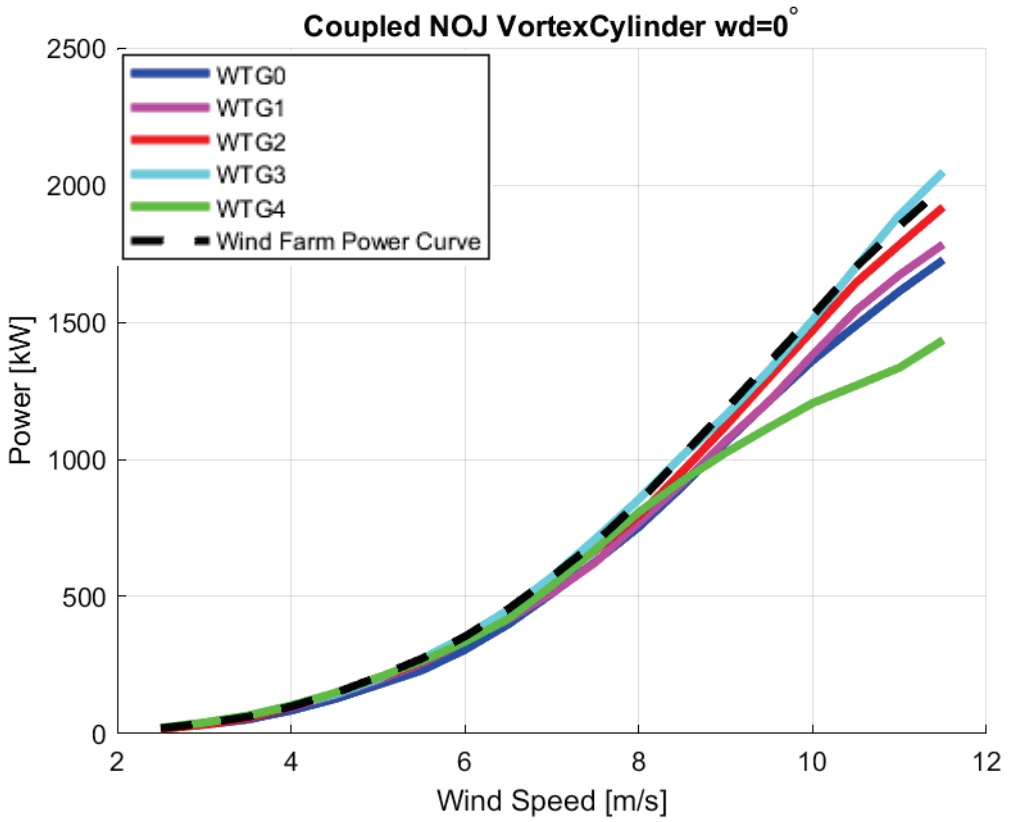

Figure 99. Power Curve of Coupled Jensen and Vortex Cylinder Model at 0° wind direction.

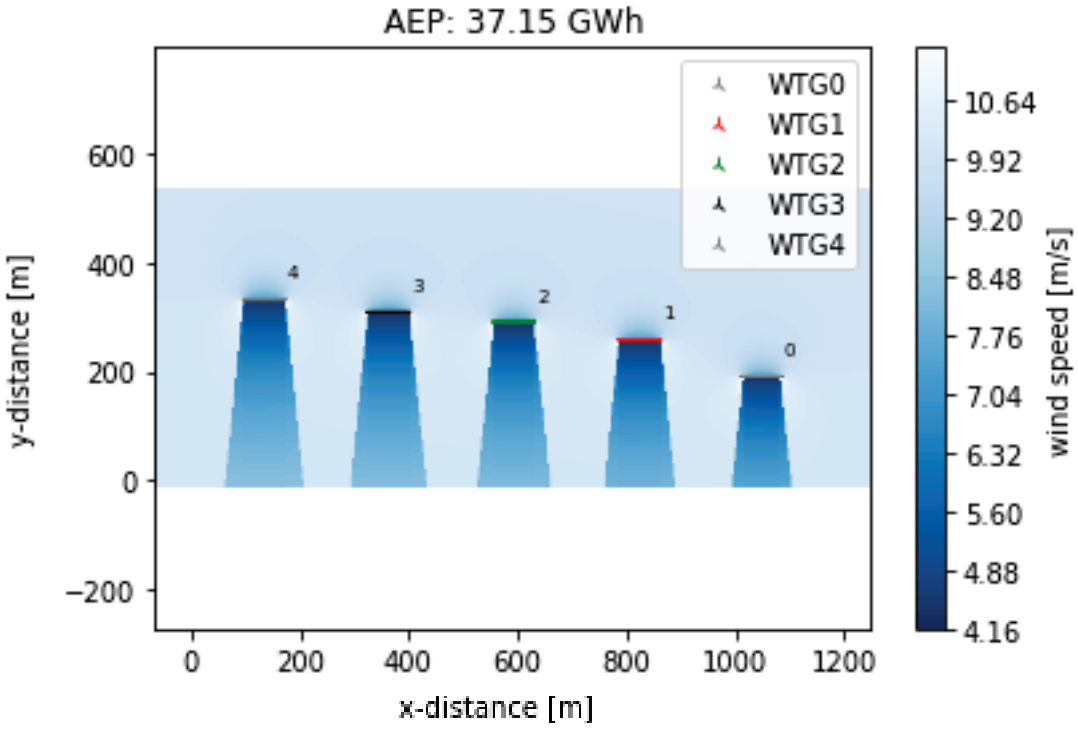

Figure 100. Flow map of Coupled Jensen and Vortex Cylinder Model at 0° wind direction.

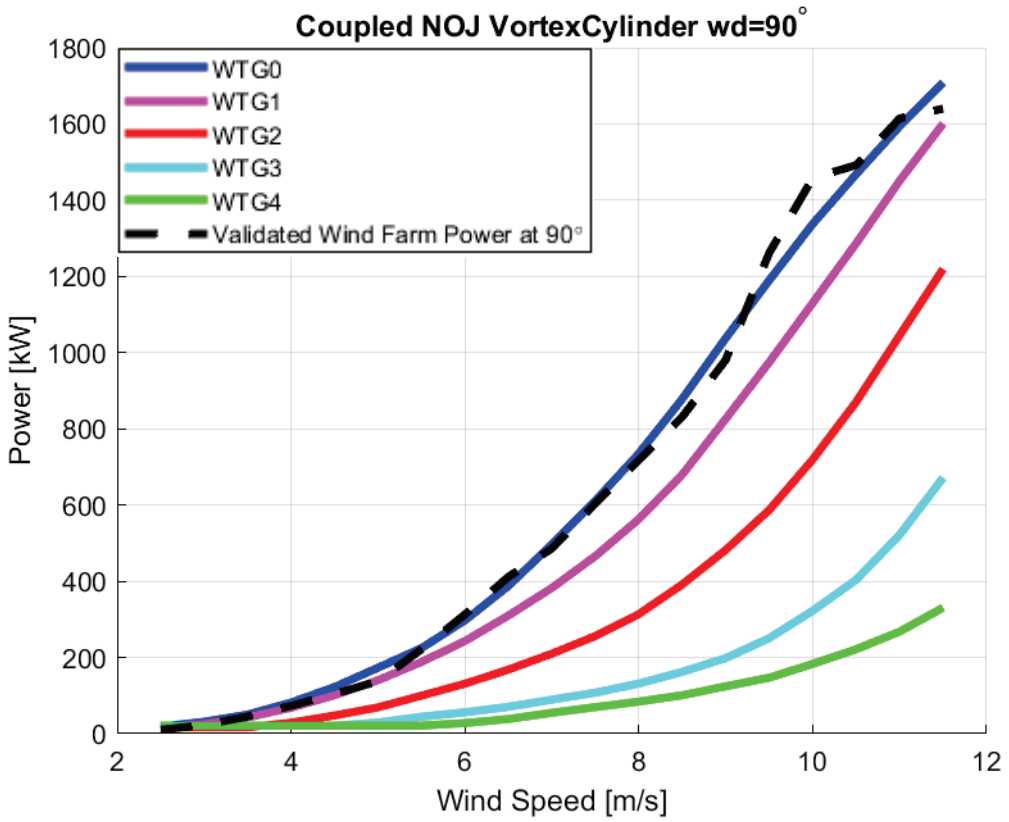

Figure 101. Power Curve of Coupled Jensen and Vortex Cylinder Model at 90° wind direction.

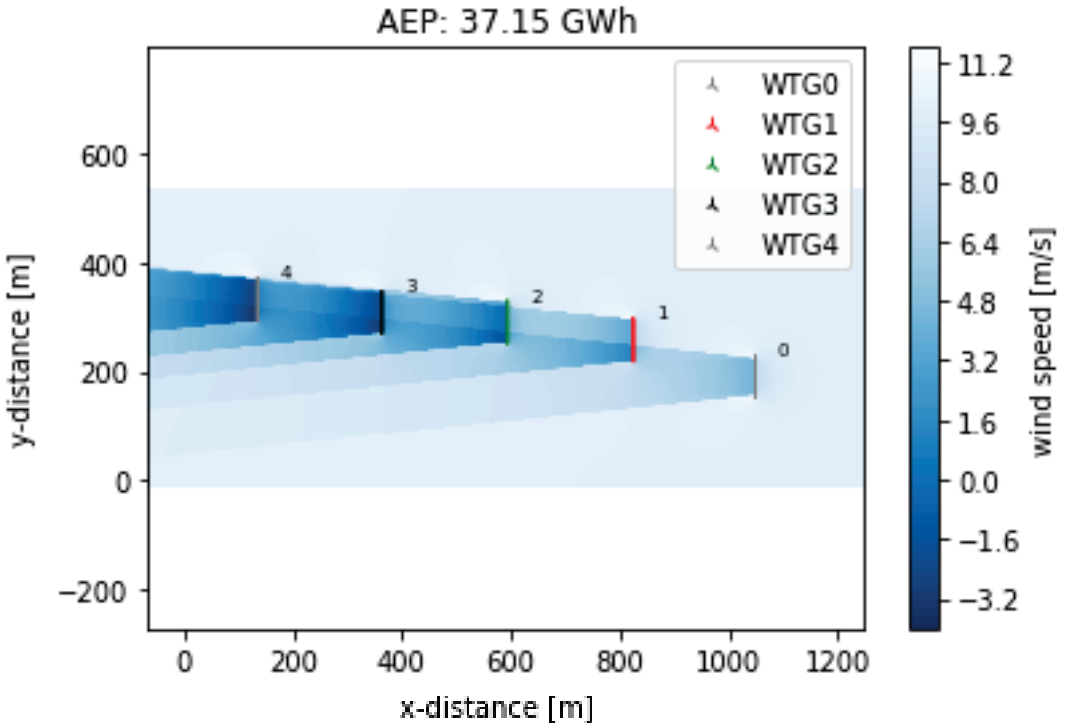

Figure 102. Flow map of Coupled Jensen and Vortex Cylinder Model at 90° wind direction.

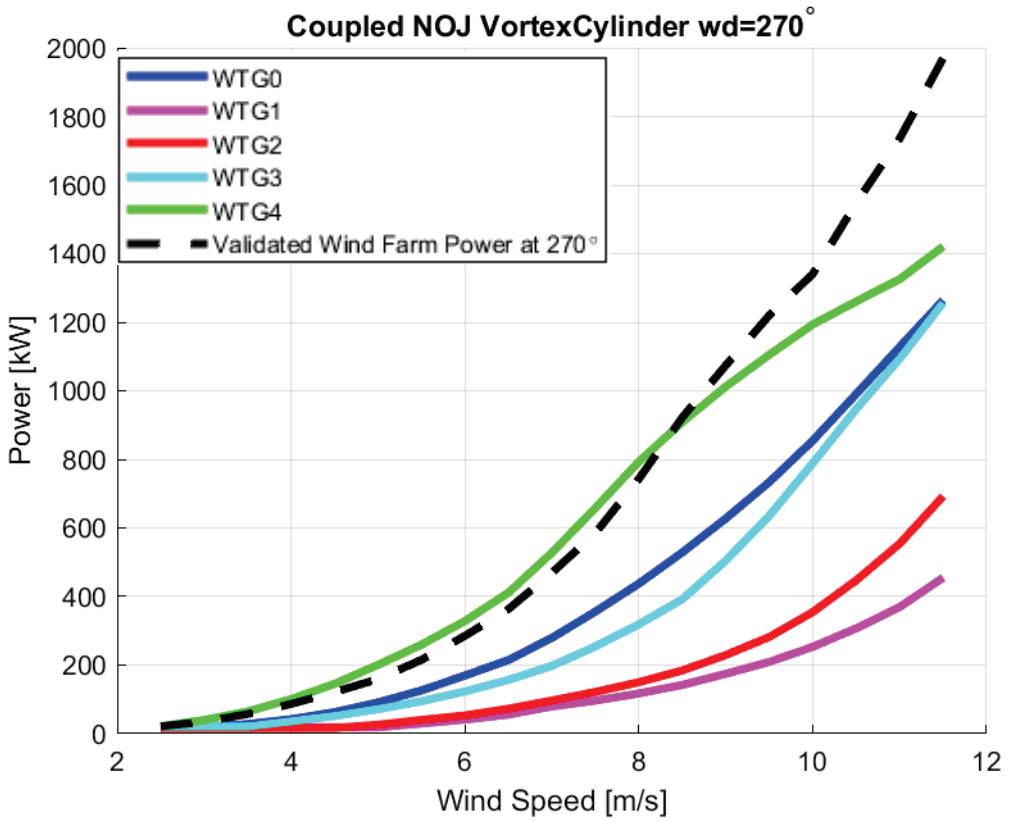

Figure 103. Power Curve of Coupled Jensen and Vortex Cylinder Model at 270° wind direction.

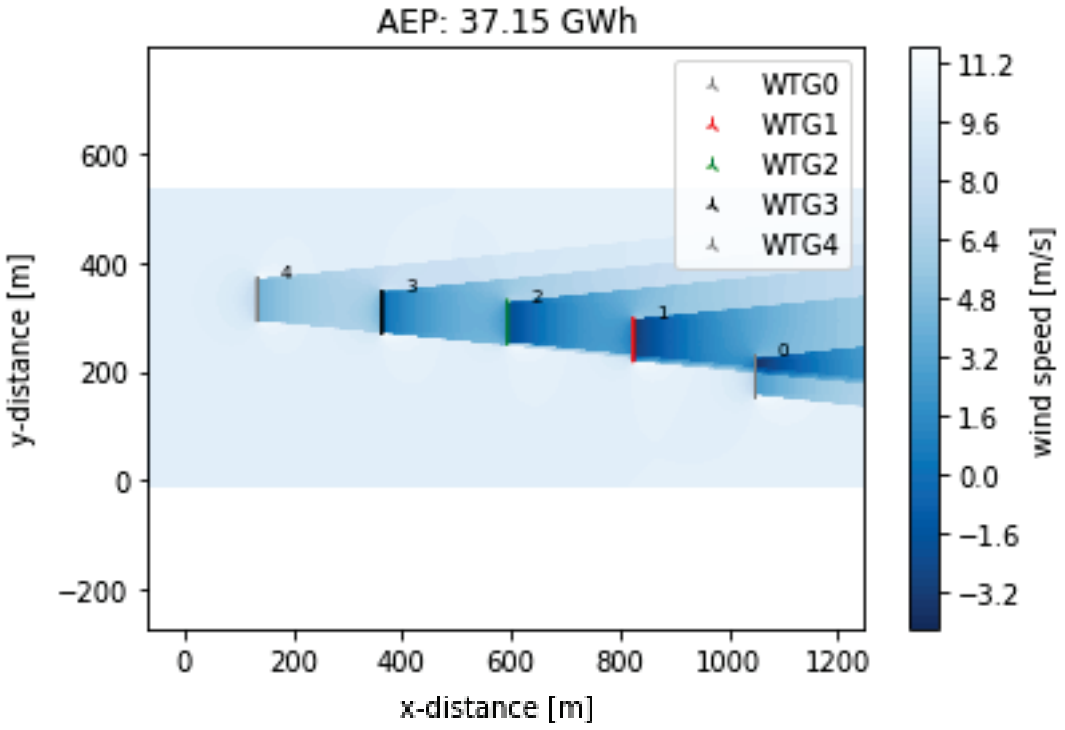

Figure 104. Flow map of Coupled Jensen and Vortex Cylinder Model at 270° wind direction.

5.9.2. Jensen-Self Similarity 2020 Coupled Model

In the coupled model, the wake effect is observed downstream and the blockage effect is ideally observed upstream, although the area upstream of the rear turbine is also in the downstream area of the front turbine. That is, at the 90° and 270° wind directions, wake and blockage effects are intertwined for the WTG1-2-3.

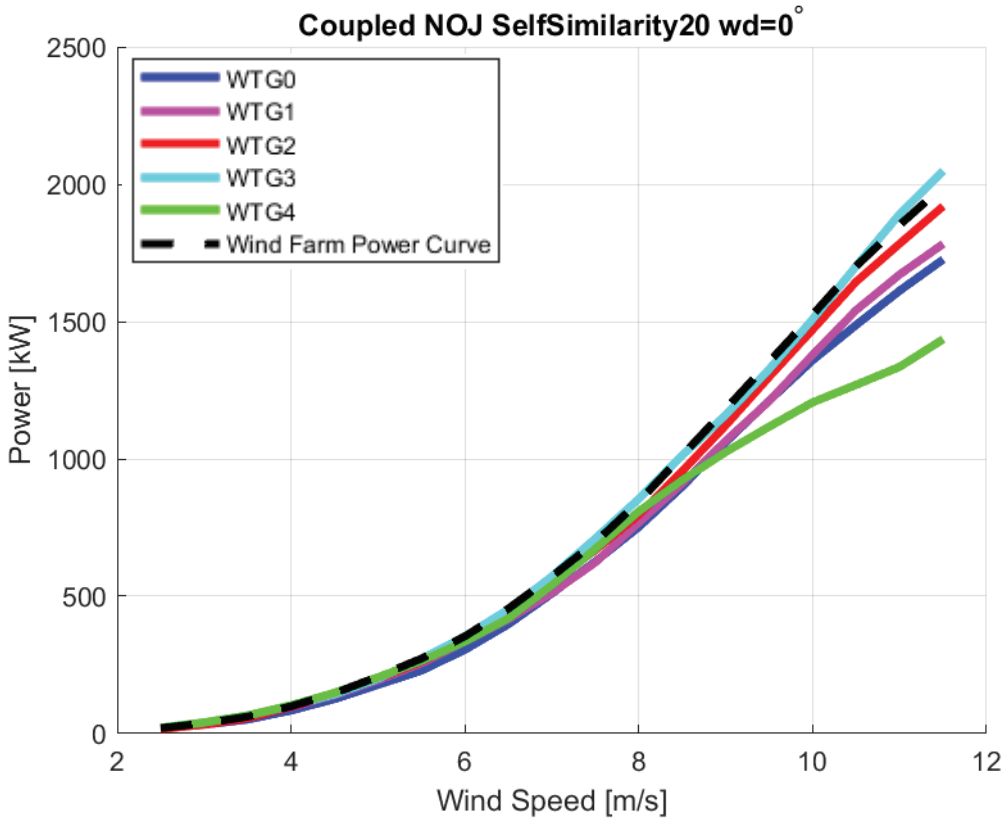

Figure 105. Power Curve of Coupled Jensen and Self Similarity 2020 Model at 0° wind direction.

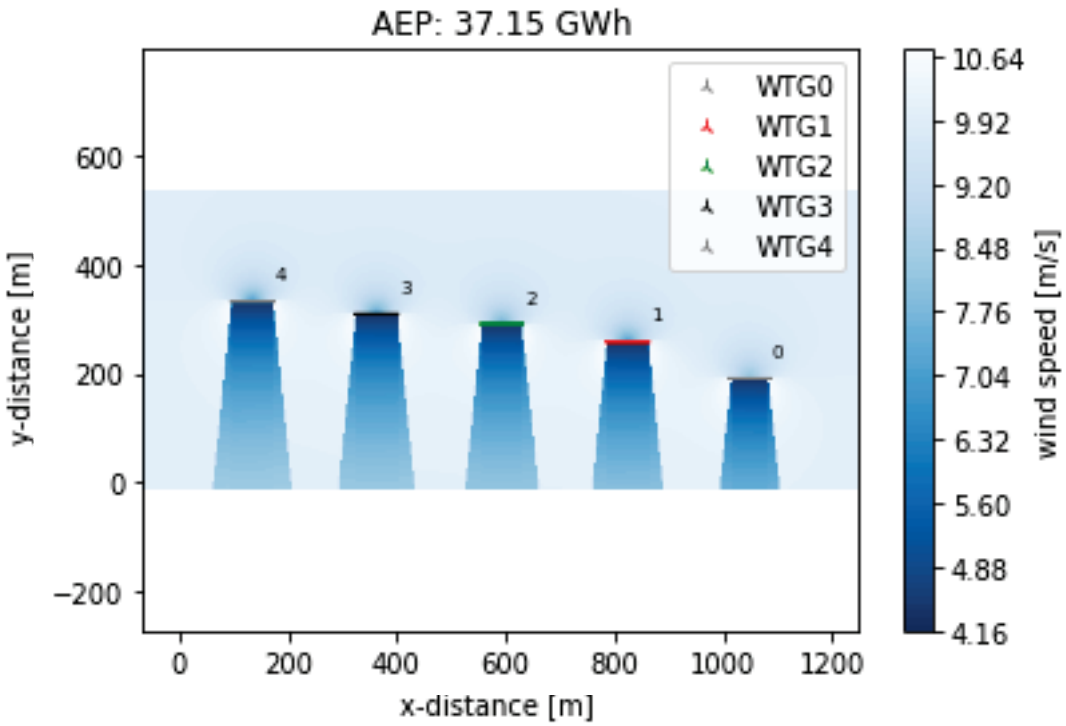

Figure 106. Flow map of Coupled Jensen and Self Similarity 2020 Model at 0° wind direction.

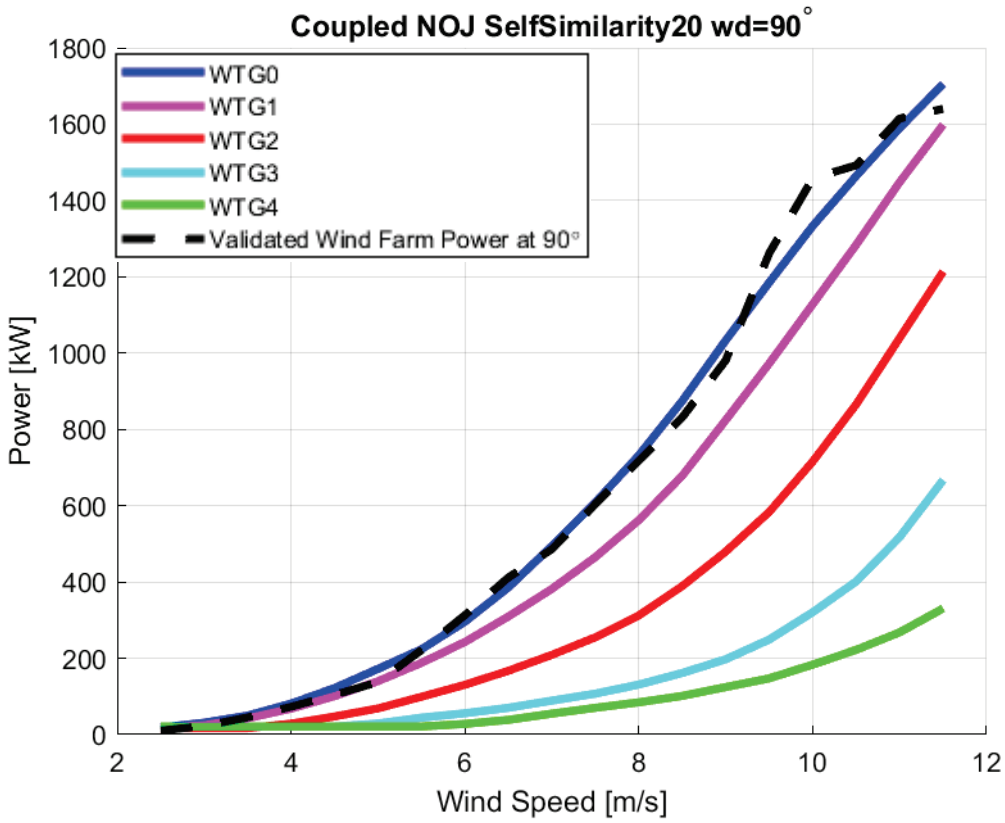

Figure 107. Power Curve of Coupled Jensen and Self Similarity 2020 Model at 90° wind direction.

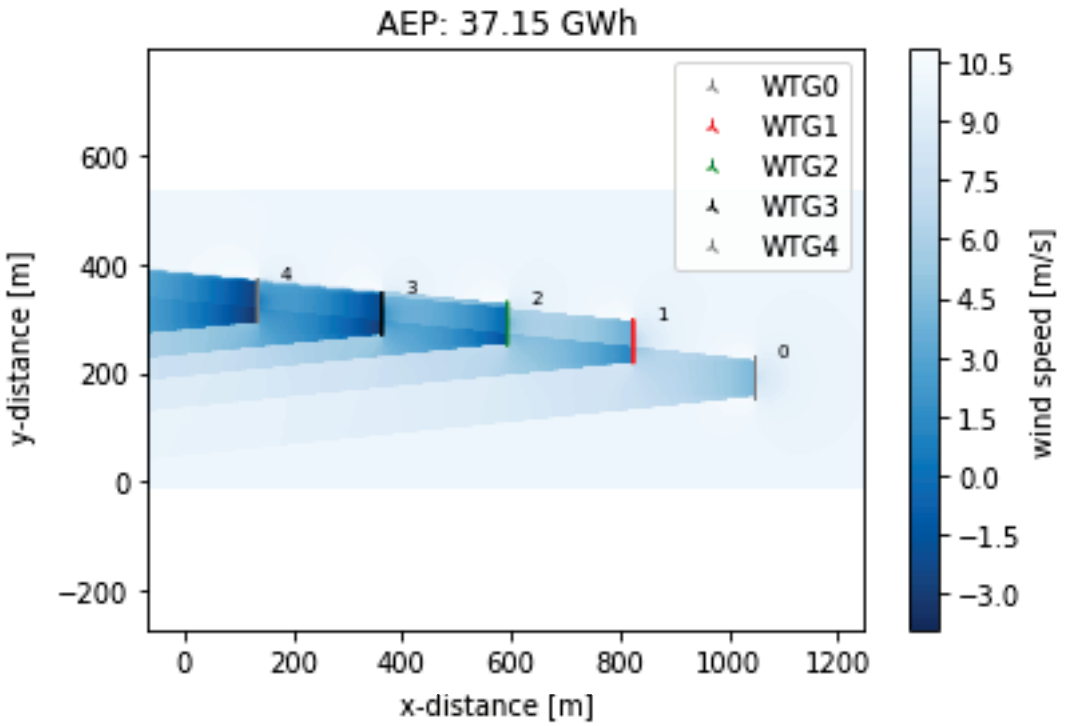

Figure 108. Flow map of Coupled Jensen and Self Similarity 2020 Model at 90° wind direction.

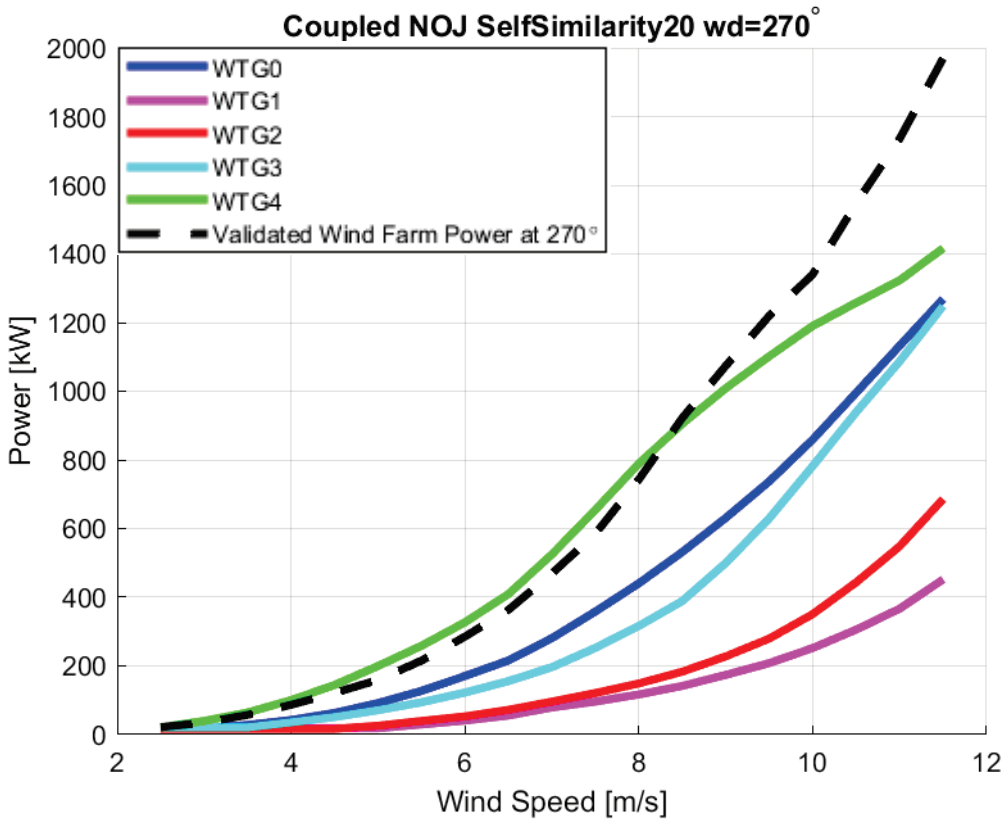

Figure 109. Power Curve of Coupled Jensen and Self Similarity 2020 Model at 270° wind direction.

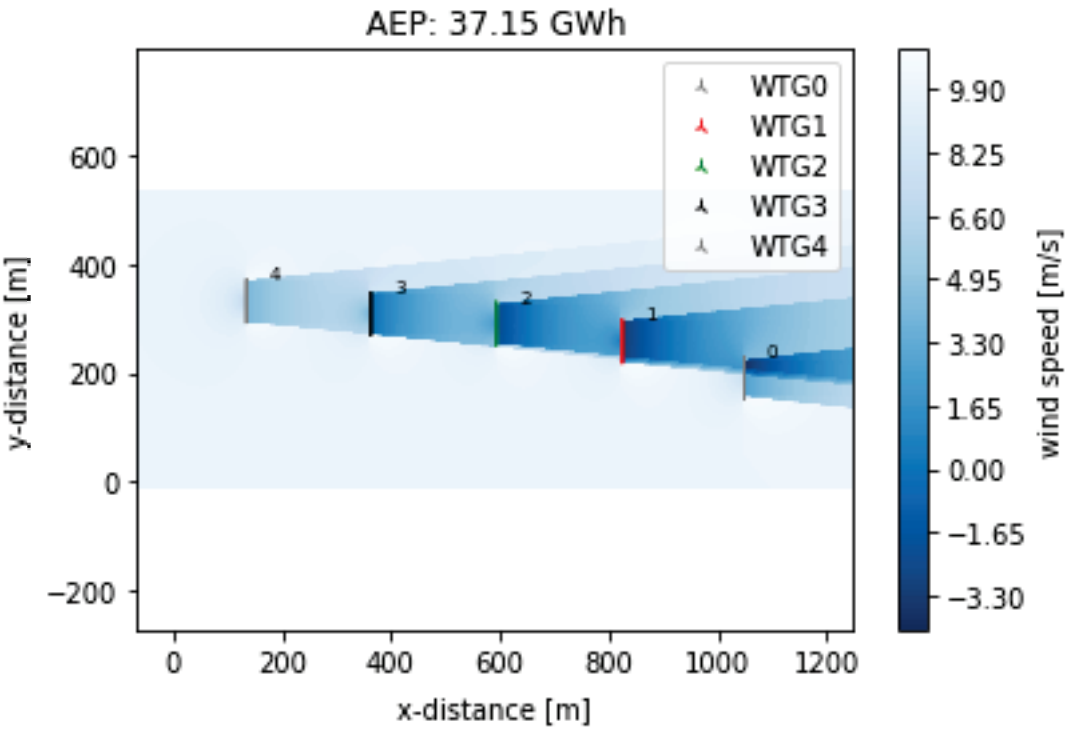

Figure 110. Flow map of Coupled Jensen and Self Similarity 2020 Model at 270° wind direction.

5.9.3. Larsen-Vortex Cylinder Coupled Model

The characteristic of the Larsen wake model is observed in the coupled model. The wake effect, which concentrates in a straight line just behind the turbine in the downstream area, loses its effect in the lateral area. Blockage effect is more minimal than wake.

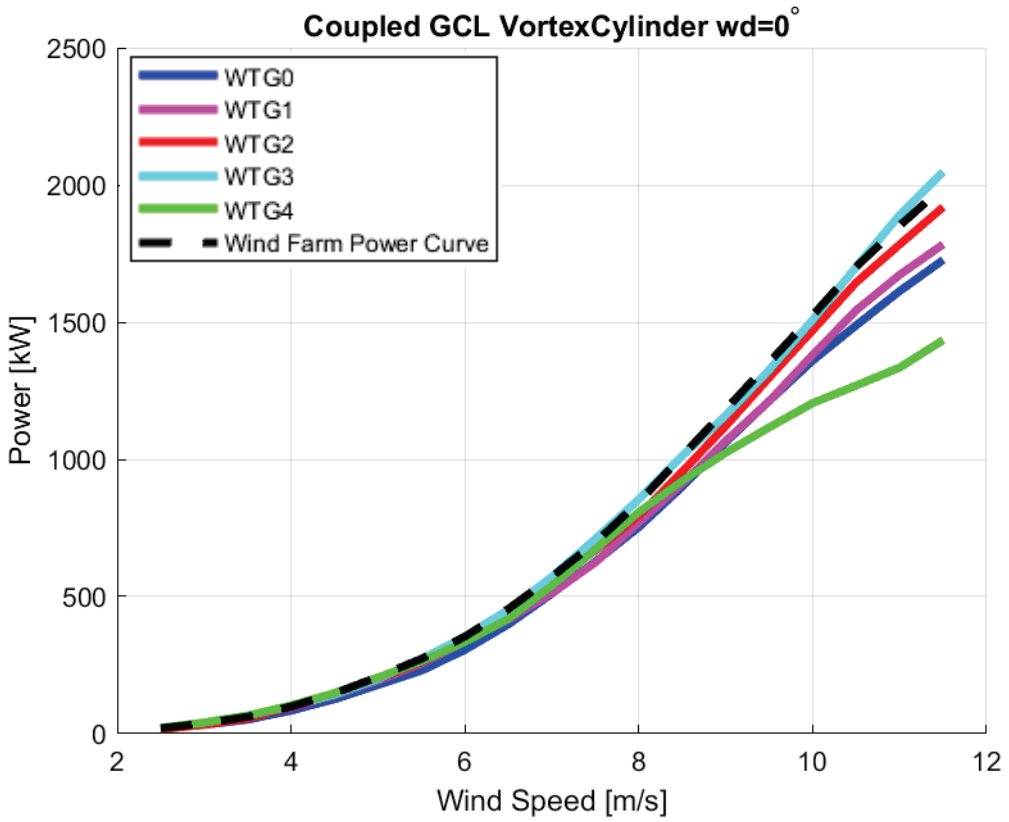

Figure 111. Power Curve of Coupled Larsen and Vortex Cylinder Model at 0° wind direction.

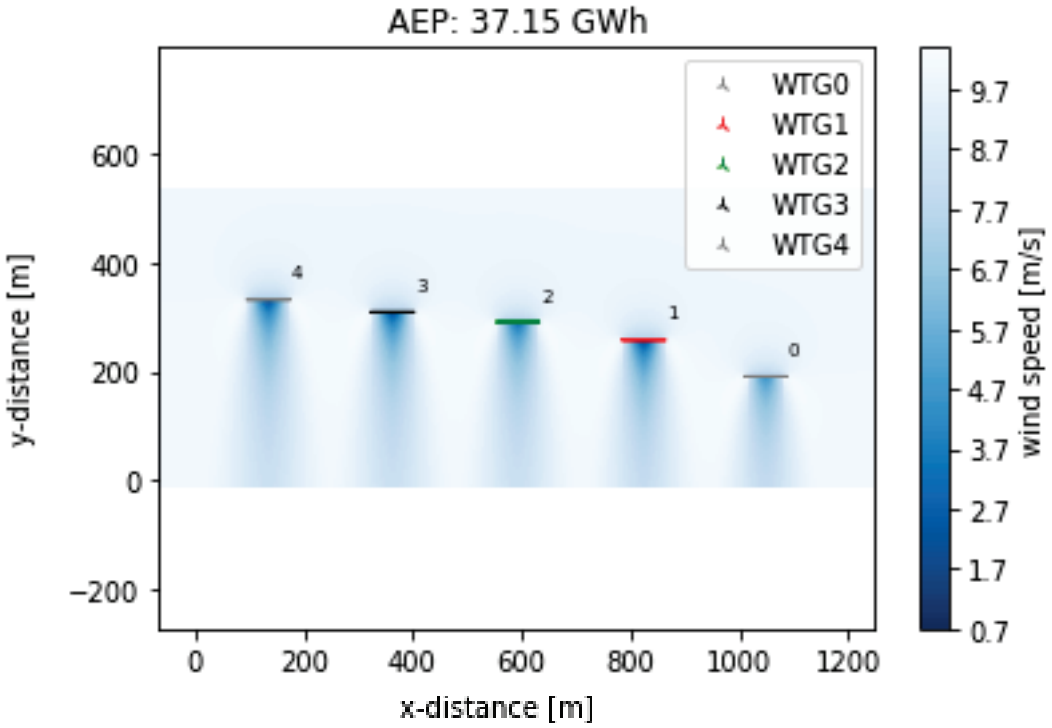

Figure 112. Flow map of Coupled Larsen and Vortex Cylinder Model at 0° wind direction.

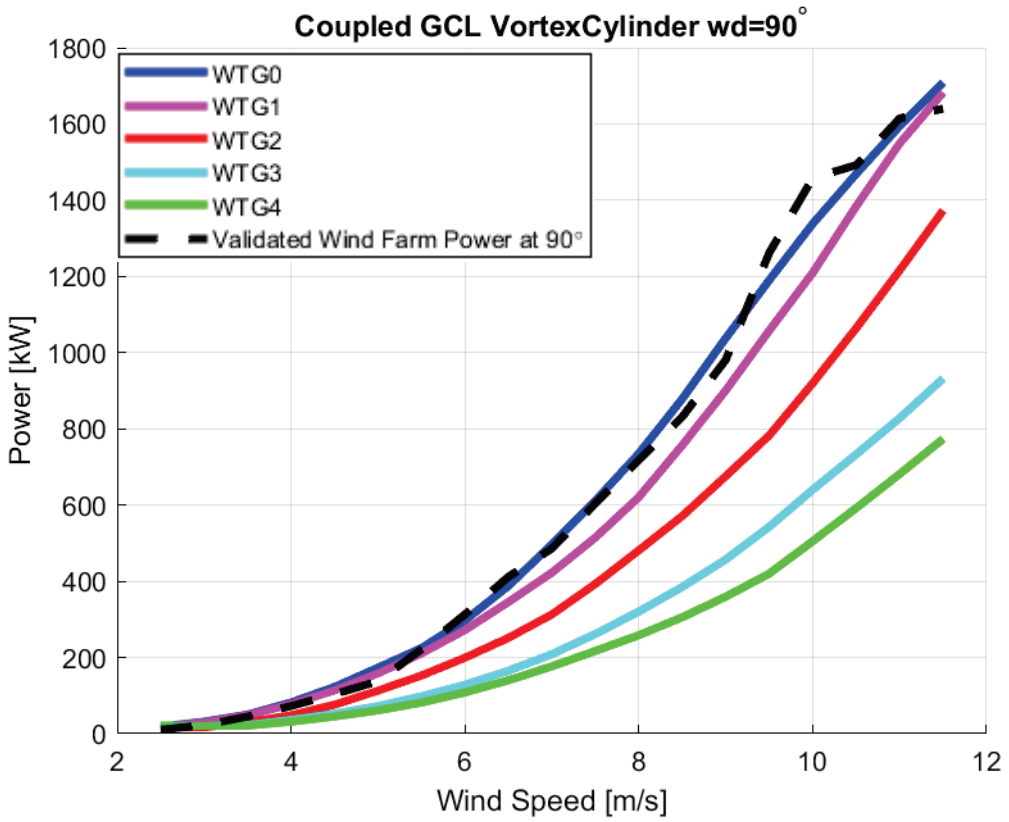

Figure 113. Power Curve of Coupled Larsen and Vortex Cylinder Model at 90° wind direction.

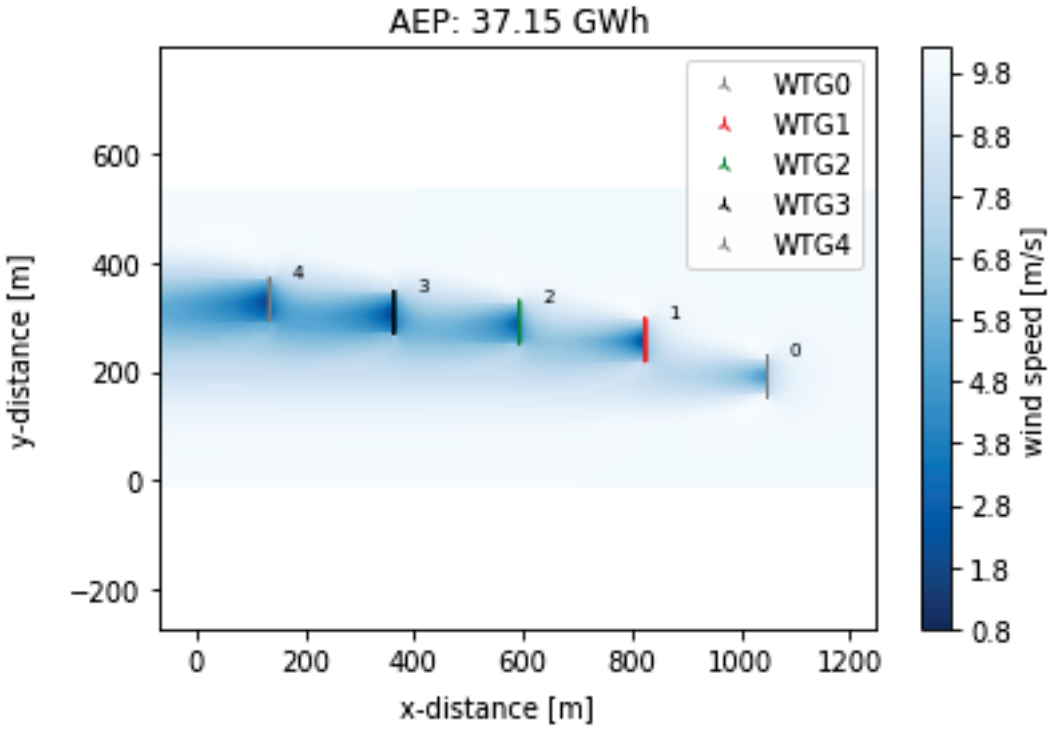

Figure 114. Flow map of Coupled Larsen and Vortex Cylinder Model at 90° wind direction.

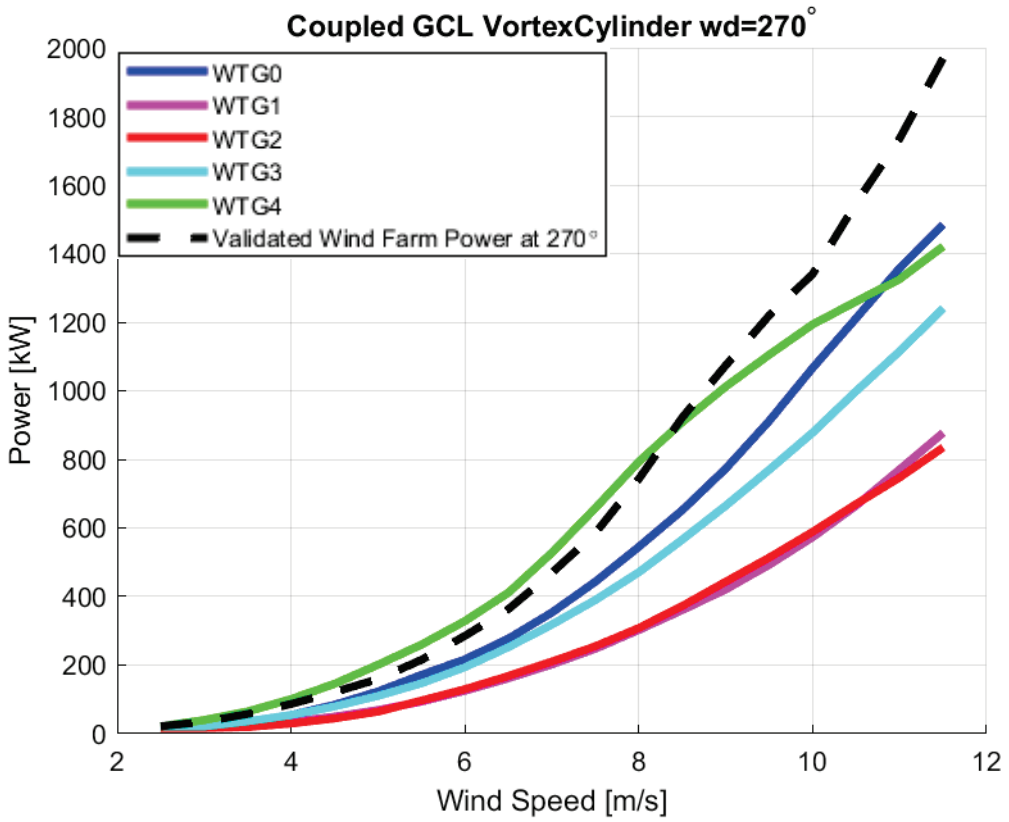

Figure 115. Power Curve of Coupled Larsen and Vortex Cylinder Model at 270° wind direction.

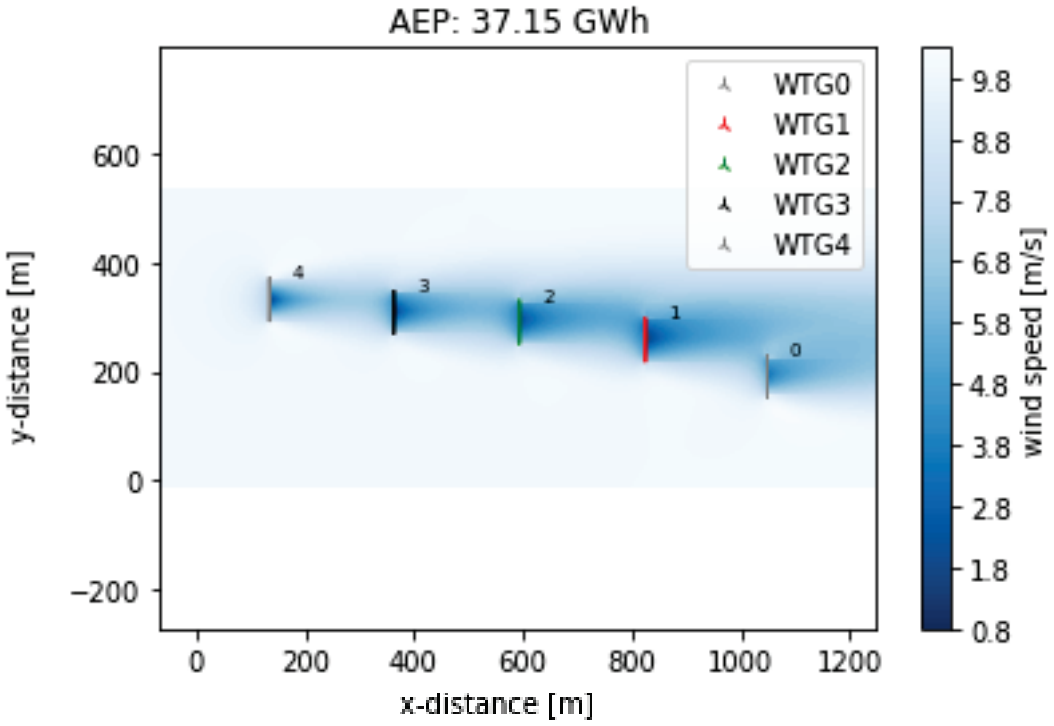

Figure 116. Flow map of Coupled Larsen and Vortex Cylinder Model at 270° wind direction.

5.9.4. Larsen-Self Similarity 2020 Coupled Model

When examining only the blockage effect, the self similarity 2020 model spreads linearly. In the coupled model, it spreads relatively more circularly.

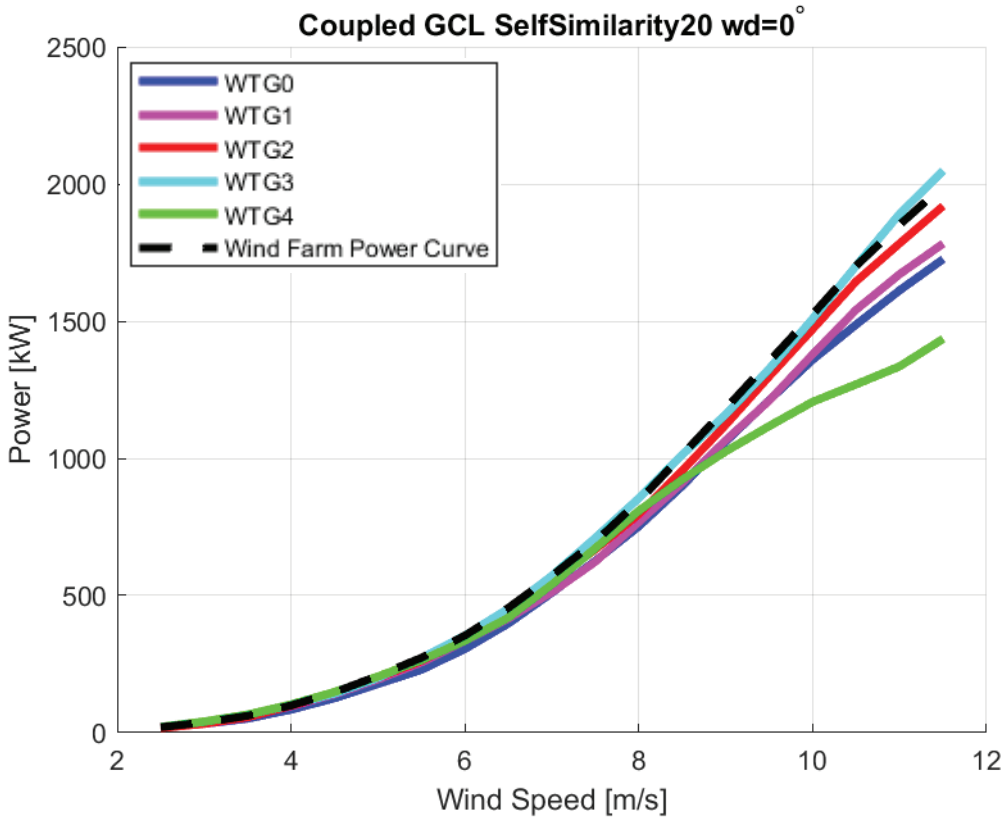

Figure 117. Power Curve of Coupled Larsen and Self Similarity 2020 Model at 0° wind direction.

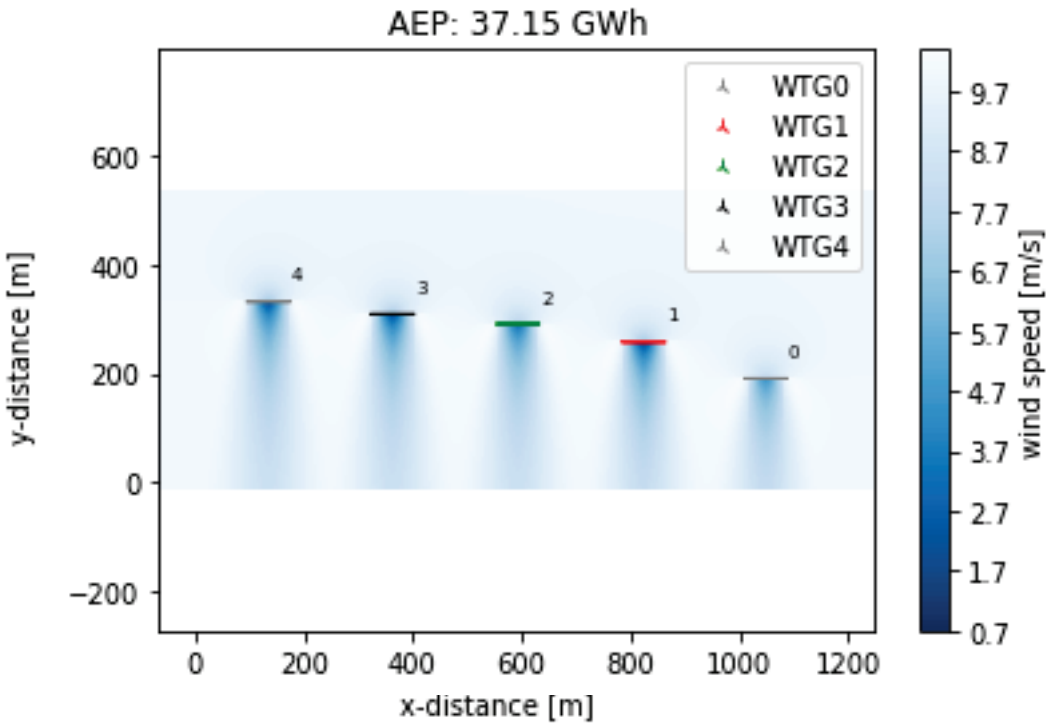

Figure 118. Flow map of Coupled Larsen and Self Similarity 2020 Model at 0° wind direction.

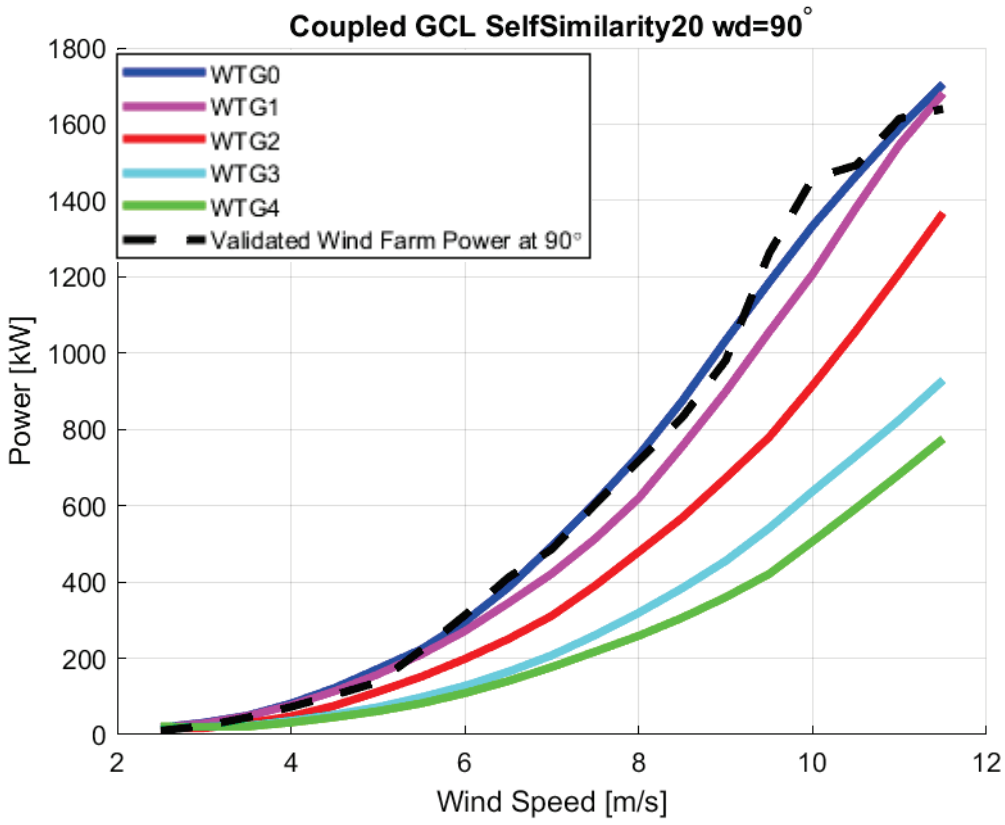

Figure 119. Power Curve of Coupled Larsen and Self Similarity 2020 Model at 90° wind direction.

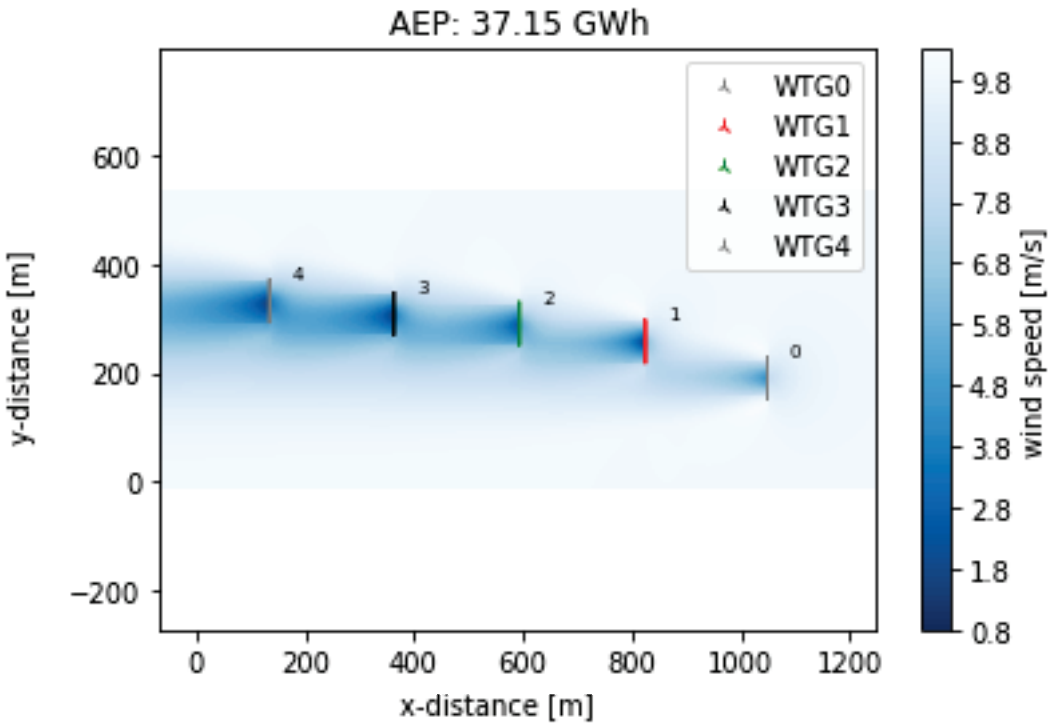

Figure 120. Flow map of Coupled Larsen and Self Similarity 2020 Model at 90° wind direction.

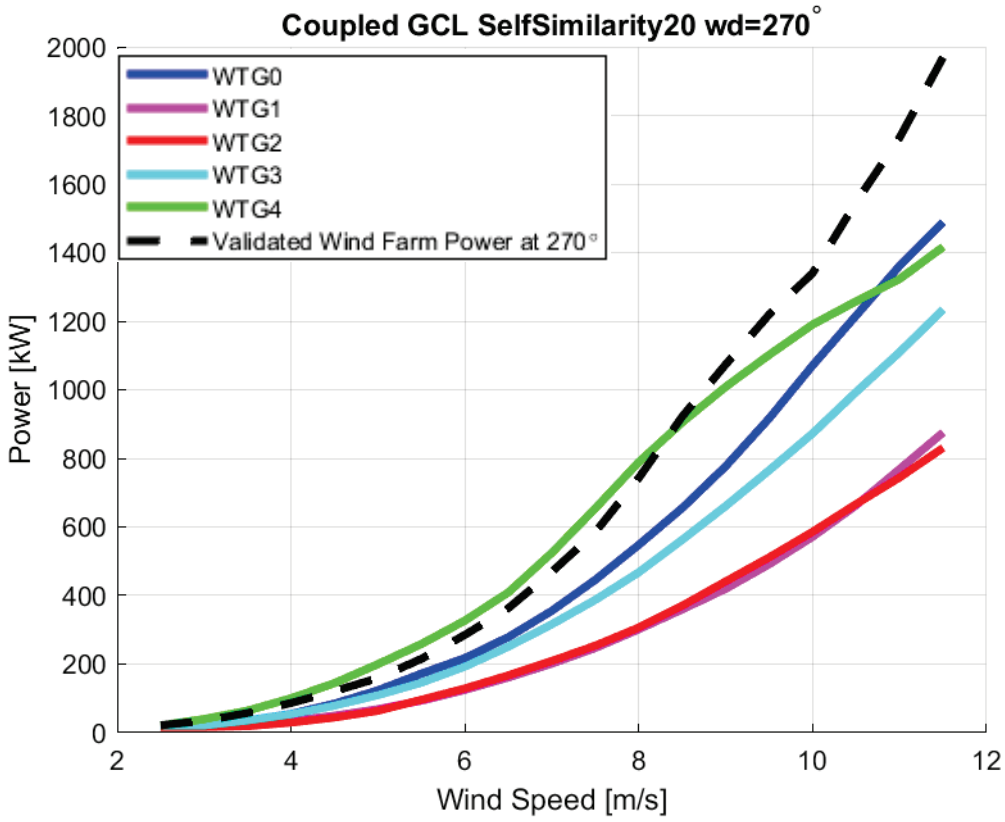

Figure 121. Power Curve of Coupled Larsen and Self Similarity 2020 Model at 270° wind direction.

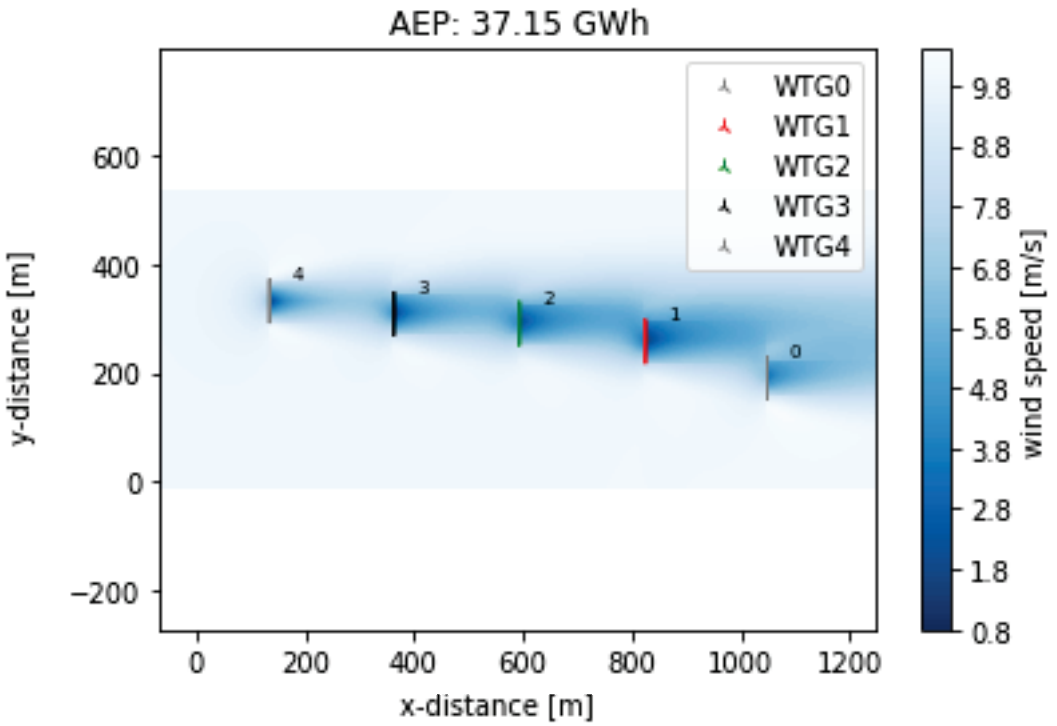

Figure 122. Flow map of Coupled Larsen and Self Similarity 2020 Model at 270° wind direction.

5.9.5. Turbo Gaussian-Vortex Cylinder Coupled Model

As with other coupled models, power results are very similar to wake model results. Because the effect of the blockage model is small. As seen in Figure 124-126-128, the wake area is distinct, linear and wide. Since the wind speed decrease in the wake effect is too much compared to the blockage, the wind speed change in the induction zone is not obvious.

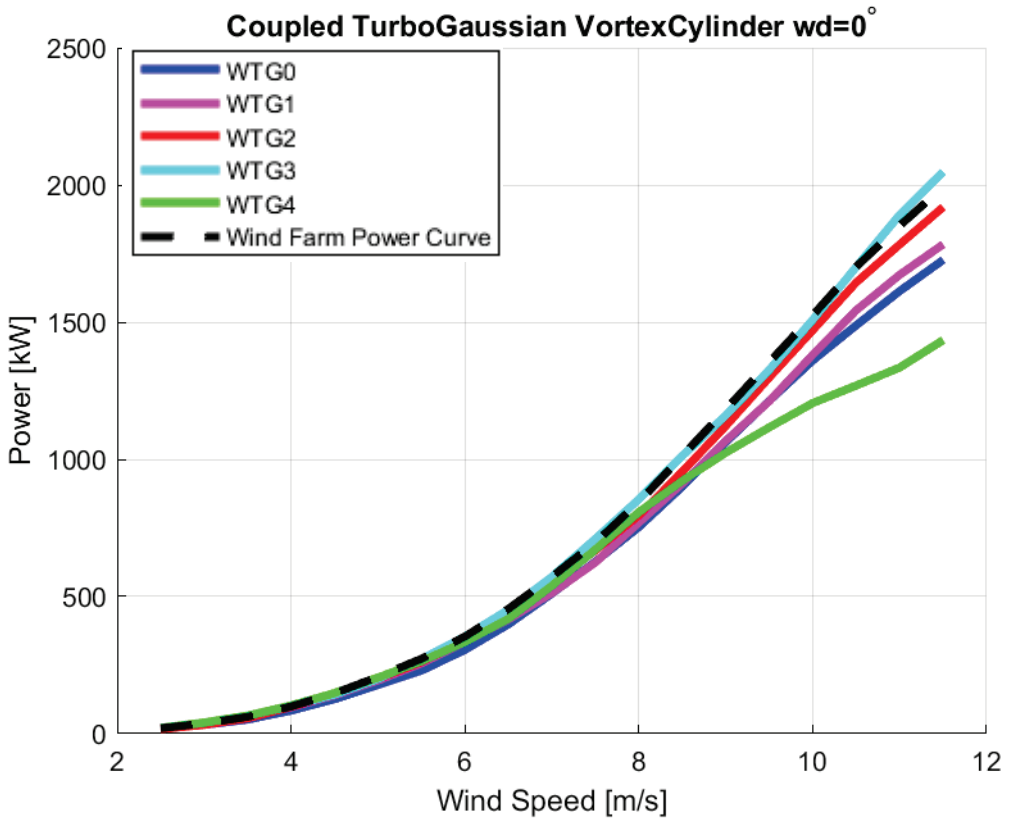

Figure 123. Power Curve of Coupled Turbo Gaussian and Vortex Cylinder Model at 0° wind direction.

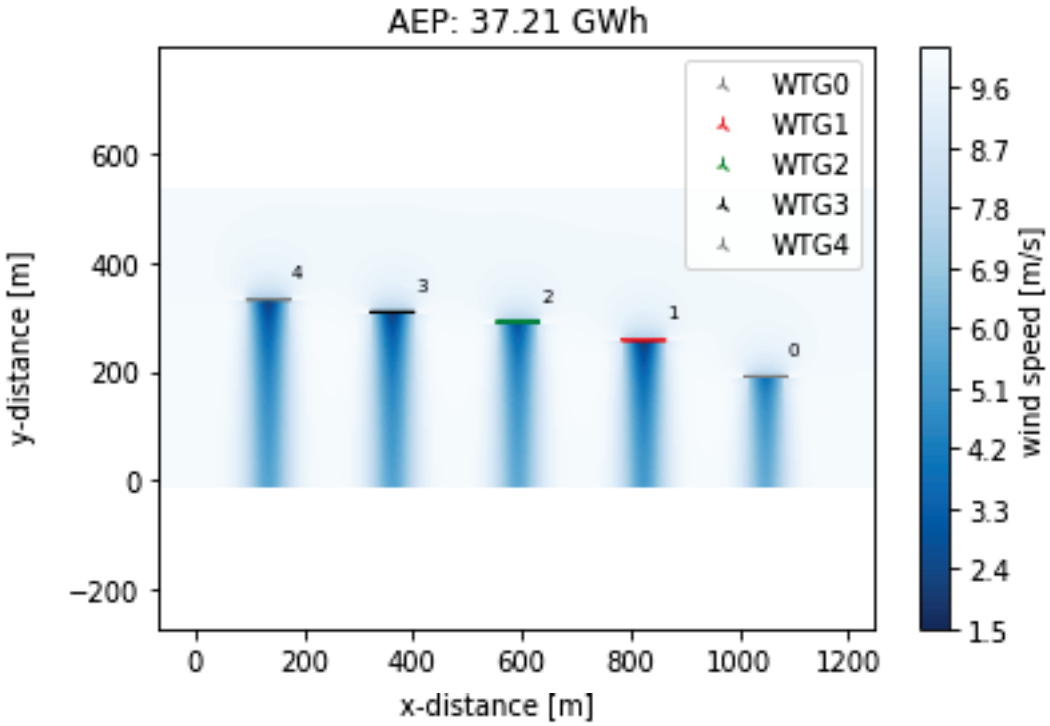

Figure 124. Flow map of Coupled Turbo Gaussian and Vortex Cylinder Model at 0° wind direction.

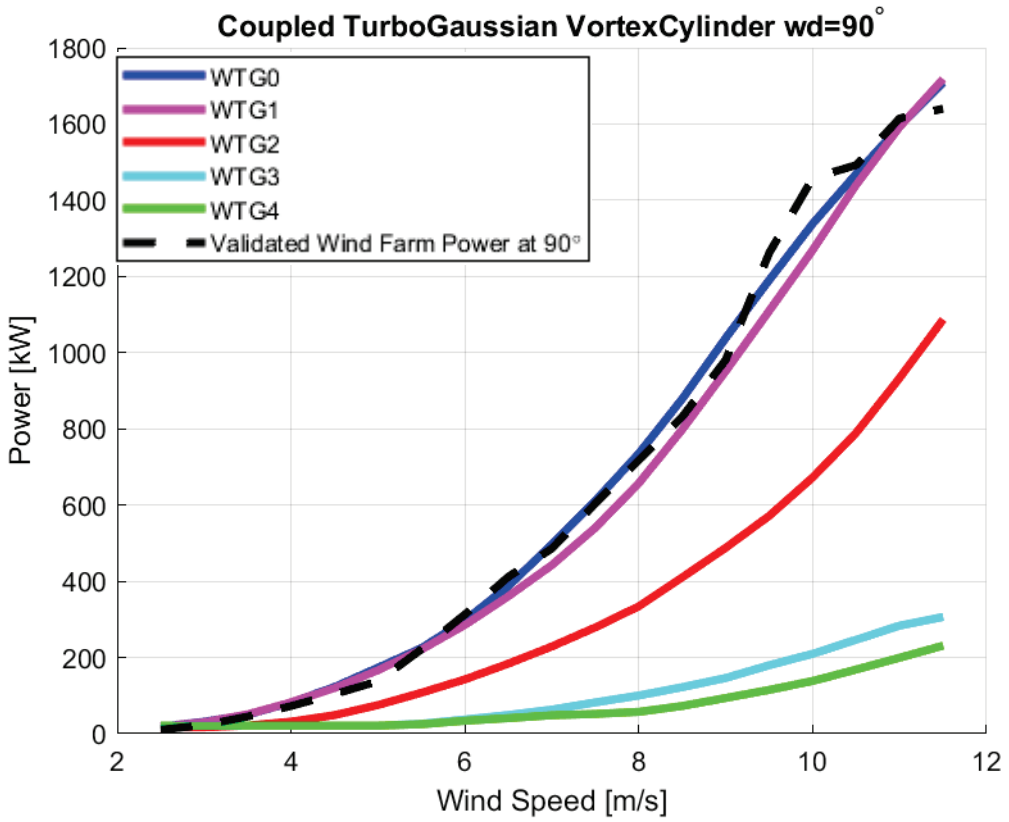

Figure 125. Power Curve of Coupled Turbo Gaussian and Vortex Cylinder Model at 90° wind direction.

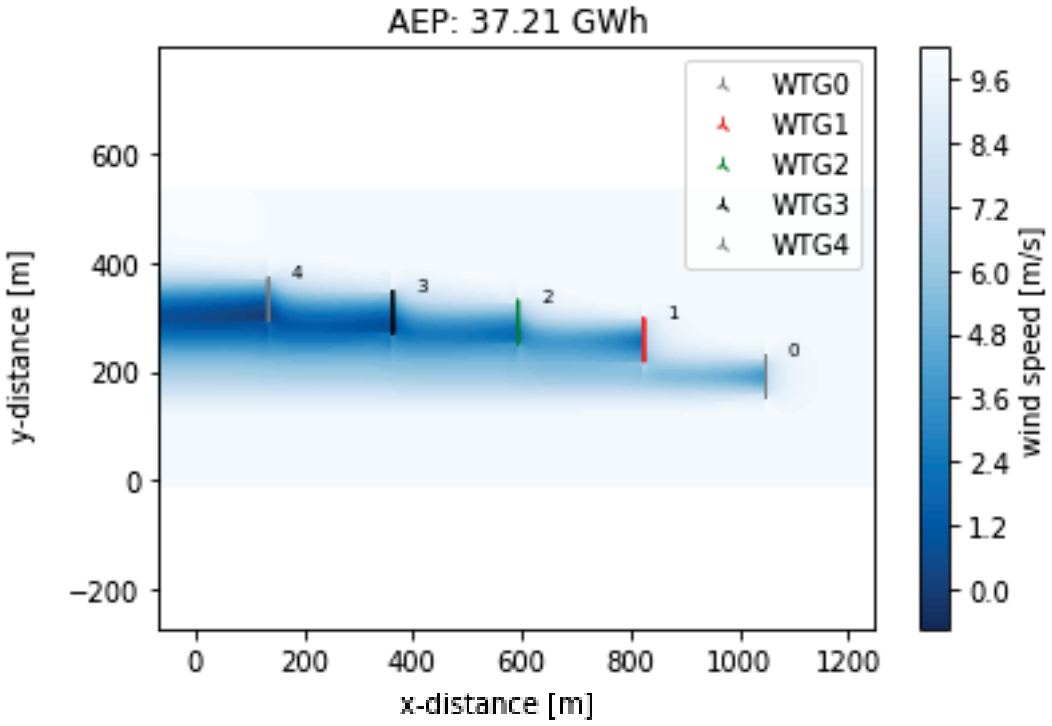

Figure 126. Flow map of Coupled Turbo Gaussian and Vortex Cylinder Model at 90° wind direction.

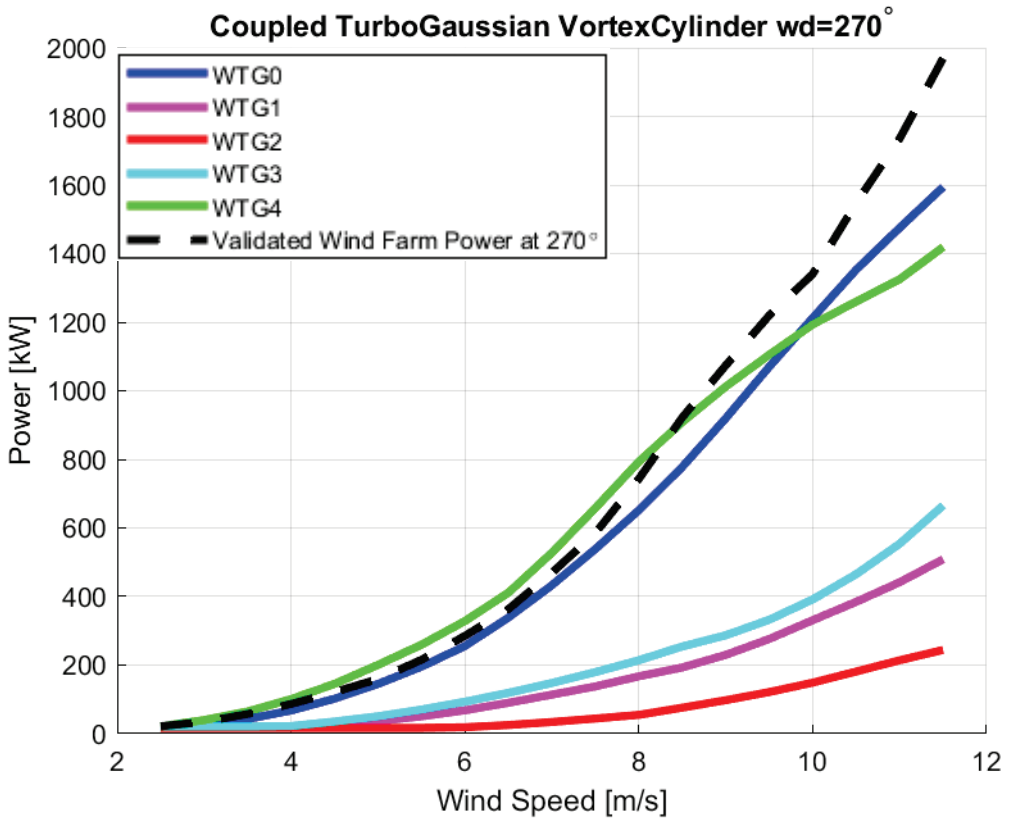

Figure 127. Power Curve of Coupled Turbo Gaussian and Vortex Cylinder Model at 270° wind direction.

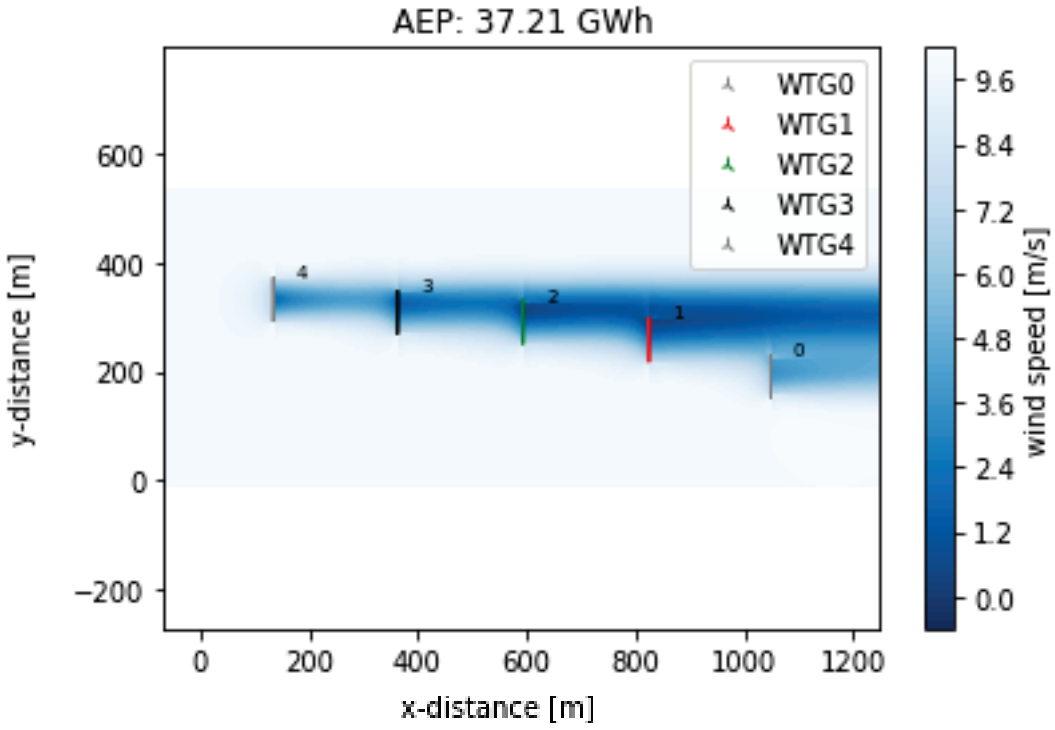

Figure 128. Flow map of Coupled Turbo Gaussian and Vortex Cylinder Model at 270° wind direction.

5.9.6. Turbo Gaussian-Self Similarity 2020 Coupled Model

In the last coupled model, Turbo Gaussian-Self Similarity 2020, wake and blockage effects are observed separately. Power curve data has parallel results with wake model. In addition, as with other flowmaps, WTG2-3-4 is under wake effect at 0° wind direction while WTG1 is under partial wake effect. WTG1-2-3 is under wake effect at 270° wind direction while partial wake effect is observed at WTG0.

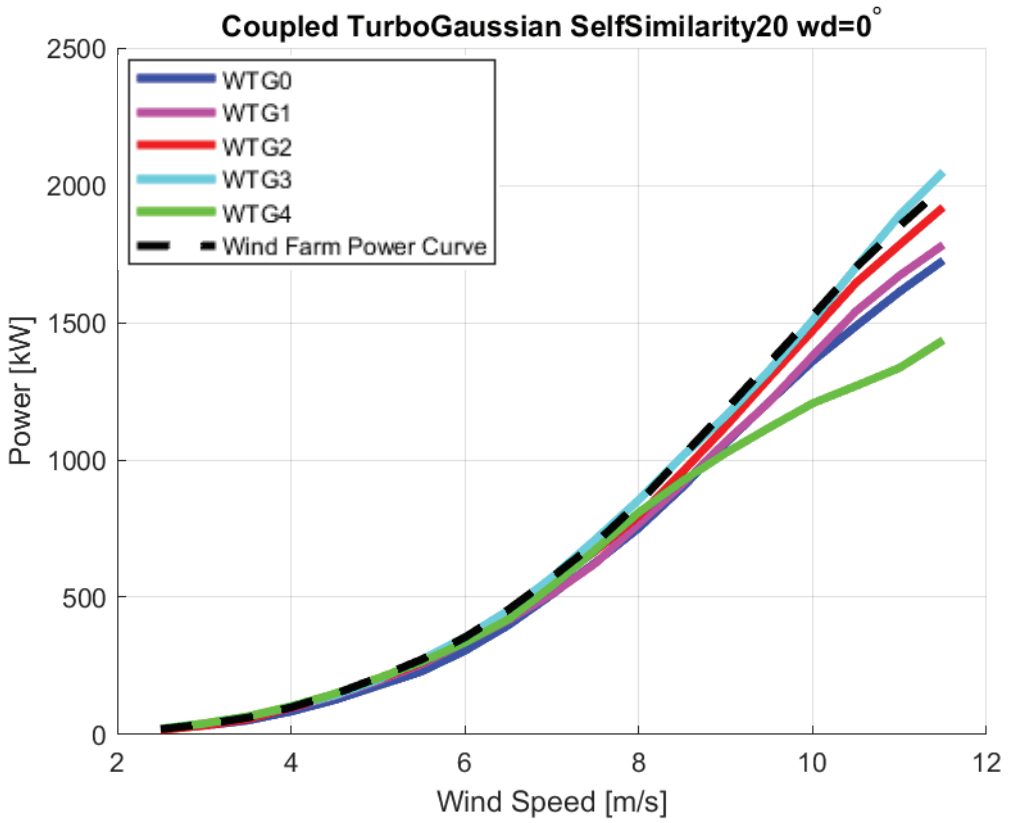

Figure 129. Power Curve of Coupled Turbo Gaussian and Self Similarity 2020 Model at 0° wind direction.

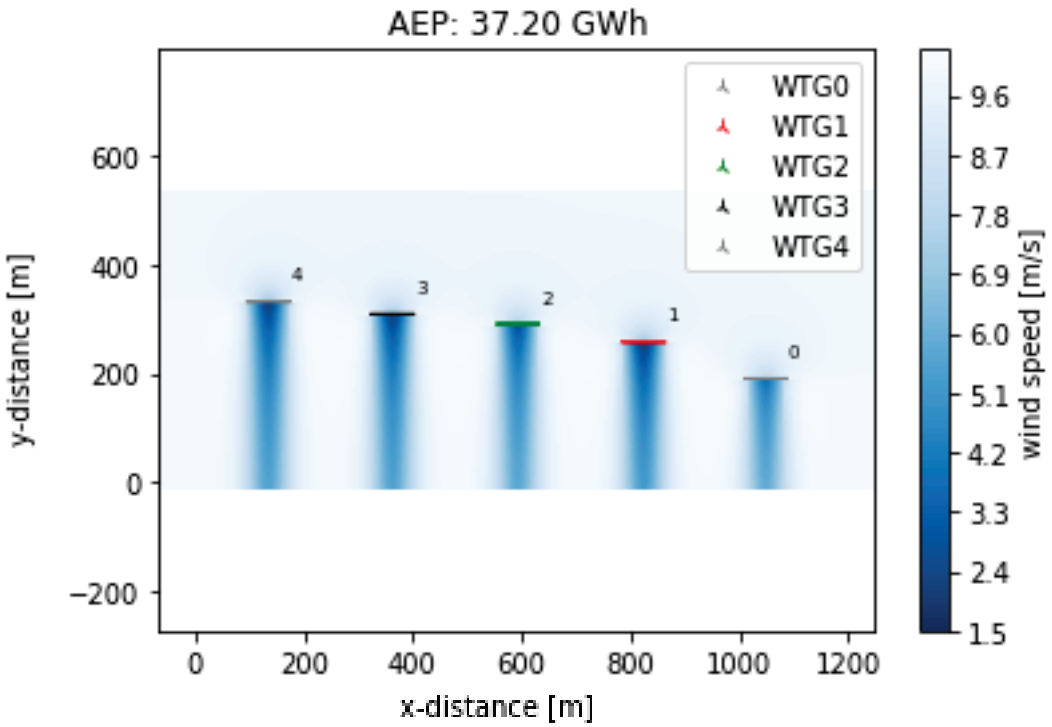

Figure 130. Flow map of Coupled Turbo Gaussian and Self Similarity 2020 Model at 0° wind direction.

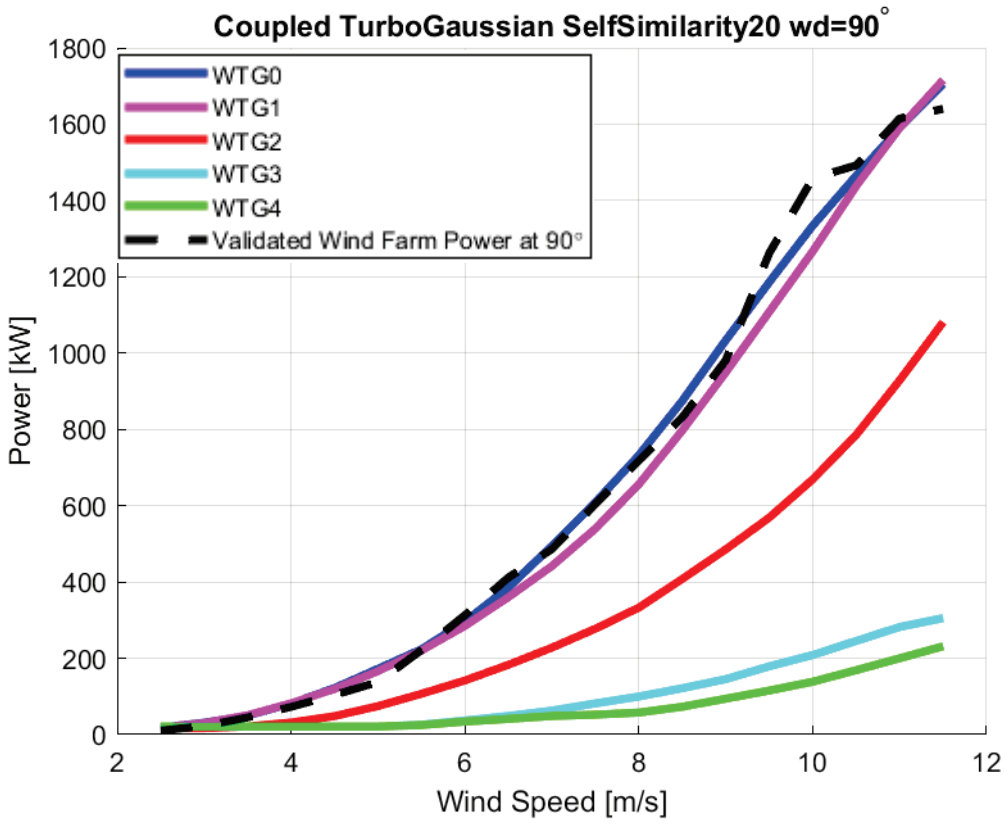

Figure 131. Power Curve of Coupled Turbo Gaussian and Self Similarity 2020 Model at 90° wind direction.

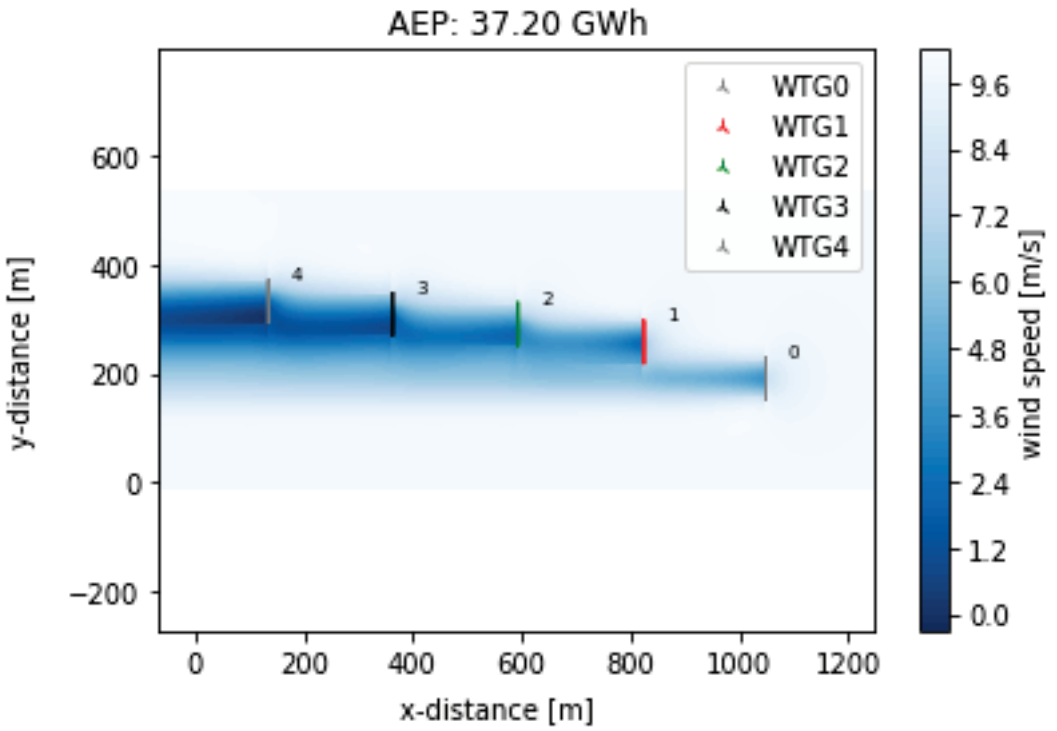

Figure 132. Flow map of Coupled Turbo Gaussian and Self Similarity 2020 Model at 90° wind direction.

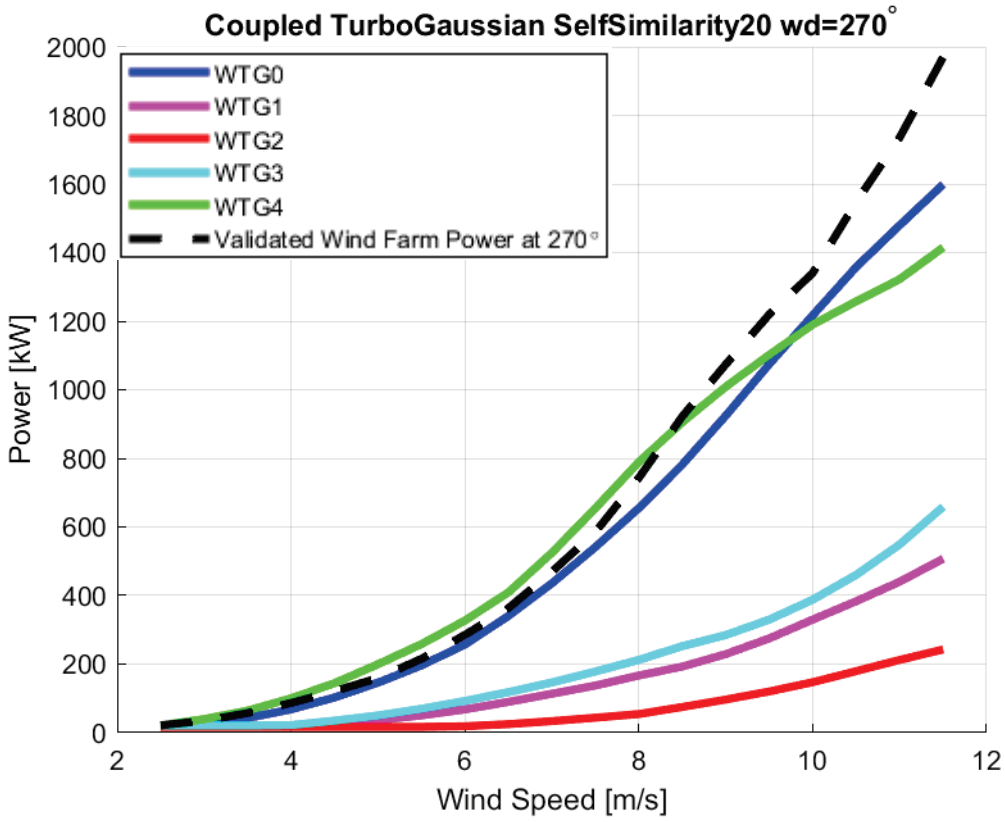

Figure 133. Power Curve of Coupled Turbo Gaussian and Self Similarity 2020 Model at 270° wind direction.

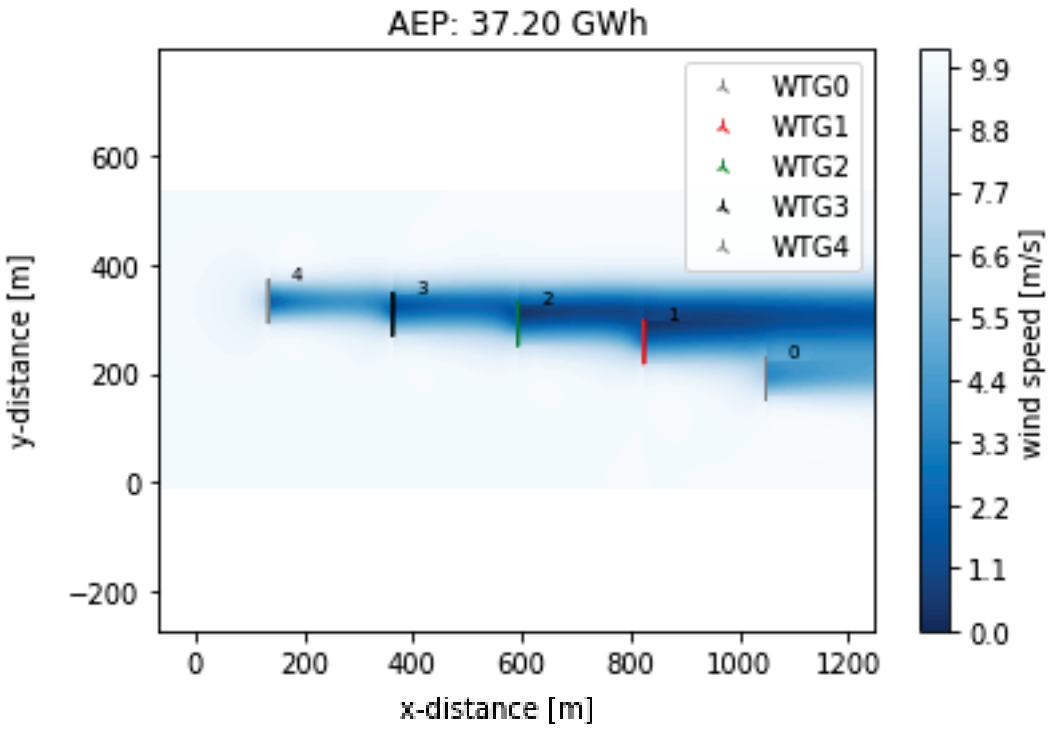

Figure 134. Flow map of Coupled Turbo Gaussian and Self Similarity 2020 Model at 270° wind direction.

As seen in Table 4, model results seem to converge to reality, except for the exceptional cases of WTG4. The wake model results of the turbine WTG0, which is at the forefront in 90° wind direction, are almost the same as the SCADA results. This is because it is exposed to free stream airflow, not the wake effect. The blockage effect has a more minor impact than wake. Further developments can be done to get the desired result from coupled models. One of the biggest factors is that the site is not complex and the number of turbines is low. In a wind farm with more turbines, the difference between the model results will become evident.

Table 4. Wake-Blockage-Coupled Model Reuslts and Wind Farm Power Results Comparison

Models	WTG0 wd=90	WTG4 wd=90	WTG0 wd=270	WTG4 wd=270
			(%)	
NOJ	0.22	-64.69	-23.53	-10.88
NOJ Local	0.22	-68.11	-25.18	-10.88
NOJ Turbo	0.22	-70.77	-21.75	-10.88
GCL	0.22	-63.01	-22.66	-10.88
GCL Local	0.22	-32.83	-18.35	-10.88
Gaussian	0.22	-62.97	-12.42	-10.88
Gaussian Turbo	0.22	-55.60	-7.92	-10.88
Hybrid Induction	-1.20	-10.71	1.28	-11.79
Rankine Half Body	-0.99	-10.71	1.28	-11.66
Vortex Cylinder	-0.97	-10.71	1.26	-11.64
Vortex Dipole	-0.99	-10.71	1.28	-11.66
Self Similarity	-1.15	-10.69	1.42	-11.76
Self Similarity 20	-1.29	-10.66	1.54	-11.86
Coupled GCL VortexCylinder	-1.11	-62.67	-21.19	-11.81
Coupled NOJ VortexCylinder	-1.15	-86.47	-36.86	-11.82
Coupled Turbo Gaussian VortexCylinder	-1.10	-89.78	-10.42	-11.83
Coupled GCL Self Similarity20	-1.46	-62.58	-20.85	-12.05
Coupled NOJ Self Similarity20	-1.49	-86.45	-36.52	-12.06
Coupled Turbo Gaussian Self Similarity20	-1.44	-89.76	-10.07	-12.07

CHAPTER 6

CONCLUSION

This study examines and compares wake and blockage models of the two effects together and validates all models with wind farm SCADA data.

For the data obtained from SCADA to be ready, the data is filtered and prepared for validation.

Wake models are examined, and suitable wake models are observed according to the complexity of the field, its size, and the distance between the turbines. To SCADA data

There may be many reasons why there is no significant difference between Blockage models. The blockage effect affects power production less than a wake. Due to the smallness of the effect, the difference may be tiny. The small size of the wind farm and the single-row turbine negatively affect the observation of the blockage effect. In this case, it is reasonable to choose the easiest and fastest model to calculate.

As a result of literature review and theoretical background research, it is understood that the blockage induction zone is also effective, that is, in the front of the turbine. Wake is observed downstream where turbulent flow is present. While the downstream of the first turbine is in the wake effect, the blockage effect is also observed when the same area is the induction zone of the second turbine. In other words, observing a wake+blockage region between two turbines is possible.

When creating models in PyWake, only the wake or only blockage model is run, without any extra deficit model entering the model during wake or just blockage model review. But when it is desired to obtain a coupled model, the function is defined to the model and run together with the selected deficit model.

This study shows that examining the wake and blockage effects together is a logical option. The models converge to the actual data when selected according to the field. Still, data filtering is substantial to reach the correct result.

REFERENCES

[1] I. Energy Agency, “Renewables 2021 - Analysis and forecast to 2026,” 2021. [Online]. Available: www.iea.org/t&c/

[2] I. Energy Agency, “Net Zero by 2050 - A Roadmap for the Global Energy Sector,” 2050. [Online]. Available: www.iea.org/t&c/

[3] T. Göçmen, P. van der Laan, P. E. Réthoré, A. P. Diaz, G. C. Larsen, and S. Ott, “Wind turbine wake models developed at the technical university of Denmark: A review,” *Renewable and Sustainable Energy Reviews*, vol. 60. Elsevier Ltd, pp. 752–769, Jul. 01, 2016. doi: 10.1016/j.rser.2016.01.113.

[4] A. Crespo and J. Hernaâ Ndez, “Survey of Modelling Methods for Wind Turbine Wakes and Wind Farms.”

[5] D. Medici, S. Ivanell, J. Å. Dahlberg, and P. H. Alfredsson, “The upstream flow of a wind turbine: Blockage effect,” *Wind Energy*, vol. 14, no. 5, pp. 691–697, Jul. 2011, doi: 10.1002/we.451.

[6] N. G. Nygaard, S. T. Steen, L. Poulsen, and J. G. Pedersen, “Modelling cluster wakes and wind farm blockage,” in *Journal of Physics: Conference Series*, Sep. 2020, vol. 1618, no. 6. doi: 10.1088/1742-6596/1618/6/062072.

[7] F. Porté-Agel, M. Bastankhah, and S. Shamsoddin, “Wind-Turbine and Wind-Farm Flows: A Review,” *Boundary Layer Meteorol*, vol. 174, no. 1, pp. 1–59, Jan. 2020, doi: 10.1007/s10546-019-00473-0.

[8] W. Munters and J. Meyers, “Dynamic strategies for yaw and induction control of wind farms based on large-eddy simulation and optimization,” *Energies (Basel)*, vol. 11, no. 1, 2018, doi: 10.3390/en11010177.

[9] J. F. Manwell, J. G. McGowan, and A. L. Rogers, “Wind Energy Explained: Theory, Design and Application,” 2010.

[10] R. Mikkelsen, F. M. Technical University of Denmark. Department of Mechanical Engineering, and MEK, *Actuator disc methods applied to wind turbines*. 2003.

[11] P.-E. Réthoré, *Wind turbine wake in atmospheric turbulence*. Risø National Laboratory, 2009.

[12] N. Troldborg, *General rights Actuator Line Modeling of Wind Turbine Wakes*.

[13] G. Deskos, M. A. Abolghasemi, and M. D. Piggott, "Wake predictions from two turbine models using mesh-optimisation techniques Towards parameter-free subgrid-scale modelling in large eddy simulation View project Tidal energy operational and spatial planning optimisation View project Wake predictions from two turbine parametrisation models using mesh-optimisation techniques." [Online]. Available: https://www.researchgate.net/publication/319091606

[14] D. J. Renkema, "Validation of wind turbine wake models Using wind farm data and wind tunnel measurements Douwe J. Renkema," 2007.

[15] P. B. S. Lissaman, "ENERGY EFFECTIVENESS OF ARBITRARY ARRAYS OF WIND TURBINES.," *Journal of energy*, vol. 3, no. 6, pp. 323–328, 1979, doi: 10.2514/3.62441.

[16] A. C. Kheirabadi and R. Nagamune, "A quantitative review of wind farm control with the objective of wind farm power maximization," *Journal of Wind Engineering and Industrial Aerodynamics*, vol. 192. Elsevier B.V., pp. 45–73, Sep. 01, 2019. doi: 10.1016/j.jweia.2019.06.015.

[17] K. Nilsson *et al.*, "Large-eddy simulations of the Lillgrund wind farm," *Wind Energy*, vol. 18, no. 3, pp. 449–467, Mar. 2015, doi: 10.1002/we.1707.

[18] N. O. Jensen, "General rights A note on wind generator interaction," 1983.

[19] A. Penã, P. E. Réthoré, and M. P. van der Laan, "On the application of the Jensen wake model using a turbulence-dependent wake decay coefficient: The Sexbierum case," *Wind Energy*, vol. 19, no. 4, pp. 763–776, Apr. 2016, doi: 10.1002/we.1863.

[20] A. Niayifar and F. Porté-Agel, "A new analytical model for wind farm power prediction," in *Journal of Physics: Conference Series*, Jun. 2015, vol. 625, no. 1. doi: 10.1088/1742-6596/625/1/012039.

[21] "PyWake." https://topfarm.pages.windenergy.dtu.dk/PyWake/notebooks/Introduction.html (accessed Jun. 06, 2022).

[22] M. Bastankhah and F. Porté-Agel, "A new analytical model for wind-turbine wakes," *Renew energy*, vol. 70, pp. 116–123, 2014, doi: 10.1016/j.renene.2014.01.002.

[23] G. C. Larsen, "General rights A Simple Wake Calculation Procedure."

[24] G. C. Larsen, "General rights A simple stationary semi-analytical wake model." [Online]. Available: www.risoe.dk

[25] G. C. Larsen and Danmarks Tekniske Universitet. Risø DTU, *Dynamic wake meandering modeling*. Risø DTU - National Laboratory for Sustainable Energy, 2007.

[26] M. Sanchez Gomez, J. K. Lundquist, J. D. Mirocha, R. S. Arthur, and D. Muñoz-Esparza, "Quantifying wind plant blockage under stable atmospheric conditions", doi: 10.5194/wes-2021-57.

[27] J. Bleeg, M. Purcell, R. Ruisi, and E. Traiger, "Wind farm blockage and the consequences of neglecting its impact on energy production," *Energies (Basel)*, vol. 11, no. 6, Jun. 2018, doi: 10.3390/en11061609.

[28] T. Nishino and S. Draper, "Local blockage effect for wind turbines," in *Journal of Physics: Conference Series*, Jun. 2015, vol. 625, no. 1. doi: 10.1088/1742-6596/625/1/012010.

[29] A. Segalini and J. A. Dahlberg, "Global Blockage Effects in Wind Farms," in *Journal of Physics: Conference Series*, Jul. 2019, vol. 1256, no. 1. doi: 10.1088/1742-6596/1256/1/012021.

[30] E. Branlard, E. Quon, A. R. Meyer Forsting, J. King, and P. Moriarty, "Wind farm blockage effects: Comparison of different engineering models," in *Journal of Physics: Conference Series*, Sep. 2020, vol. 1618, no. 6. doi: 10.1088/1742-6596/1618/6/062036.

[31] E. Branlard and A. R. M. Forsting, “Assessing the blockage effect of wind turbines and wind farms using an analytical vortex model,” 2020, doi: 10.1002/we.

[32] B. J. Gribben, G. S. Hawkes, and F.-N. Consultancy, “A potential flow model for wind turbine induction and wind farm blockage,” 2019.

[33] “Egenda Enerji Urla RES.” https://www.egenda.com.tr/santrallerimiz/1015/urla-res-13-mwe-egenda-ege-enerji-uretim-as.aspx (accessed Jun. 06, 2022).

[34] P. Arthur and R. Duffy, “Effect of wind speed gradients on AEP in a wind farm cluster,” 2019. [Online]. Available: www.vindenergi.dtu.dk

[35] Bingöl Ferhat, “Adapting a Doppler laser anemometer to wind energy,” 2005.

[36] F. Bingöl, “Rüzgar Enerji Sistemleri İçin Hava Yoğunluğunun Hesaplanması,” *Journal of Polytechnic*, Jan. 2018, doi: 10.2339/politeknik.385523.

APPENDICES

APPENDIX A : Site Description

```
import numpy as np
from py_wake.site._site import UniformWeibullSite
from py_wake.wind_turbines.power_ct_functions import PowerCtTabular
from py_wake.wind_turbines import WindTurbines
wt_x = [1048 , 824 , 593 , 363 , 135]
#wt_x = [465848,465624,465393,465163,464935]
wt_y = [191 , 258 , 291 , 309 , 332]
#wt_y = [4241191,4241258,4241291,4241309,4241332]
wt_z = [437.9,455.3,470,463.3,461]
ws=[2.5,3,3.5,4,4.5,5,5.5,6,6.5,7,7.5,8,8.5,9,9.5,10,10.5,11,11.5,12,1
2.5,13,13.5,14,14.5,15]
power_wtg0=[]
power_wtg1=[]
power_wtg2=[]
power_wtg3=[]
power_wtg4=[]
ct=[]
class wts(WindTurbines):
def __init__(self, method='linear'):
WindTurbines.__init__(self,names=['WTG0’,'WTG1','WTG2','WTG3','WTG4'],
             diameters=[82 , 82 , 82, 82 , 82],
             hub_heights=[78 , 78 , 78, 78 , 78],
             powerCtFunctions=[PowerCtTabular(ws,power_wtg0,'kW',ct),
                               PowerCtTabular(ws,power_wtg1,'kW',ct),
                               PowerCtTabular(ws,power_wtg2,'kW',ct),
                               PowerCtTabular(ws,power_wtg3,'kW',ct),
                               PowerCtTabular(ws,power_wtg4,'kW',ct)])

class Ures(UniformWeibullSite):
def __init__(self, ti=.1, shear=None):
f=[0.11,0.38,0.13,0.03,0.01,0.03,0.08,0.07,0.05,0.02,0.03,0.06]
A=[7.9, 9.9, 8.2, 4.6, 4.6, 7.3, 8.3, 8.4, 7, 5.3, 5.3, 6.2]
k=[2.74,2.99,2.15,1.27,1.47,2.03,1.73,1.85,1.79,1.68,2.18,2.7]
UniformWeibullSite.__init__(self,np.array(f)/np.sum(f),A,k,ti=ti,shear
=shear)
self.initial_position = np.array([wt_x, wt_y, wt_z]).T

site = Ures()
windTurbines = wts([0,1,2,3,4])
wt_x, wt_y, wt_z = site.initial_position.T
k=0.0831644
```

APPENDIX B : Wake Model Example

```
wf_model=NOJ(site,windTurbines)
wf_model_local=NOJLocal(site,windTurbines,turbulenceModel=STF2017Turbu
lenceModel())
wf_model_turbo=PropagateDownwind(site,windTurbines,rotorAvgModel=None,
wake_deficitModel=TurboNOJDeficit(use_effective_ws=True,use_effective_
ti=False),
superpositionModel=LinearSum(),
turbulenceModel=STF2017TurbulenceModel())

tip=np.array([0, 1, 2, 3, 4])
sim_res = wf_model(wt_x, wt_y,h = [437.9,455.3,470,463.3,461],
type=tip,wd=None,
ws=[2.5,3,3.5,4,4.5,5,5.5,6,6.5,7,7.5,8,8.5,9,9.5,10,10.5,11,11.5,12,1
2.5,13,13.5,14,14.5,15,15.5,16,16.5,17,17.5,18,18.5,19,19.5,20,20.5,21
,21.5,22,22.5,23,23.5,24,24.5,25,25.5,26,26.5,27,27.5,28,28.5,29,29.5,
30,30.5,31,31.5,32,32.5,33,33.5,34],
Air_density=1.146)

print(sim_res)

res = pd.DataFrame()
res['u']=[2.5,3,3.5,4,4.5,5,5.5,6,6.5,7,7.5,8,8.5,9,9.5,10,10.5,11,11.
5,12,12.5,13,13.5,14,14.5,15,15.5,16,16.5,17,17.5,18,18.5,19,19.5,20,2
0.5,21,21.5,22,22.5,23,23.5,24,24.5,25,25.5,26,26.5,27,27.5,28,28.5,29
,29.5,30,30.5,31,31.5,32,32.5,33,33.5,34]
for i in range(0,5):
    p=sim_res.Power.sel(wt=i, wd=0)
    myname=f'p{i+1}'
    res[myname]=p.data/1000

wt_x, wt_y, wt_z = Ures().initial_position.T
        tip2=np.array([0, 1, 2, 3, 4])
        windTurbines = wts(tip2)

site = Ures()
wf_model = NOJ(site, windTurbines, k=0.04)
wf_model_local = NOJLocal(site, windTurbines,
                          turbulenceModel=STF2017TurbulenceModel())
wf_model_turbo=PropagateDownwind(site,windTurbines,rotorAvgModel=None,
wake_deficitModel=TurboNOJDeficit(use_effective_ws=True, use_effective
_ti=False),
superpositionModel=LinearSum(),
turbulenceModel=STF2017TurbulenceModel())
```

APPENDIX C : Wake Model Flowmap Example

```
noj_models = [wf_model , wf_model_local , wf_model_turbo ]

for noj_model in noj_models:

# Calculate AEP
sim_res = noj_model(wt_x, wt_y, wt_z, type=tip2)
# Plot wake map
plt.figure(sim_res.__class__.__name__)
plt.title('AEP: %.2f GWh' % sim_res.aep().sum())

flow_map = sim_res.flow_map(wd=[270], ws=[10])
flow_map.plot_wake_map(plot_windturbines=True)
plt.show()
```

APPENDIX D : Blockage Model Example

```
site = Ures()
windTurbines = wts([0,1,2,3,4])
wt_x, wt_y, wt_z = site.initial_position.T
k=0.0831644
wf_model=All2AllIterative(site,windTurbines,
wake_deficitModel=NoWakeDeficit(),
superpositionModel=LinearSum(),
blockage_deficitModel=SelfSimilarityDeficit())
wf_model_2020=All2AllIterative(site,windTurbines,
wake_deficitModel=NoWakeDeficit(),
superpositionModel=LinearSum(),
blockage_deficitModel=SelfSimilarityDeficit2020())
tip=np.array([0, 1, 2, 3, 4])
sim_res = wf_model_2020(wt_x, wt_y,h = [437.9,455.3,470,463.3,461],
type=tip,wd=None,
ws=[2.5,3,3.5,4,4.5,5,5.5,6,6.5,7,7.5,8,8.5,9,9.5,10,10.5,11,11.5,12,1
2.5,13,13.5,14,14.5,15,15.5,16,16.5,17,17.5,18,18.5,19,19.5,20,20.5,21
,21.5,22,22.5,23,23.5,24,24.5,25,25.5,26,26.5,27,27.5,28,28.5,29,29.5,
30,30.5,31,31.5,32,32.5,33,33.5,34],
Air_density=1.146)

print(sim_res)
res = pd.DataFrame()
res['u']=[2.5,3,3.5,4,4.5,5,5.5,6,6.5,7,7.5,8,8.5,9,9.5,10,10.5,11,11.
5,12,12.5,13,13.5,14,14.5,15,15.5,16,16.5,17,17.5,18,18.5,19,19.5,20,2
0.5,21,21.5,22,22.5,23,23.5,24,24.5,25,25.5,26,26.5,27,27.5,28,28.5,29
,29.5,30,30.5,31,31.5,32,32.5,33,33.5,34]

for i in range(0,5):
    p=sim_res.Power.sel(wt=i, wd=270)
    myname=f'p{i+1}'
    res[myname]=p.data/1000
wt_x, wt_y, wt_z = Ures().initial_position.T
        tip2=np.array([0, 1, 2, 3, 4])
        windTurbines = wts(tip2)

site = Ures()
wf_model = All2AllIterative(site, windTurbines, wake_deficitModel=NoWa
keDeficit(),
superpositionModel=LinearSum(), blockage_deficitModel=SelfSimilarityDe
ficit())

wf_model_2020 = All2AllIterative(site, windTurbines, wake_deficitModel
=NoWakeDeficit(),
superpositionModel=LinearSum(), blockage_deficitModel=SelfSimilarityDe
ficit2020())
```

APPENDIX E : Blockage Model Flowmap Example

```
SelfSimilarity_models = [wf_model , wf_model_2020]

for SelfSimilarity_model in SelfSimilarity_models:

# Calculate AEP
 sim_res = SelfSimilarity_model(wt_x,wt_y,wt_z,type=tip2)
# Plot wake map
plt.figure(sim_res.__class__.__name__)
plt.title('AEP: %.2f GWh' % sim_res.aep().sum())
#plt.title(wake_model)

flow_map = sim_res.flow_map(wd=[90], ws=[10])
flow_map.plot_wake_map(plot_windturbines=True)
plt.show()
```

APPENDIX F : Coupled Model Example

```
site = Ures()
windTurbines = wts([0,1,2,3,4])
wt_x, wt_y, wt_z = site.initial_position.T
k=0.0831644

wf_model = All2AllIterative(site, windTurbines, wake_deficitModel=Turb
oGaussianDeficit(),superpositionModel=LinearSum(),blockage_deficitMode
l=VortexCylinder())
tip=np.array([0, 1, 2, 3, 4])
sim_res = wf_model(wt_x, wt_y,h = [437.9,455.3,470,463.3,461],
type=tip,wd=None,
ws=[2.5,3,3.5,4,4.5,5,5.5,6,6.5,7,7.5,8,8.5,9,9.5,10,10.5,11,11.5,12,1
2.5,13,13.5,14,14.5,15,15.5,16,16.5,17,17.5,18,18.5,19,19.5,20,20.5,21
,21.5,22,22.5,23,23.5,24,24.5,25,25.5,26,26.5,27,27.5,28,28.5,29,29.5,
30,30.5,31,31.5,32,32.5,33,33.5,34],
Air_density=1.146)

print(sim_res)
res = pd.DataFrame()
res['u']=[2.5,3,3.5,4,4.5,5,5.5,6,6.5,7,7.5,8,8.5,9,9.5,10,10.5,11,11.
5,12,12.5,13,13.5,14,14.5,15,15.5,16,16.5,17,17.5,18,18.5,19,19.5,20,2
0.5,21,21.5,22,22.5,23,23.5,24,24.5,25,25.5,26,26.5,27,27.5,28,28.5,29
,29.5,30,30.5,31,31.5,32,32.5,33,33.5,34]
for i in range(0,5):
    p=sim_res.Power.sel(wt=i, wd=270)
    myname=f'p{i+1}'
    res[myname]=p.data/1000
wt_x, wt_y, wt_z = Ures().initial_position.T
        tip2=np.array([0, 1, 2, 3, 4])
        windTurbines = wts(tip2)

site = Ures()
wf_model = All2AllIterative(site, windTurbines, wake_deficitModel=Turb
oGaussianDeficit(),superpositionModel=LinearSum(), blockage_deficitMod
el=VortexCylinder())
```

APPENDIX G : Coupled Model Flowmap Example

```
vortexcylinder_models = [wf_model]

for vortexcylinder_model in vortexcylinder_models:

# Calculate AEP
Sim_res = vortexcylinder_model(wt_x, wt_y, wt_z,type=tip2)
# Plot wake map
plt.figure(sim_res.__class__.__name__)
plt.title('AEP: %.2f GWh' % sim_res.aep().sum())

flow_map = sim_res.flow_map(wd=[90], ws=[10])
flow_map.plot_wake_map(plot_windturbines=True)
plt.show()
```